DEPARTMENT OF THE AIR FORCE

AIR UNIVERSITY

AIR FORCE INSTITUTE OF TECHNOLOGY

Wright-Patterson Air Force Base, Ohio

AFIT/GAE/AA/88D-35

MACROCRACK-MULTIPLE DEFECT INTERACTION CONSIDERING ELASTIC, PLASTIC, AND VISCOPLASTIC EFFECTS

THESIS

LeRoy K. Smith
Captain, USAF

AFIT/GAE/AA/88D-35

Approved for public release; distribution unlimited

AFIT/GAE/AA/88D-35

MACROCRACK - MULTIPLE DEFECT INTERACTION CONSIDERING ELASTIC, PLASTIC, AND VISCOPLASTIC EFFECTS

THESIS

Presented to the Faculty of the School of Engineering

of the Air Force Institute of Technology

Air University

In Partial Fulfillment of the

Requirements for the Degree of

Master of Science in Aeronautical Engineering

LeRoy K. Smith, B.S.

Captain, USAF

December 1988

Acknowledgments

I am especially grateful to Dr A.N. Palazotto for the many hours he spent reviewing my efforts and providing constructive guidance during this research. I also want to thank Dr T. Nicholas of the Air Force Materials Laboratory for recommending and sponsoring this effort.

I also wish to extend special thanks to my father, Roy, for encouraging me to pursue a career in engineering. Finally, my deepest appreciation goes to my wife, Lori, for her loving support and patience during the many long hours.

LeRoy K. Smith

Contents

List of Symbols

a	Half crack or defect length
$[D]$	Elastic material property matrix
D_o	Bodner material constant
D_2^P	Second invariant of plastic strain rate
E	Elastic modulus
J	J-integral value
J_2	Second invariant of deviatoric stress
$[K]$	Elastic stiffness matrix
K_1	Elastic stress intensity
m	Bodner material constant
n	Bodner material constant
R	Minimum to maximum load ratio
R_p	Irwin plastic zone radius
r	Bodner Material constant/Radial distance
S	Defect ratio of crack length
W	Strain energy density
W_p	Plastic strain energy density
Z	Bodner model state variable
Z_o, Z_1, Z_2	Bodner model constants
$\delta( )$	Virtual quantity
δ	Spacing ratio of defect length
S_{ij}	Deviatoric stress tensor
${}^0S_{ij}$	2nd Piola-Kirkhoff Stress Tensor
F_i	Body force (neglected in this analysis)

List of Symbols (Cont'd)

T_i	External surface traction
e_{kl}	Increment of linear strain
ε_{ij}	Total strain tensor
ε^{e}_{ij}	Elastic component of total strain
ε^{p}_{ij}	Plastic component of total strain
σ_{ij}	Components of stress tensor
σ_{ys}	Material yield stress
η_{ij}	Incremental nonlinear strain
λ	Scalar constant

List of Figures

List of Figures (Cont'd)

List of Figures Cont'd

List Of Tables

Abstract

A finite element investigation was conducted to analyze an axial tension specimen with collinear defects placed symmetrically about a center crack. The material modeled was IN-718, a nickel-based superalloy used in jet engines. The effects of crack/defect interaction were compared using elastic, elastic plastic, and viscoplastic constitutive models. A 2-D nonlinear finite element code called SNAP was used. This program has the capability to simulate crack growth and closure by releasing or closing nodes along the crack plane.

Elastic stress intensity solutions were developed for two different finite width specimens. The stress intensity versus crack length plots compared well with infinite theory. Results reflect the defect can partially shield the crack from finite width effects. A critical spacing was also noted where the stress intensity of the crack exceeded the stress intensity for the combined length of the crack and defect.

Finite element analysis of a crack/defect configuration, considering elastic-plastic and elastic-viscoplastic effects, provided crack opening profiles, plastic zone profiles, and stress/strain fields. In general, the defect has a prominent influence range equal to approximately one defect length for all constitutive models. The presence of a defect increases the magnitude of the crack opening and stress/strain fields in front of the crack tip.

I. Introduction

Background

The United States Air Force has adopted fracture mechanics as a design criteria for aircraft engines through the Engine Structural Integrity Program (ENSIP) which was instituted as a Military Standard (1) in 1984. The damage tolerance policy is based on "retirement for cause". This policy requires the determination of crack growth rates such that inspection intervals will be set to one-half the time required for an existing crack to grow to a critical size. Linear elastic fracture mechanics (LEFM) provides a good estimate of remaining life for components subjected to moderate temperatures and loads. However, components such as turbine disk blades are subjected to both high stresses (200 ksi) and high temperatures (1200 F) which leads to interaction between creep and crack growth. For these components, the Air Force Office of Scientific Research (AFOSR) has set forth a philosophy that damage tolerances should be characterized by near-tip stress, strain, and displacement fields with emphasis on non-continuum description of structural materials. Application of damage tolerant concepts yielded a 40 to 1 benefit to cost ratio and extended part life by a factor of four for the F100-PW-200 core engine (2).

Approach

In response to the above directives, several studies were conducted using elastic-plastic and viscoplastic finite

element analysis (3-9). The geometries considered include both axial and compact tension specimens with emphasis on single crack phenomena. The goal of the present work is to build upon these efforts by incorporating collinear defects with a center-cracked axial tension specimen.

Two primary objectives were set forth in this study. The first objective was to investigate the influence of collinear defects on the stress intensity solutions of the center-cracked tension specimen. This was accomplished using the J-Integral method developed by Rice (10). The second objective was to investigate crack growth in close proximity to the defects under both monotonic and cyclic loading. The material was IN-718, a nickel-based superalloy used in turbine blades for jet engines. The material behavior was modeled with elastic-plastic constitutive equations using the Von Mises criterion (11) and the viscoplastic flow law developed by Bodner and Partom (12) for high temperature effects.

Finite element analysis was conducted with a program called SNAP (13). The SNAP program was modified by Mercer (8) to allow crack growth and closure by the incorporation of spring type boundary nodes along the crack line in a manner similar to Newman (14). Additional modifications were made to allow up to 5000 degrees of freedom and variable crack growth rates under monotonic loading. Four-noded linear isoparametric elements were used.

Literature Review

Single Cracks

As previously stated, several studies have been undertaken using elastic-plastic and viscoplastic effects to characterize the behavior of a single crack. A summary of related work is provided here.

Zahoor and Abou-Sayed (3) performed elastic-plastic analysis on a center-cracked tension specimen. Both constant strain triangles and 4-noded quadrilateral elements were used. Crack tip blunting effects were noted by prominent element rotation at the crack tip.

Hinnerichs (4) examined constant load creep crack growth for a center-cracked specimen of IN-100 at high temperatures with a program he developed called "VISCO". A procedure, referred to as the hybrid method, was developed for determining crack extension using calculations of viscoplastic deformation with no crack growth. In this procedure, the difference between total crack deformation and viscoplastic deformation is attributed to crack extension. Extremely good crack growth predictions were made for the axial tension geometry.

Nicholas and others (5) investigated plasticity induced closure involving short cracks. They found, from an analytical point of view, that closure requires some amount of crack extension in order to develop residual strains behind the crack tip. The plastic wake effect developed

very rapidly for fully reversed loading but required longer propagation distances to develop under positive load ratios.

Wilson and Palazotto (6) investigated viscoplastic fatigue in an IN-100 compact tension specimen with R = 0.1. They found that a large majority of plastic straining occurs within the first three load cycles and the stress field remains relatively constant after one to three cycles.

Henkel and Palazotto (7) compared viscoplastic fatigue in a compact tension and a center-cracked specimen with R = -1. They found the size of the plastically strained region at the crack tip is a major factor determining the amount of closure behind the crack tip. In addition, incomplete closure behind the crack tip was noted at full negative load for both specimens.

Mercer (8) did an extensive viscoplastic study of a crack growing from a notch under cyclic loading. He found that the notch has a region of influence equal to one notch radius. It was also noted that a highly loaded short crack has more crack tip plasticity than a long crack at a lower load level to produce the same stress intensity. Chestnut (9) did follow-on research for large round notches and proved a similar influence range of one notch radius.

Multiple Cracks

Limited publications were found in the area of multiple crack interaction. The work summarized below discusses infinite plate analysis.

Matake and Imai (15) investigated the behavior of a small collinear defect located in front of a long crack. The possibility of pop-in behavior induced by the main and subcrack was demonstrated. Pop-in behavior is characterized as an abrupt load dropping when the crack and defect combine during fracture testing. Under constant load this phenomenon is characterized as an abrupt drop in the stress intensity of the combined crack and defect. Analytical equations for the stress intensity solution at each crack tip were developed. These equations are discussed under Fracture Mechanics Theory.

Rose (16) represented microcracks in front of the main crack by using point-source complex potentials. Simultaneous equations for parameters characterizing the strength of the equivalent point sources are then solved. This method proved to be accurate to within five percent of the exact solution.

Chang (17) addressed the problem of noncoplanar crack interaction and developed equations for the stress intensity based on asymptotic approximations of the normal stresses at the crack tips.

Yoda (18) did an experimental investigation of crack coalescence in glass. He noted that the crack velocity increases with the stress intensity factor as the cracks approached each other.

Ang (19) considered two collinear cracks of equal length and provides a boundary integral solution to this problem.

He also presents an exact solution for the stress intensity factor for the outer tip of the cracks.

Rubinstein (20) developed an exact solution for a macrocrack interacting with a periodically distributed collinear array of microcracks. He found that if the microcracks were spaced far enough apart one need only consider the leading microcrack in the interaction with the main crack. For this case, he found the critical spacing to be two microcrack lengths.

Summary of Findings

The review of the literature reflects significant accomplishments in 2-D analysis of single cracks under various geometries and material behavior models. In the area of multiple cracks, substantial work has been done for linear elastic analysis in an infinite plane. However, multiple cracks under finite geometries and nonlinear effects is completely open for study.

II. Theory

Equations of Motion

Finite element modeling is a well developed technique for approximating the "exact" equations of motion for a body undergoing deformation. The SNAP finite element code developed by Brockman (13) is based on an incremental virtual work expression that characterizes a body deforming from a state (k-1) to a state (k) and is given by:

$$\int_{{}^0V} \left[D_{ijkl}(e_{kl})\delta e_{ij} + {}_{(k-1)}{}^0S_{ij}\delta\eta_{ij} \right] dVol$$

$$= \int_{{}^0V} {}_kF_i\delta u_i \; dVol + \int_{{}^0S_1} {}_kT_i\delta u_i dA - \int_{{}^0V} {}_{(k-1)}{}^0S_{ij}\delta e_{ij} dVol \qquad (2.1)$$

Where:

D_{ijkl} = Incremental material constitutive matrix

e_{kl} = Incremental linear strain

η_{ij} = Incremental nonlinear strain

T_i = Surface Tractions

F_i = Body Forces

${}^0S_{ij}$ = 2nd Piola-Kirkhoff stress tensor

$\delta( )$ = Virtual quantity

Mercer (8) provides a detailed derivation of the above equation.

The corresponding finite element expression in total Lagrangian form is written (neglecting body forces) as:

$$k\left[[K_t] + [K_g]\right](U) = {}_k(T) - {}_{k-1}(I) \qquad (2.2)$$

Where: $[K_t]$ = Tangent stiffness matrix

$[K_g]$ = Geometric stiffness matrix

$\langle u \rangle$ = Nodal displacement vector

$\langle T \rangle$ = External force vector

$\langle I \rangle$ = Internal force vector

The total stiffness matrix is divided into tangent and geometric components to account for nonlinear material behavior and large displacements respectively. The nonlinear plasticity problems were solved using the initial stiffness method. This method uses the stiffness matrix formulated with the first increment of displacement for the entire solution. During a load increment the internal forces in the elements may not be in exact equilibrium with the applied forces. This extra force is considered a residual force and is applied to the next time increment. Equilibrium for the current load step is met when the residual force and displacement corrections are less than user specified tolerances. A detailed description of the initial stiffness technique is given by Owen and Hinton (11).

Constitutive Models

Three constitutive models were used in this analysis for calculating stresses and strains in the elements. A brief description of each is provided below.

Linear Elastic

The linear elastic constitutive model follows the classical relation:

$$\langle \sigma \rangle = [D]\langle \varepsilon \rangle \qquad (2.3)$$

where: $\langle \sigma \rangle = \langle \sigma_{11} \ \sigma_{22} \ 0 \ \sigma_{12} \rangle^T$

$\langle \varepsilon \rangle = \langle \varepsilon_{11} \ \varepsilon_{22} \ \varepsilon_{33} \ \varepsilon_{12} \rangle^T$

$[D]$ = Elastic constitutive matrix

Elastic-Plastic

For this model, total strains are decomposed into elastic and plastic parts:

$$\varepsilon_{ij} = \varepsilon_{ij}^{e} + \varepsilon_{ij}^{p} \qquad (2.4)$$

Incremental plastic strains are calculated via a Prandtl-Reuss relation (11) as:

$$d\varepsilon_{ij}^{p} = d\lambda \, S_{ij} \qquad (2.5)$$

Where: $d\lambda = \dfrac{3 \, d\bar{\sigma}}{2 \, \bar{\sigma} \, H}$

S_{ij} = Deviatoric stress = $\sigma_{ij} - \dfrac{\delta_{ij}\sigma_{kk}}{3}$

H = Slope of stress-plastic strain curve

$\bar{\sigma}$ = Effective stress = $\sqrt{[3/2(S_{ij}S_{ij})]}$

The corresponding matrix form of the equation is given by Yamada (21):

$$\langle d\sigma \rangle = [Dep]\langle d\varepsilon \rangle \qquad (2.6)$$

where: $d\sigma$ = incremental stress

$d\varepsilon$ = incremental strain

[Dep] = elastic-plastic constitutive Matrix

Mercer (8) shows the elastic-plastic matrix in expanded form.

For this model, a Von Mises yield criterion is used to determine when the material exceeds a critical value of recoverable elastic energy. For the case of uniaxial tension, yielding occurs when the effective stress exceeds the yield stress of the material.

Bodner-Partom Viscoplasticity

The Bodner-Partom flow law accounts for viscoplastic behavior as well as rate sensitivity and strain hardening effects (12). The model description given by Mercer (8) is presented here for completeness.

For small strains, the total strain rate is decomposed into elastic and plastic parts by :

$$\dot{\varepsilon}_{ij} = \dot{\varepsilon}_{ij}^{e} + \dot{\varepsilon}_{ij}^{p} \qquad (2.7)$$

Where: $\dot{\varepsilon}_{ij}^{e}$ = Elastic strain rate

$\dot{\varepsilon}_{ij}^{p}$ = Viscoplastic strain rate

The viscoplastic strain rates are calculated using a Prandtl-Ruess type relation:

$$\dot{\varepsilon}_{ij}^{p} = \left[\left[D_0^2 \exp\left[-\left\{\frac{Z^2}{3J_2}\right\}^n \frac{n+1}{n}\right]\right]\left\{\frac{1}{J_2}\right\}\right]^{\frac{1}{2}} S_{ij} \qquad (2.8)$$

where S_{ij} is the deviatoric stress and J_2 is the second deviatoric stress invariant.

The constant n controls the model's strain rate

sensitivity, while D_0 is the maximum value of strain rate in shear. The Z parameter is an internal state variable which accounts for the degree of material work hardening and is expressed as:

$$Z = Z_1 + (Z_0 - Z_1)\exp(-m\,\bar{W}_p) \qquad (2.9)$$

where Z_0 and Z_1 are the material's initial and maximum values of hardness respectively, and the constant (m) controls the rate of work hardening. The term $\bar{W}_p$ accounts for the plastic work including thermal recovery of hardening at high temperature and is defined as:

$$\bar{W}_p = \int \sigma \dot{\varepsilon}^p \, dt + \int \frac{\dot{Z}_{rec}}{m(Z_1 - Z)} \, dt \qquad (2.10)$$

The rate of thermal recovery of hardness is:

$$\dot{Z}_{rec} = -AZ_1 \left\{ \frac{Z - Z_2}{Z_1} \right\}^r \qquad (2.11)$$

where Z_2 is the minimum expected value of the hardening at a given temperature. The constants (A) and (r) are material parameters which are chosen to match low strain rate (secondary creep) test data. Secondary creep is defined as the balanced condition when the rate of work hardening equals the rate of thermal recovery (4). The recovery term becomes essential in high temperature analysis.

Stresses are calculated using the following equation:

$$\{d\sigma\} = [D]\,[\{d\varepsilon\} - \{d\varepsilon^p\}] \qquad (2.12)$$

where [D] is the elastic stiffness matrix.

Owen and Hinton (11) set forth the following equation for

calculating the plastic strain rate:

$$\left\{d\dot{\varepsilon}_{ij}^{P}\right\}^{i} = dt^{i}\left[(1-\phi)\left\{\dot{\varepsilon}_{ij}^{P}\right\}^{i-1} + \phi\left\{\dot{\varepsilon}_{ij}^{P}\right\}^{i}\right] \quad (2.13)$$

Where for:

$\phi = 0$ Euler integration scheme (fully explicit)

$\phi = 1$ Fully implicit scheme

$\phi = \frac{1}{2}$ Crank-Nicolson rule, or semi-implicit

A semi-implicit scheme is employed in the SNAP code to calculate the viscoplastic strains. This scheme is unconditionally stable as described by Hughes and Taylor (22) which allow larger load increments to be applied during the solution. However, accuracy is decreased if the load steps become too large. Chestnut (9) provides a discussion on how the viscoplastic solution proceeds in the SNAP code.

Beaman (23) determined the Bodner-Partom material parameters for IN-718 listed in table 2.1 below.

Table 2.1: Bodner-Partom Parameters for IN-718 @ 1200 F

Parameter	Description	Value
E	Elastic Modulus	23.5 x 10 ksi
n	Strain rate exponent	3.0
D_0	Strain rate limit	10^6 sec^{-1}
Z_0	Initial hardness	235.3 ksi
Z_1	Maximum hardness	260.3 ksi
Z_2	Minimum hardness	104.1 ksi
m	Hardening rate exponent	2.875 ksi
A	Hardening recovery coeff	1.5×10^{-3} sec^{-1}
r	Hardening recovery exponent	7.0

Linear Elastic Fracture Mechanics

Fracture mechanics studies the effects of externally applied loads and specimen geometry on crack tip stresses, displacements, and growth rates. Specimen thickness and the stress intensity factor provide the similitude parameters necessary for linear fracture toughness comparisons. Broek (24) states that the analysis is considered linear as long as the plastic zone in front of the crack tip is small, which is when the stress is low with respect to the yield stress ($\sigma < 0.8\ \sigma_{ys}$). When the stresses are higher, the plastic zone will spread beyond the point at which it is a unique function of the stress intensity factor. The development of fracture mechanics is well described by Broek (24) and therefore will not be elaborated upon here. The equations used for this analysis are briefly described below.

Center-Cracked Plate

For linear analysis, the stress at the crack tip is expressed by the stress intensity factor which for mode one loading (opening mode) is given by:

$$K_1 = \beta\, \sigma \sqrt{\pi a} \qquad (2.14)$$

Where: β = finite boundary correction factor

σ = far field stress

a = half crack length

In order to apply equation 2.14 to a finite element

model, the proper correction factor for the finite width and height was required. Isida (25) developed finite boundary corrections (β) for a variety of boundary conditions with the use of Laurent expansions of complex potentials satisfying the stress free relations along the crack. Table 2.2 lists a representative example of the finite width corrections for an axial tension specimen subjected to uniaxial loading. The accuracy of the finite boundary corrections are regarded as correct up to four figures (25). The half height/half width ratios of 0.4 and 1.0 were used in the mesh validation efforts of this study.

Table 2.2 Finite Boundary Corrections (25)

c/b		0.4	0.6	0.8	1.0
γ =	0.0	1.0000	1.0000	1.0000	1.0000
	0.1	1.069	1.033	1.021	1.014
	0.2	1.256	1.130	1.083	1.055
	0.3	1.520	1.285	1.184	1.123
	0.4	1.843	1.497	1.323	1.216
	0.5	2.247	1.773	1.496	1.334
	0.6	2.806	2.123	1.702	1.481
	0.7	3.670	2.550	1.940	1.680

Where: γ = crack half length/specimen half width

c/b = specimen half height/specimen half width

Macrocrack - Multiple Defect (Infinite Plate)

The presence of defects or large inclusions near primary cracks in ductile materials have been observed in

experimental work. It is known that the growth and nucleation of such defects in the vicinity of a primary crack play an important role in high temperature creep growth (4). The presence of defects can also shield the primary crack thereby directly affecting the toughness of the material (16). However, quantitative effects of crack/defect interaction are not very well understood. The aim of this work is to provide some insight into this interaction.

For this analysis, a defect is defined as a through-the-thickness crack that is approximately one-fifth or less than the length of the primary or macrocrack. The substantially smaller defect length makes a favorable argument for limiting crack growth to the macrocrack tip only.

A crack with collinear defects placed symmetrically about the y axis as shown in Figure 2.1 was selected. Collinear analysis simplified the finite element mesh development and and allowed direct comparison to existing analytical equations for the stress intensity factor as described below.

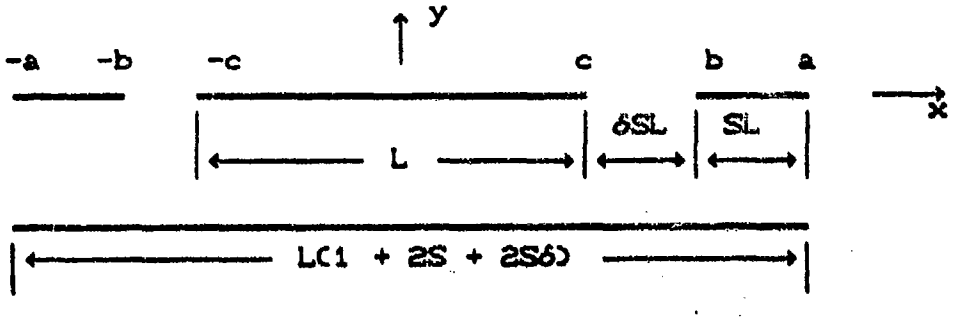

Fig. 2.1 Macrocrack - Multiple Defect Geometry

Matake and Imai (15) studied the case of a macrocrack with two collinear defects for an infinite plate. They obtained analytical expressions for the stress intensities at each tip of the crack and defect for the case of a uniform tensile stress normal to the crack plane. The mode one stress intensity solutions for the above geometry are:

$$K_a = \sigma \sqrt{\frac{\pi L}{2}(1 + 2S + 2S\delta)}\ \frac{1}{k}\left\{1 - \frac{E(k)}{K(k)}\right\} \qquad (2.15)$$

$$K_b = \sigma \sqrt{\frac{\pi L}{2}(1 + 2S\delta)}\ \frac{n}{k}\left\{\frac{1}{n^2}\ \frac{E(k)}{K(k)} - 1\right\} \qquad (2.16)$$

$$K_c = \sigma \sqrt{\frac{\pi L}{2}}\ \frac{1}{n}\ \frac{E(k)}{K(k)} \qquad (2.17)$$

Where:

$$k = \sqrt{\frac{1 + S + 2S\delta}{(1 + \delta)(1 + S + S\delta)}} \qquad (2.18)$$

$$n = \sqrt{(1 - k^2)} \qquad (2.19)$$

σ = far field stress

S = defect ratio of crack length

δ = spacing ratio of defect length

K(k) and E(k) are complete elliptic integrals of the first and second kinds and are given by the following equations:

$$K(k) = \int_0^{\frac{\pi}{2}} \frac{d\phi}{\sqrt{(1 - k^2 \sin^2\phi)}} \qquad (2.20)$$

$$E(k) = \int_0^{\frac{\pi}{2}} \sqrt{(1 - k^2 \sin^2 \phi)} \; d\phi \qquad (2.21)$$

Stress Intensity Methods

The elastic stress intensity factor can be determined for crack problems in finite element analysis using the J-integral, compliance methods, and extrapolation of the stress and displacement fields near the crack tip. For this study, the J-integral and stress extrapolation technique were used. A description of each method is given below.

J - Integral

Rice (10) has shown the J-integral as defined along a contour around the crack tip (Fig. 2.2) is the change in potential energy for a virtual crack extension (da).

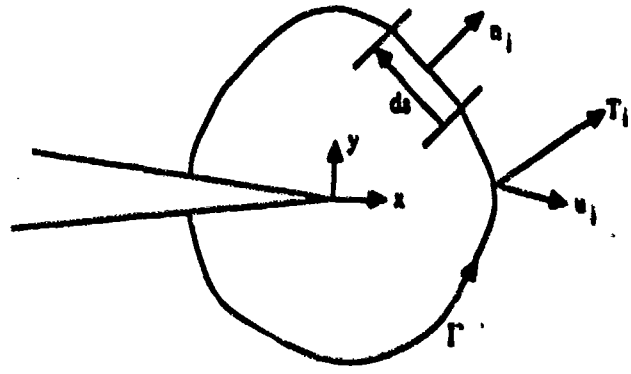

Fig. 2.2 J-Integral Contour Path

The J-integral is given by:

$$J = \int \left(W dy - T_i \frac{\partial u}{\partial x} ds \right) \qquad (2.22)$$

Where: W = strain energy density

$= (1/2)\sigma_{ij}\varepsilon_{ij}$ (Elastic)

$= (1/2)\sigma_{ij}\varepsilon_{ij} + \int_0^{\varepsilon^P_{mn}} \sigma_{ij} d\varepsilon^P_{ij}$ (Elastic-Plastic)

T_i = traction vector along contour path

u = displacement vector along contour path

da = increment of distance along the contour

ε_{ij} = elastic strain tensor

ε^P_{ij} = plastic strain tensor

σ_{ij} = stress tensor

The stress intensity factor is then calculated from the J-integral by:

$$K_1 = \sqrt{E\,J} \qquad \text{(Plane Stress)} \qquad (2.23)$$

Where: E = Modulus of Elasticity.

Stress Extrapolation

With this technique, The stresses normal to the crack tip are used to determine the stress intensity factor. The stress in the vicinity of the crack front is given by:

$$\sigma_y = \frac{K_1}{\sqrt{2\pi r}} \cos(\phi/2)\,[1 + \sin(\phi/2)\sin(\phi/2)] \qquad (2.24)$$

For the case of $\phi = 0^\circ$ the resulting expression for K_1 is:

$$K_1 = \sqrt{2\pi r}\ \sigma_y \qquad (2.25)$$

Where: σ_y = stress in y direction

r = radial distance from crack tip

The averaged stress intensity value for the crack tip is extrapolated to $r = 0$ based on the method described by Broek (24).

Irwin Plastic Zone

The basic theory behind linear elastic analysis of a crack states that an infinite stress field is present at the crack tip. In actuality, this cannot occur since the metal will plastically deform once the yield stress is met. The plastically deformed region is known as the plastic zone and a rough estimate of its size was set forth by G.R. Irwin as discussed by Broek (24). The approximation is a circular region in front of the crack tip with a radius given as:

$$R_p = \frac{\sigma^2 a}{\sigma_{ys}^2} \qquad (2.26)$$

Where: R_p = plastic zone radius

σ = far field stress

σ_{ys} = material yield stress

a = crack half length

A comparison between the above equation and the plastic zone size generated with the finite element technique follows in the discussion of results.

III. Finite Element Models

This analysis modeled a 0.1 inch thick axial tension specimen subjected to a uniaxial load normal to the crack plane. With this approach, the effects of finite boundary conditions normally present in experimental work will be analytically modeled. Figure 3.1 depicts the configuration of the crack and defects in the axial tension specimen. Due to symmetry only one fourth of the specimen was modeled with the finite element mesh.

Generation

Two different size meshes were generated to evaluate the finite width effects on the crack/defect configuration. The first mesh (Fig. 3.2) is a symmetric mesh with a height and width of 0.5 inch. The second mesh (Fig. 3.3) has a height of 0.5 inch and an extended width of 1.232 inches. Four noded isoparametric elements were placed in a reduction pattern to transition smoothly into the small elements along the crack/defect region. The crack/defect region of both meshes consists of 0.002 inch square elements. This size was selected to correspond with the meshes generated by Mercer (8). Mercer proved this size of element in the crack tip region gave adequate stress/strain data, plasticity solutions, and stress intensity solutions for modeling crack growth with a similar magnitude of stress.

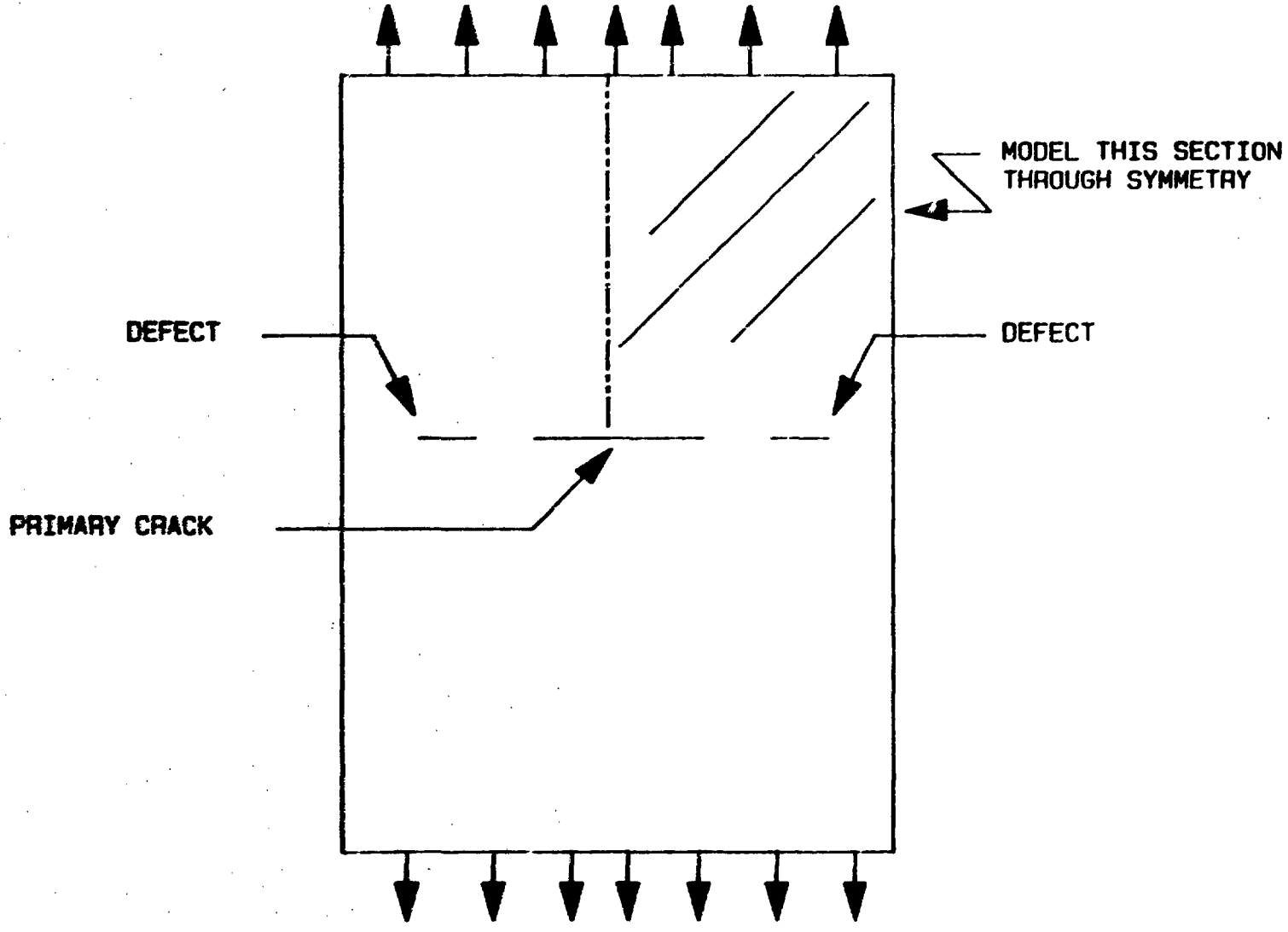

FIGURE 3.1 AXIAL TENSION SPECIMEN WITH CRACK AND DEFECTS

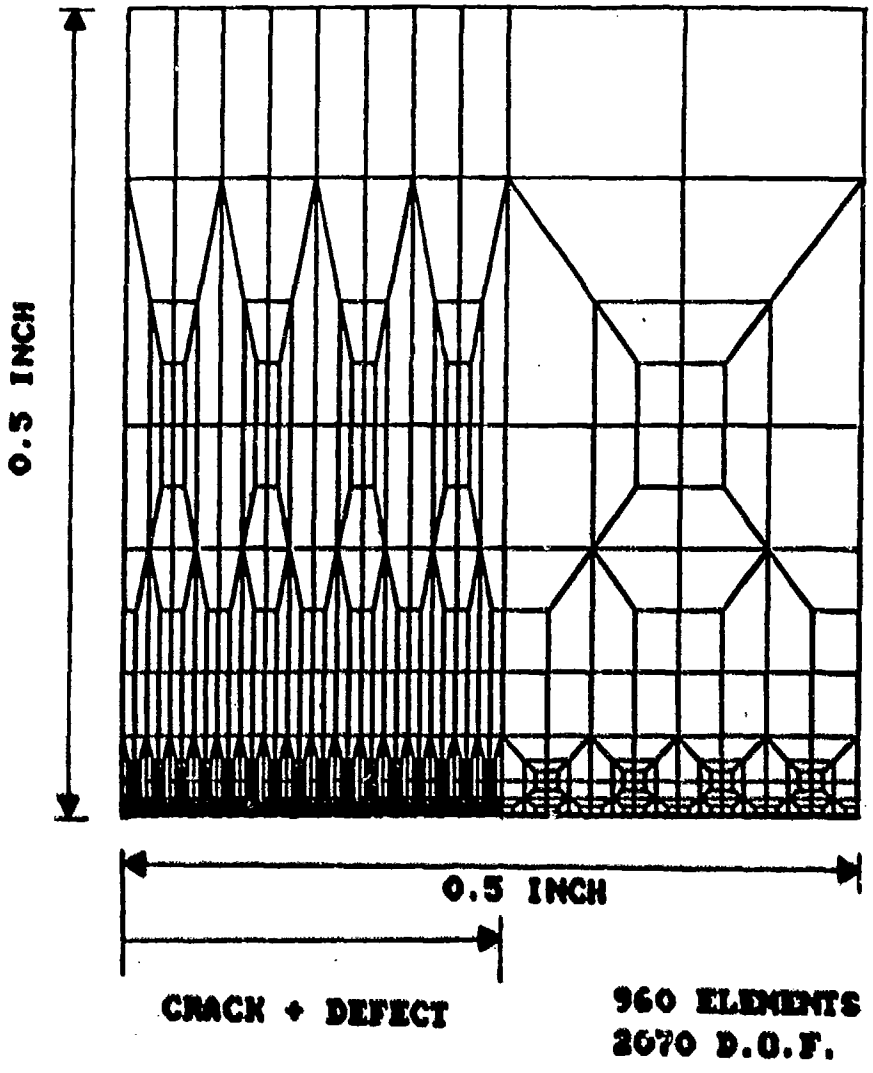

FIGURE 3.2 SYMMETRIC MODEL OF AXIAL TENSION SPECIMEN

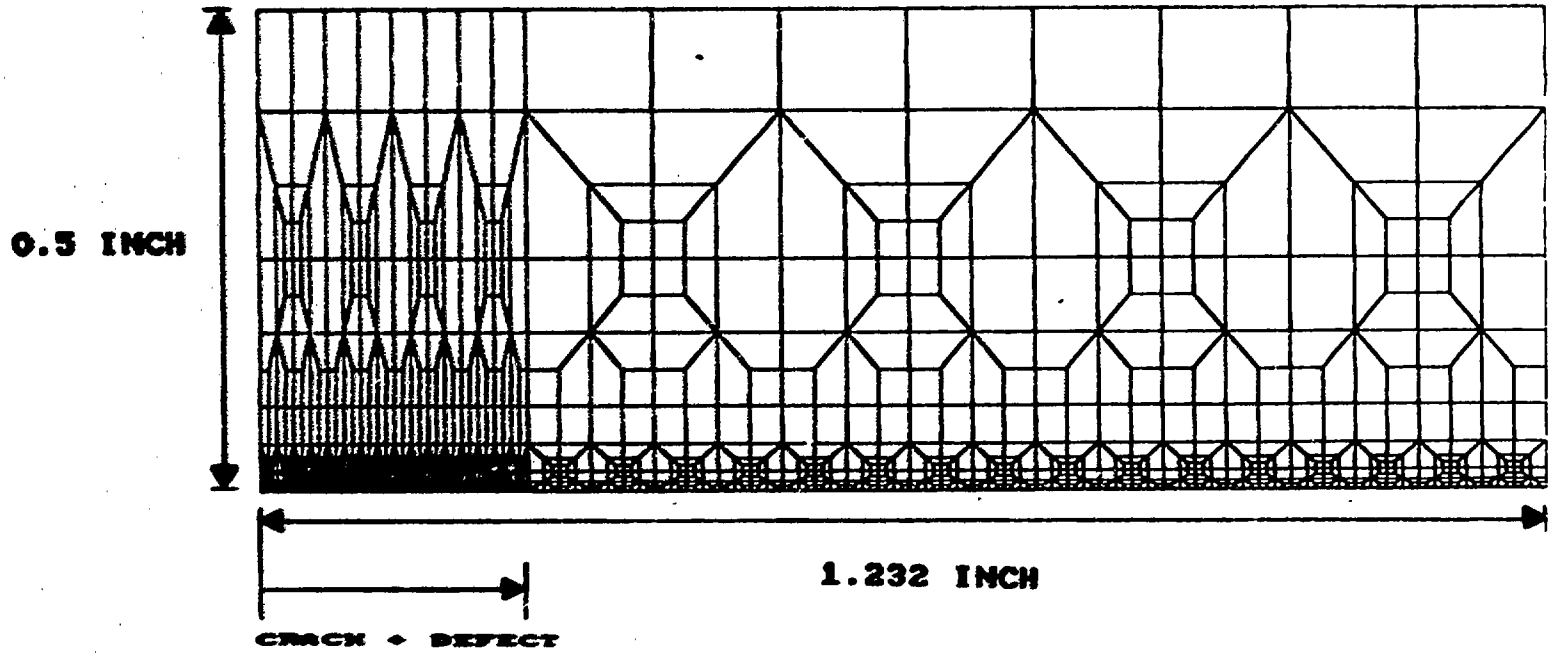

FIGURE 3.3 EXTENDED MODEL OF AXIAL TENSION SPECIMEN

The crack/defect region for this analysis was approximately five times larger than the work of Mercer (8) and Chestnut (9) and the number of elements required to generate the models increased on the same order of magnitude. This raised a concern that the computer processing time for nonlinear analysis would become prohibitive. To reduce this problem, the aspect ratio of the elements was increased to a range between two and four as the mesh diverged from the crack/defect region. Cook (26) states that aspect ratios up to two will yield good stress results and aspect ratios as high as seven will yield good displacement results.

The program PDA-PATRAN was used to develop the finite element meshes needed for this analysis. Due to the size of the meshes (2070 and 3228 D.O.F. respectively) it was beneficial to band the resulting stiffness matrix to conserve memory and processing time. A matrix is "banded" if all nonzero coefficients cluster about the diagonal. Cook (26) provides detailed information about optimization techniques. A program called SWAP (Appendix B) was used to convert the neutral files generated by PDA-PATRAN to NASTRAN input decks to accomplish the bandwidth optimization. Optimization reduced the bandwidth from 288 to 75. The SWAP program was then used to convert the optimized neutral file to a SNAP input deck.

Validation

To validate the mesh configuration four examples of a center cracked plate were performed on the symmetric mesh. The far field stress was 12 ksi normal to the crack plane. Both the J-integral and stress extrapolation technique were used to determine the stress intensity for each crack size. Figure 3.4 shows an example of the stress extrapolation technique using equation 2.24. The averaged stress intensity value for the crack tip is extrapolated to r = 0 based on the method described by Broek (24). Equation 2.14 with the corresponding finite width correction given by Isida (25) for the particular crack size was used to calculate the theoretical value of the stress intensity. The results were accurate to within 2 percent or less. Tables 3.1 and 3.2 provide a summary of the crack sizes and results.

Table 3.1: Center Cracked Plate Stress Intensity

Crack a	K_1 Theory	K_1 Stress	Percent Error
0.100 in	7.10	6.96	1.80
0.144 in	9.03	8.89	1.50
0.176 in	10.30	10.30	1.20
0.200 in	11.57	11.68	1.00

Table 3.2: Center Cracked Plate Stress Intensity

Crack a	K_1 Theory	K_1 J-Int.	Percent Error
0.100 in	7.10	7.04	0.70
0.144 in	9.03	8.93	1.00
0.176 in	10.30	10.36	0.60
0.200 in	11.57	11.46	0.80

Figure 3.5 depicts the path location used for the J-integral. Three different length paths were used with negligible differences (less than 0.1 percent) being recorded for paths ranging from 30 to 94 elements. The elements in the paths have an aspect ratio of one and a size of 0.002 in. This analysis and the work of Mercer (8) confirm the independence of the J-integral routine to element size. However, it was found that the algorithm contained in the SNAP code requires the element aspect ratio be less than two. As long as the path selected followed this criterion, the J-integral results were independent of path length. For aspect ratios between two and four, up to seven percent error below the theoretical values was noted in the calculations for the stress intensity. The writer believes this error is accumulated in the weight function technique used for the contour path. This technique extrapolates the stress values at the element gaussian points (containing the contour path) to points along the

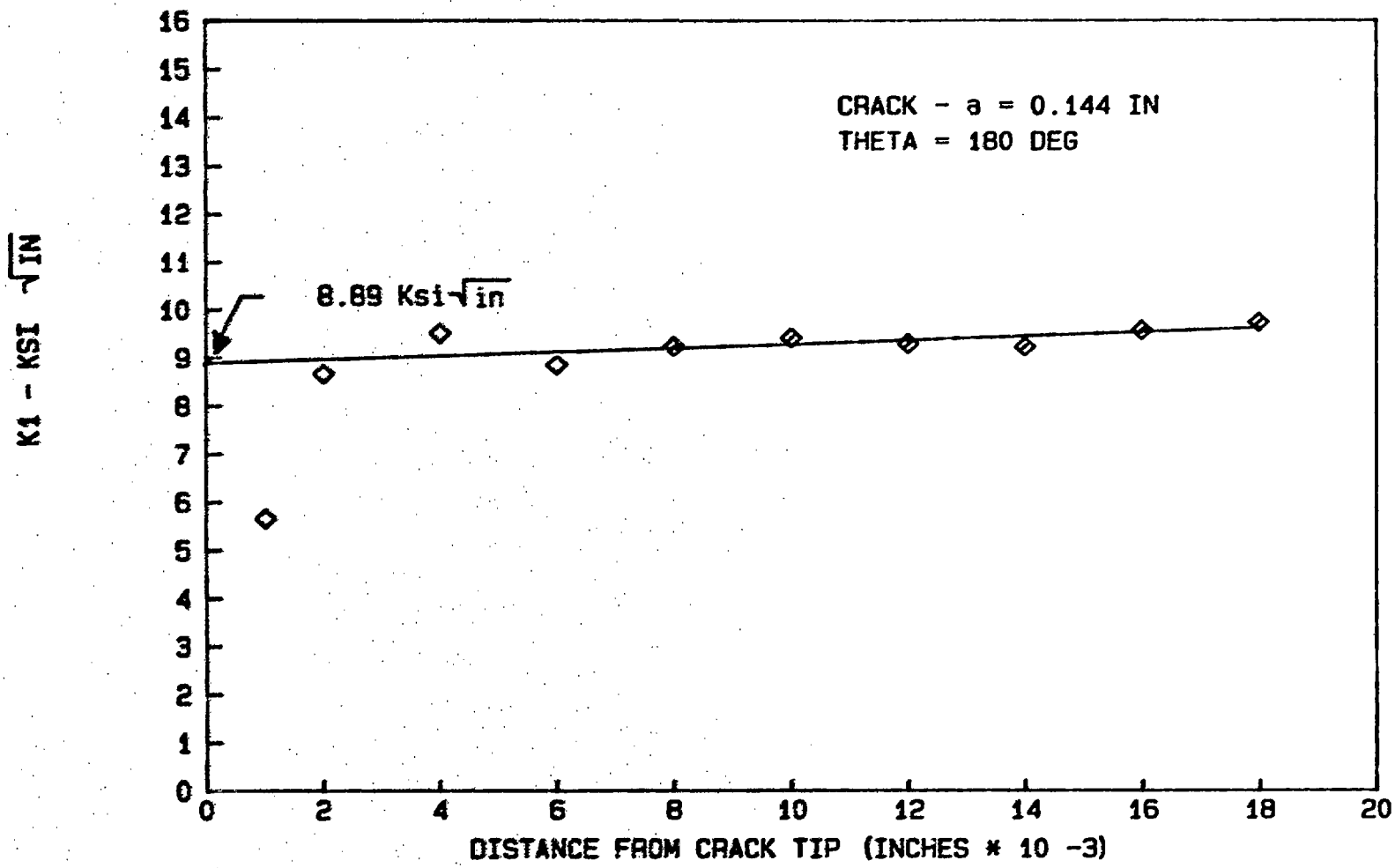

FIGURE 3.4 STRESS EXTRAPOLATION OF STRESS INTENSITY FACTOR

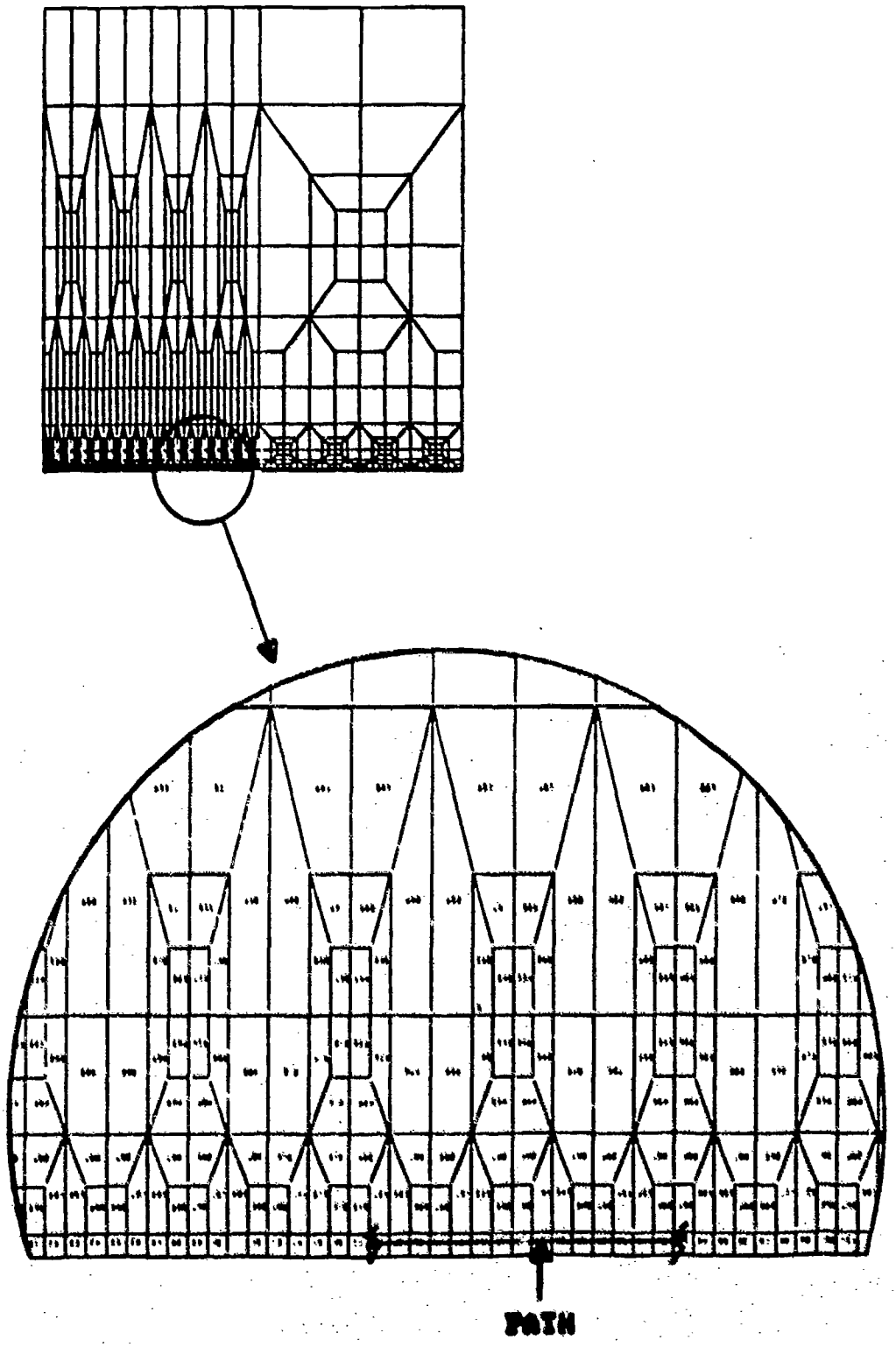

FIGURE 3.5 J - INTEGRAL PATH

path itself. Those elements with aspect ratios greater than two slightly underestimate the true stress field as noted by Cook (28). The small error in each element is then accumulated along the contour path resulting in a total error of seven percent.

IV. Results and Discussion

The problem of a crack interacting with collinear defects was analyzed with linear elastic, elastic-plastic, and viscoplastic constitutive equations. The results of each constitutive model are presented below.

Linear Elastic Analysis

The purpose of the linear analysis was to compare the the finite element solutions of crack/defect interaction to existing infinite plate theory. The results given below show that finite element analysis provided comparable solutions.

The first objective was to determine the influence range of a defect on the crack stress intensity factor. Three different length defects were studied with the symmetric mesh. As pointed out in section II, a defect is defined as a through-the-thickness crack that is approximately one-fifth or less the length of the primary crack. The J-integral method was used to measure the stress intensity of a crack subjected to a far field load of 18 kips (36 ksi) normal to the crack plane. Rubenstein (20) used the method of complex stress potentials to analyze the defect influence range. He determined the defect influenced the stress intensity of the primary crack at a distance equal to two times the defect length (2a). Based on his efforts, the

initial crack/defect spacing was set to two times the defect length for this study. At this distance, the addition of a defect provided a one percent or less increase in the stress intensity for a center cracked axial tension specimen. The crack tip was then moved toward the defect in 0.002 inch increments until a three percent increase was present in the stress intensity over the center crack solution. As shown in table 4.1, a distance equal to 1.1 defect lengths was required. Once inside this range, a sharp increase in the stress intensity gradient begins to occur which is also reflected in the analytical solutions in Figure 4.1.

Table 4.1: Defect Influence on Stress Intensity Solution

Crack a (in)	Defect a (in)	Spacing (in)	CCP ksi√in	CCP w/Defect ksi√in	Percent Increase
0.214	0.010	0.022	36.47	37.47	2.77
0.194	0.015	0.032	33.18	34.32	3.44
0.172	0.020	0.044	30.57	31.73	3.79

* Far Field Stress = 36 ksi

An analytical comparison was then conducted to determine if the defect influence range on the crack stress intensity was independent of crack length. Figure 4.1 shows a comparison between the center cracked plate solution (eq. 2.14) and the macrocrack-multiple defect solution (eq. 2.17) for crack sizes ranging from 0.132 - 2.016 inches. The

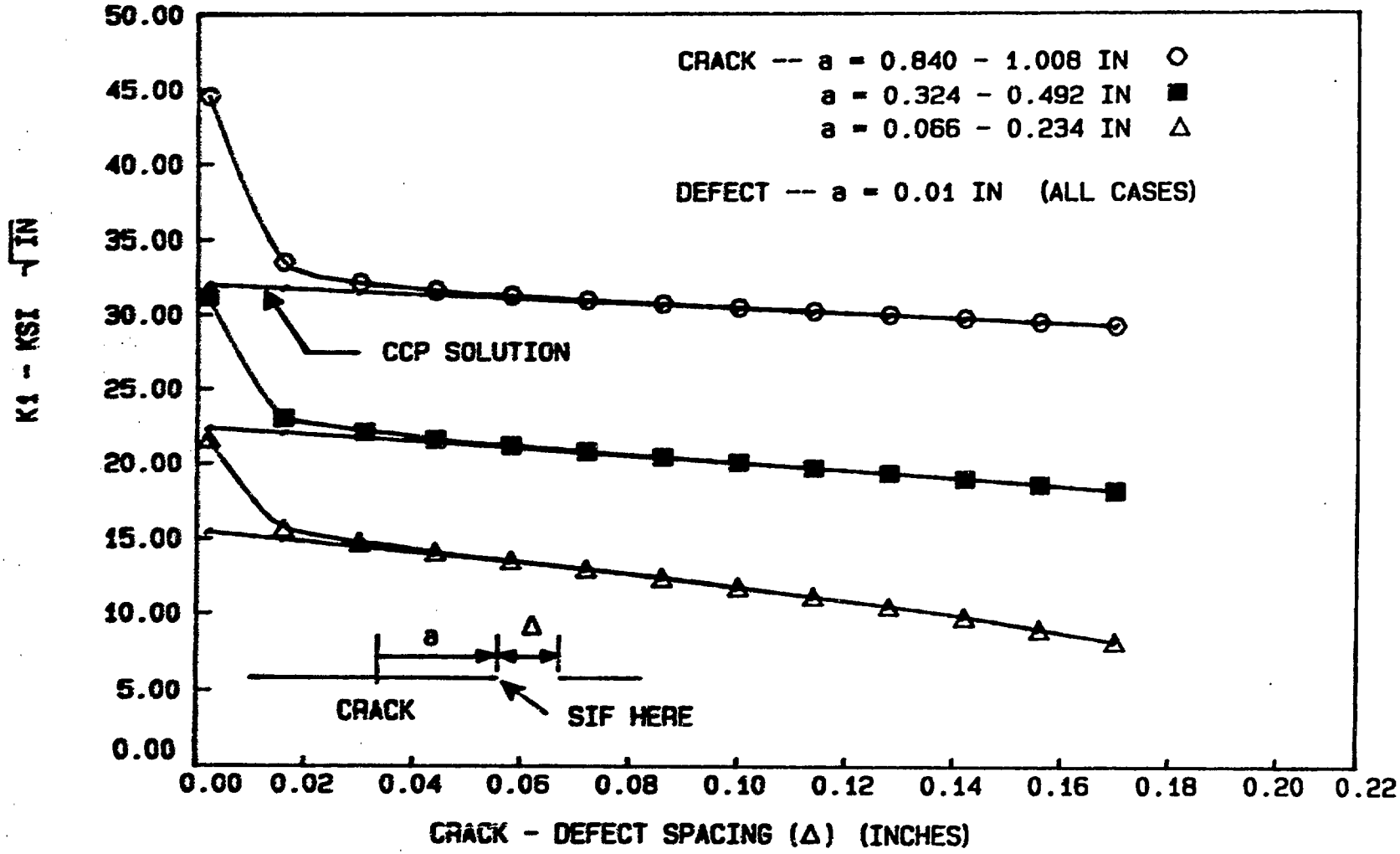

FIGURE 4.1 CRACK STRESS INTENSITY VERSUS CRACK SIZE COMPARISON

results indicate that crack length doesn't have a measurable effect on the defect influence range. Furthermore, the analytical solution confirmed a prominent defect influence range of approximately one defect length.

The second objective in the linear analysis was to analyze finite boundary influences on the crack and defect stress intensity solutions and compare the finite element results to the macrocrack-multiple defect solutions given by equations 2.15 - 2.17.

Figures 4.2 - 4.4 show a comparison of the crack stress intensity versus the defect spacing for the same three defects used in the first objective. A far field load of 6 kips (12 ksi) was applied to the specimen. The 6 kip load ensured the size of the plastic zone in front of the crack tip would be insignificant for the linear analysis. The stress intensity results via finite element analysis compare well with the plots given by infinite theory. Furthermore, a small four to five percent decrease in the stress intensity range was noted for the extended width mesh (figure 3.3) which is 1.5 times wider than the symmetric mesh (figure 3.2). The small drop in the stress intensity indicates that the a defect will essentially shield the crack tip from the finite width of the plate. The majority of the increase in the crack stress intensity over infinite theory appears to be due to the finite height of each mesh. The finite height in each case is constraining the area over

which the stress field can act thereby forcing a direct stress increase in the local region.

An individual comparison of Figures 4.2 - 4.4 shows that as the defect increases in size, so too will the influence range of the defect and the magnitudes of the stress intensity solutions for a given crack/defect spacing. For this analysis, doubling the defect size resulted in a ten percent increase in the stress intensity at a crack/defect spacing of 2 mils.

Figures 4.2 - 4.4 also show that the crack stress intensity will exceed the stress intensity of the combined length (crack + defect) when the defect is in close proximity to the crack. This occurs since two stress singularities (i.e. crack and defect tips) in close proximity will generate a larger stress concentration at the primary crack.

Figures 4.5 and 4.6 provide a direct analysis of the spacing where the crack stress intensity will exceed the the stress intensity of the combined length (crack + defect) for the symmetric and extended width mesh respectively. This spacing is termed a "critical spacing" by Tamako and Imai (15). If the crack tip is inside the critical spacing and the far field stress is increased such that the crack stress intensity equals the toughness of the material (i.e. stress intensity for catastrophic crack growth), the crack will propagate into the defect. When the crack combines with the

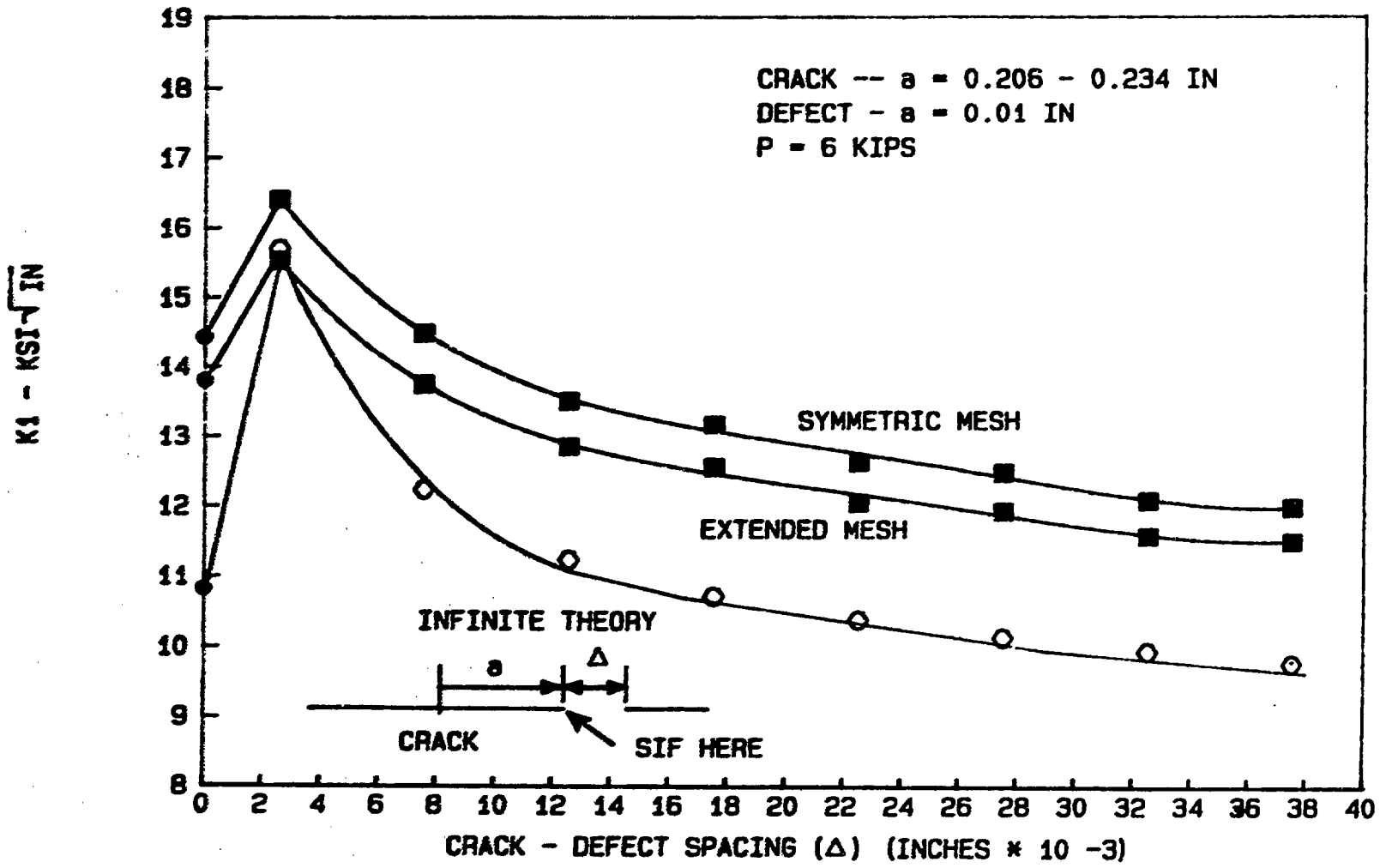

FIGURE 4.2 CRACK STRESS INTENSITY VERSUS DEFECT SPACING

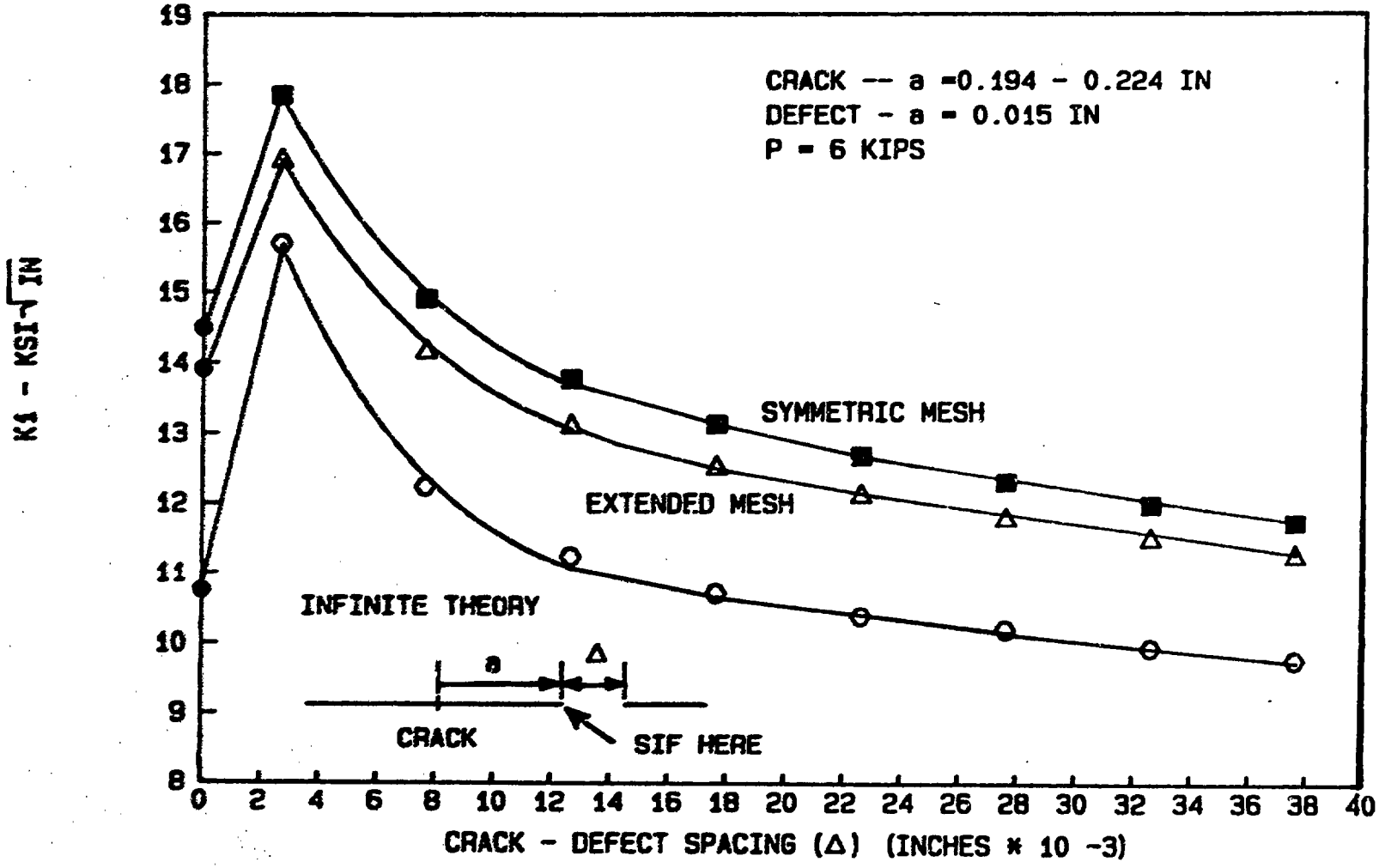

FIGURE 4.3 CRACK STRESS INTENSITY VERSUS DEFECT SPACING

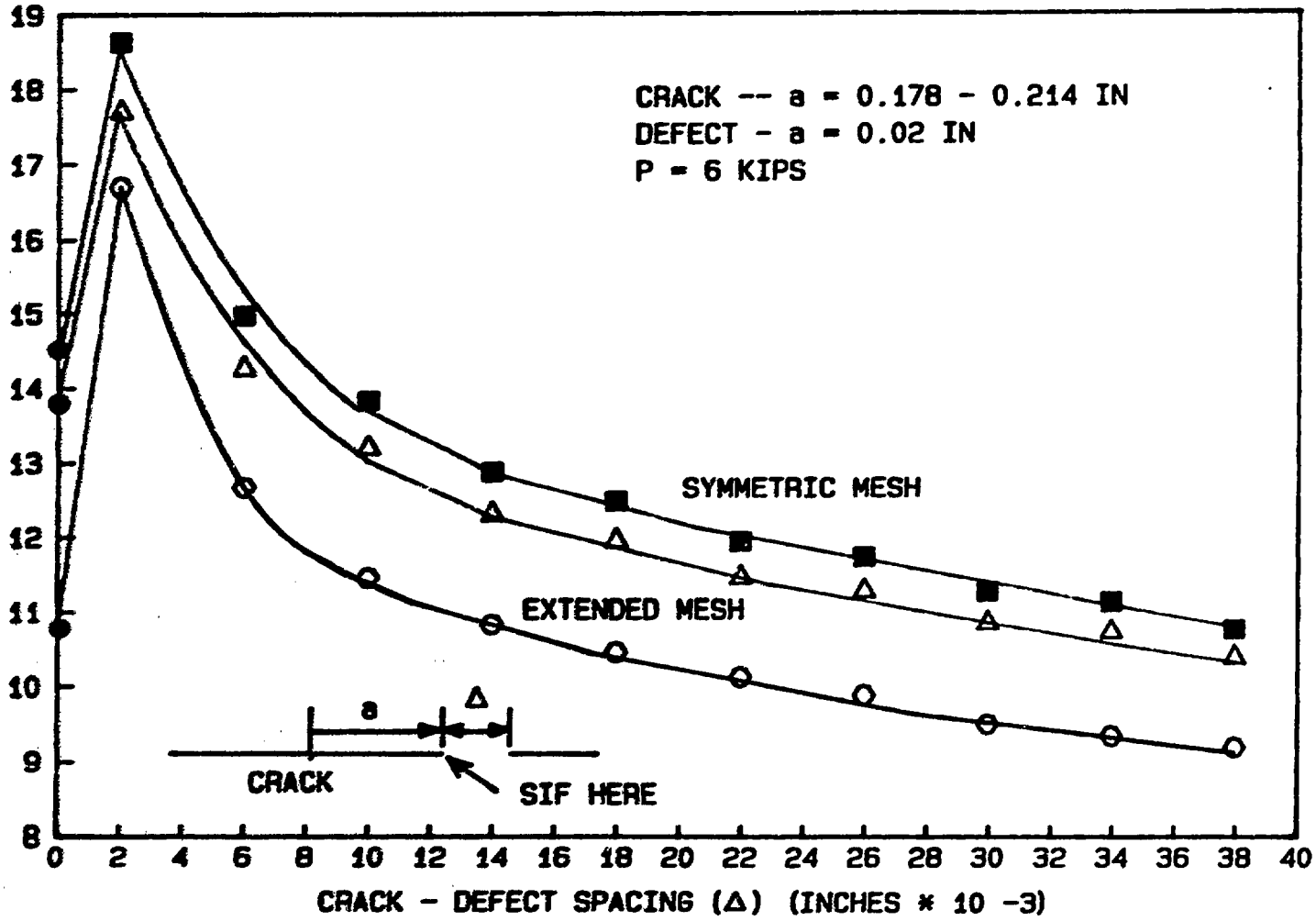

FIGURE 4.4 CRACK STRESS INTENSITY VERSUS DEFECT SPACING

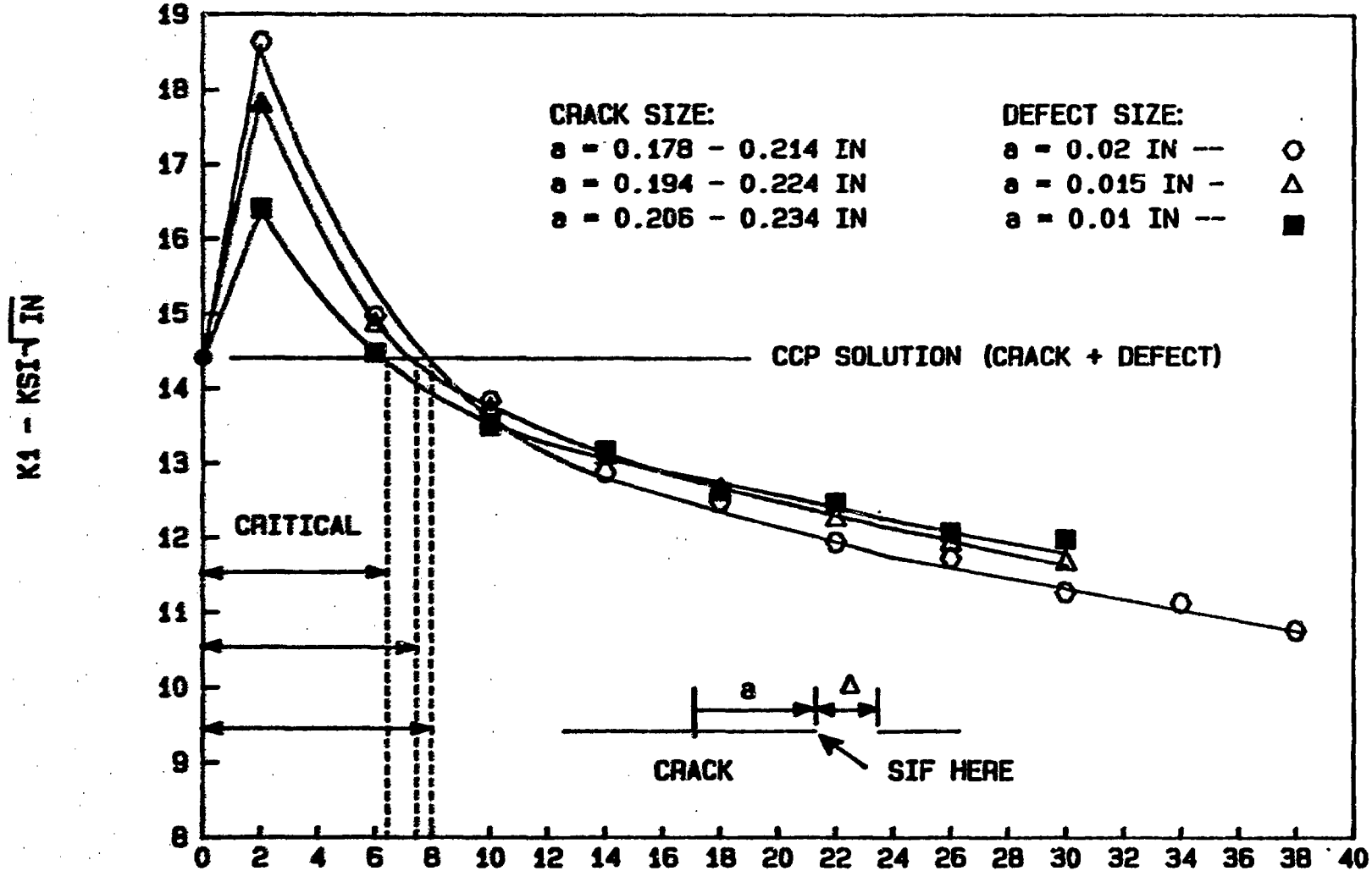

FIGURE 4.5 CRITICAL SPACING FOR SYMMETRIC MESH, P = 6 KIPS

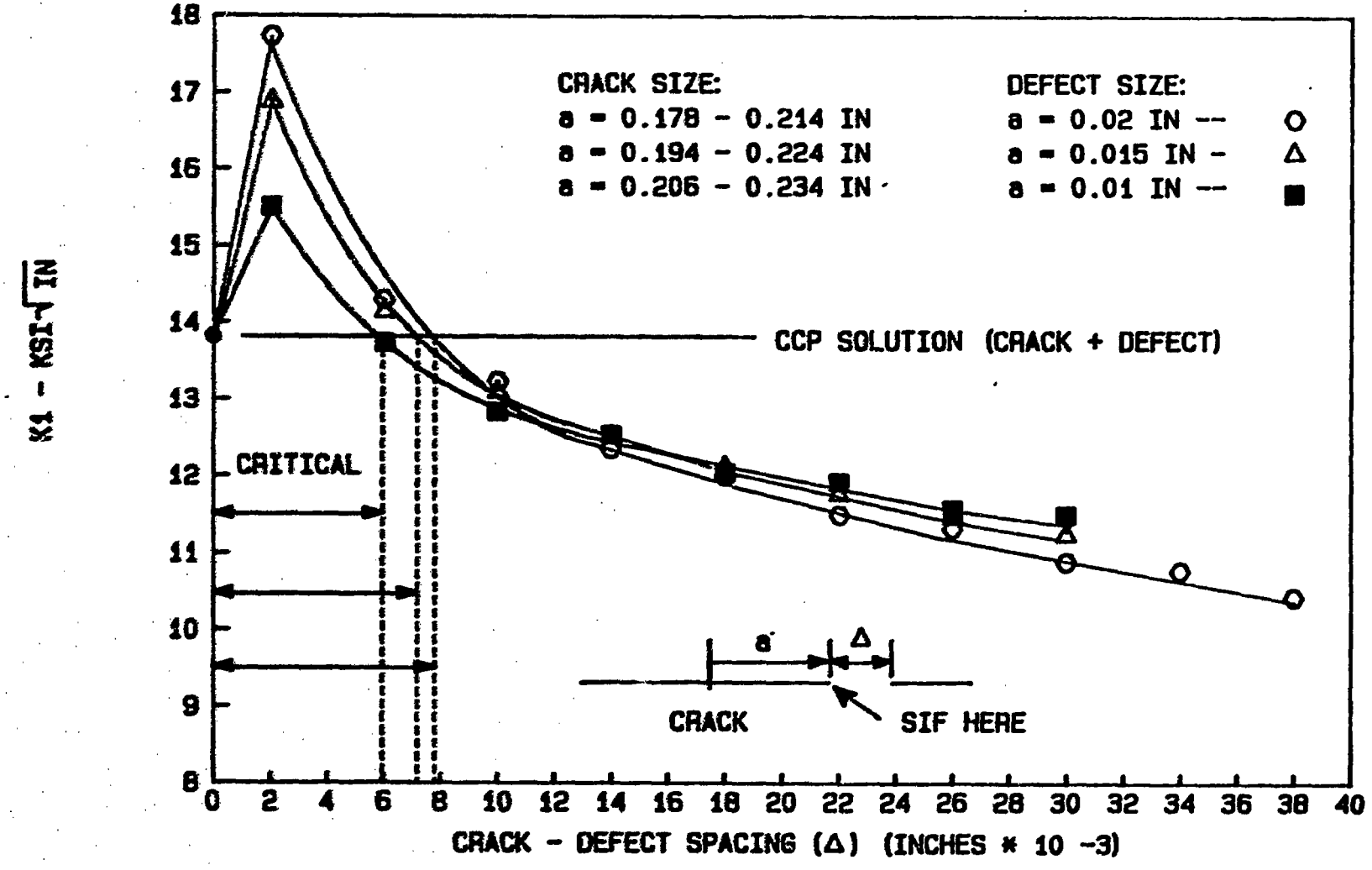

FIGURE 4.6 CRITICAL SPACING FOR EXTENDED MESH, P = 6 KIPS

defect, the stress intensity will drop below the toughness value to the the combined crack and defect stress intensity. An increase in load will then be required to increase the new main crack stress intensity to the toughness value for propagation to continue. This phenomenon is referred to by Tamake and Imai (15) as pop-in behavior.

The critical spacing for the defects used in this analysis ranged between 6 to 8 mils which is approximately 40 to 60 percent of the respective defect lengths. Doubling the defect size resulted in a 33 percent increase in the critical spacing for both the symmetric and extended width meshes. Here we note that defect size definitely increases the critical spacing, but due to the limited data no exact correlations between defect size and critical spacing can be made. A five percent drop in the critical spacing was also evident between the symmetric and extended width mesh indicating finite width has a small influence on the critical spacing. The small influence of the width is again due to the defect shielding the primary crack.

Figures 4.7 - 4.9 show a comparison of the stress intensity of the outside tip of the defect to infinite theory. Again, comparative trends to infinite theory were obtained. For this case, the stress intensities calculated with the extended width mesh converged very close to infinite theory. This result follows the intuitive prediction that the outer tip of the defect will be

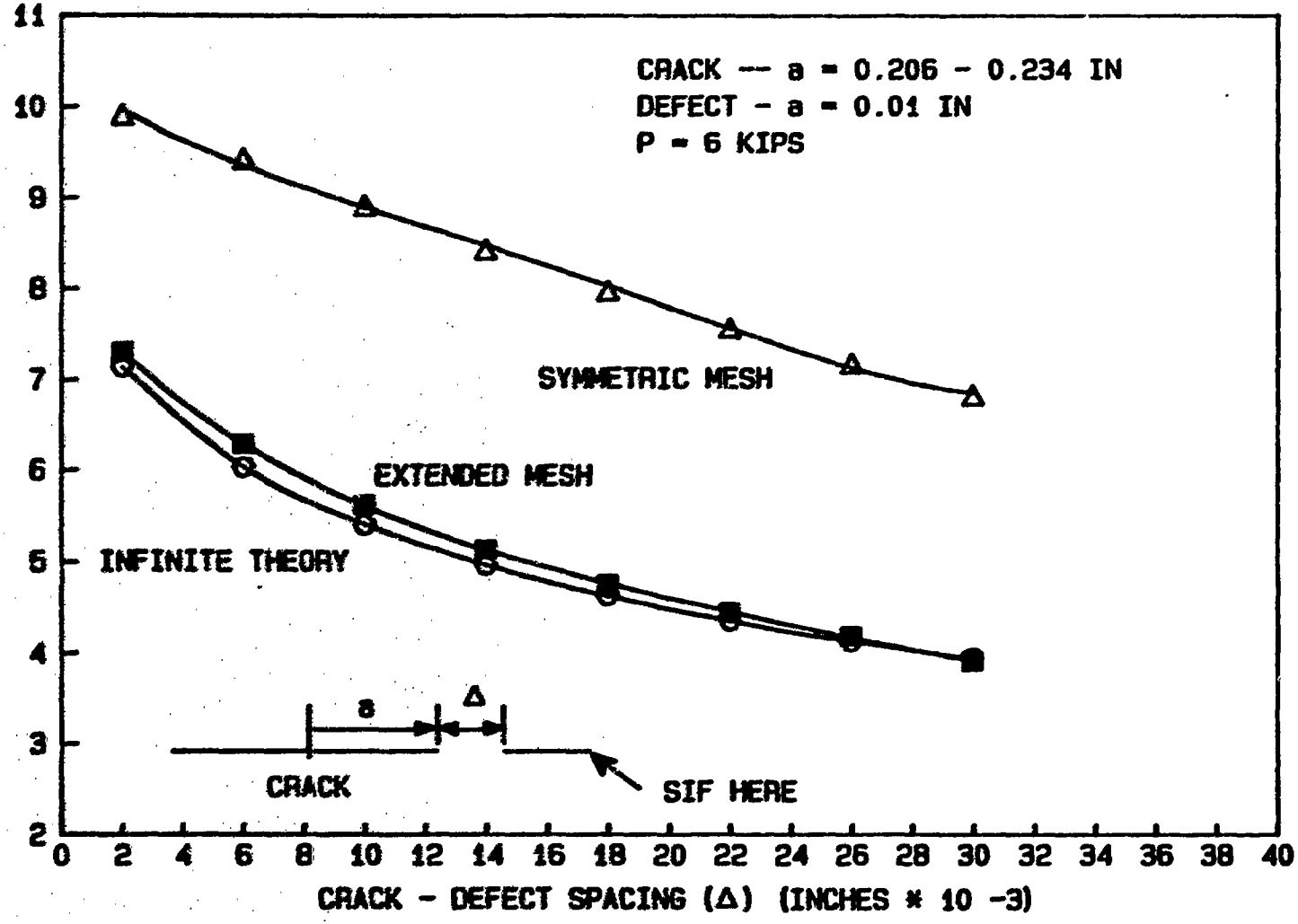

FIGURE 4.7 DEFECT STRESS INTENSITY VERSUS DEFECT SPACING

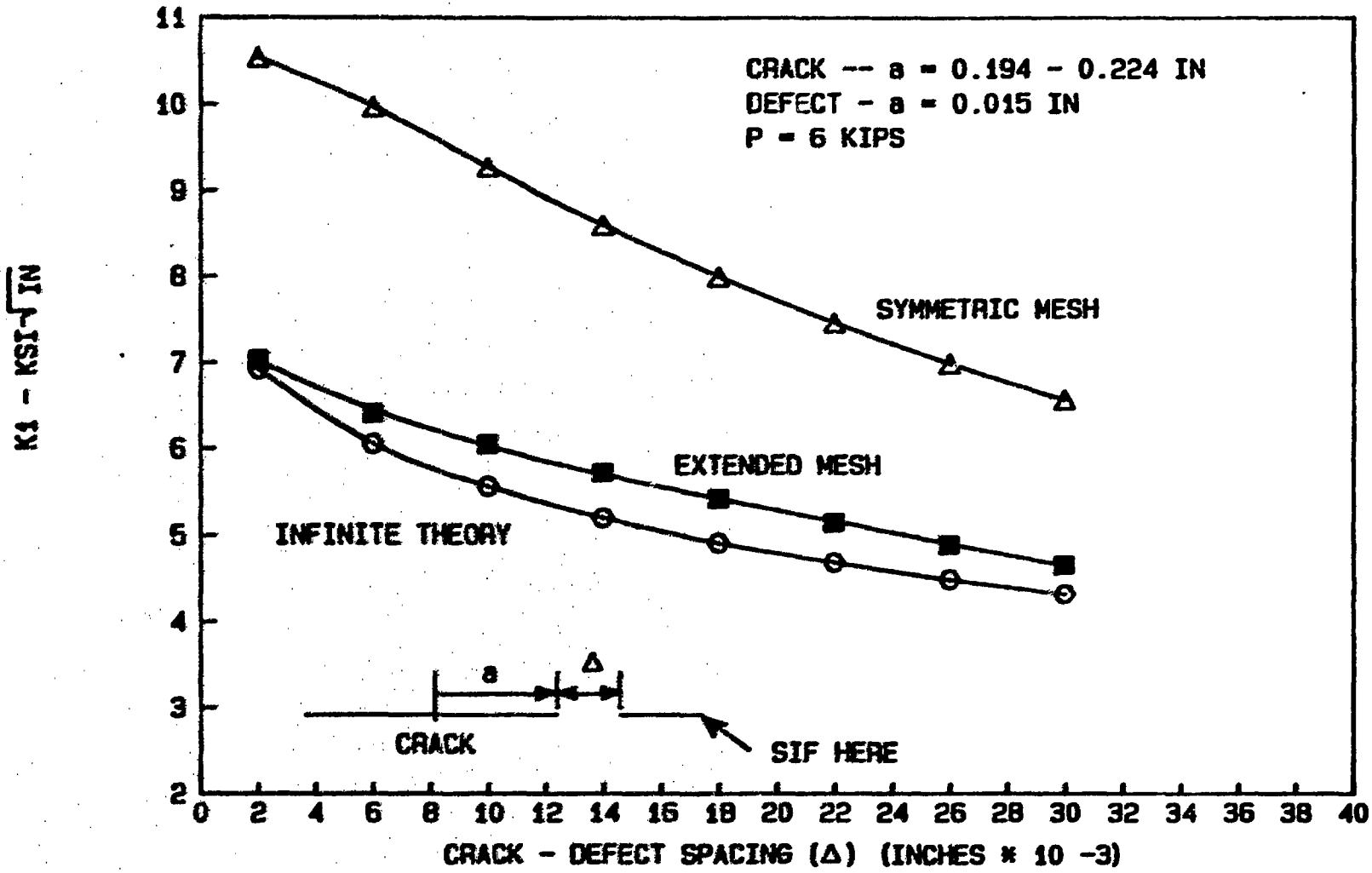

FIGURE 4.8 DEFECT STRESS INTENSITY VERSUS DEFECT SPACING

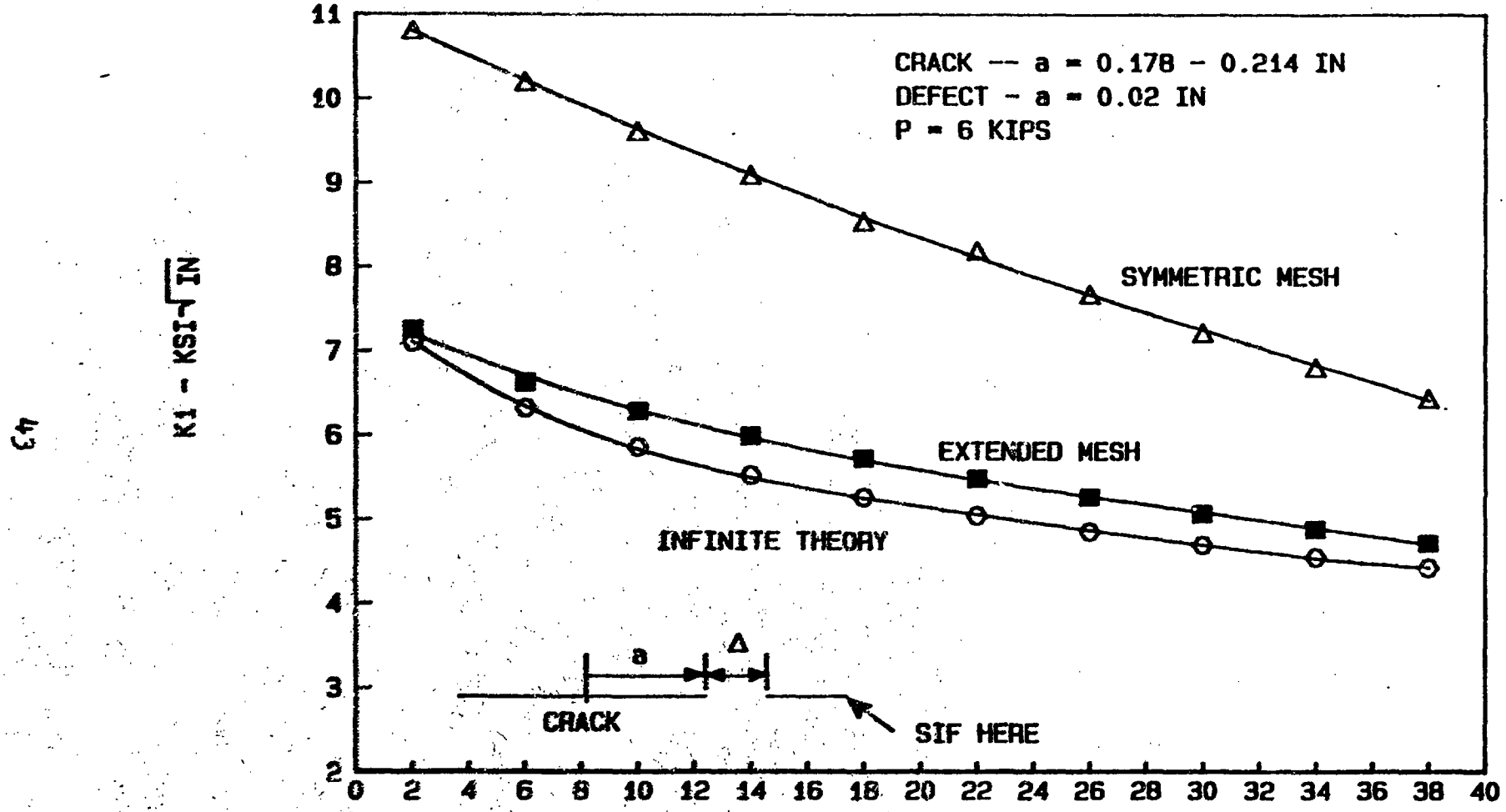

FIGURE 4.9 DEFECT STRESS INTENSITY VERSUS DEFECT SPACING

primarily influenced by the width rather than the height of the specimen.

The linear analysis conducted so far in this study validated the program and finite element meshes against available theory.

Elastic-Plastic Analysis

The elastic-plastic analysis used small displacement formulation for calculating strain displacement relationships. The range of the problem considered was established by the nonlinear validation efforts performed by Mercer (8) with the SNAP code. He determined that small displacement theory was valid for an elastic stress intensity of 35 - 45 ksi$\sqrt{in}$ for a center cracked plate with a material yield stress of 140 ksi. Based on his efforts, this study selected 35 ksi$\sqrt{in}$ as the elastic stress intensity to be used for initial crack lengths. This value allowed an investigation of crack growth within a plastic regime as well as imply a strain small enough so that small displacement theory could be imposed.

To limit the amount of computer time, two primary cracks of initial half length (a) = 0.100 inch and (a) = 0.200 inch; and one defect of half length (a) = 0.01 inch were selected. In addition, the crack/defect spacing was set so that the plastic zones ahead of the crack and defect overlapped. The proper load (25 and 18 Kips) was then

applied to the specimen to generate a stress intensity of 35 ksi$\sqrt{in}$ for each crack length. At full load, the element in front of the crack tip had a stress of 160 ksi and six percent strain.

This portion of the analysis used the elastic-plastic relations of Eqs. 2.4 - 2.6. The crack could not be grown in this part of the analysis since attempts to grow the crack toward the defect resulted in negative values along the diagonal of the stiffness matrix during equation solution. This was occurring since the stress/strain curve is essentially flat at six percent strains. As a result, the elastic-plastic analysis consisted of individual cases of crack size and defect spacing.

Figures 4.10 and 4.11 show the shape of the plastic zone developed for a fixed defect position and increasing crack lengths. In Figure 4.10 the primary crack is approximately half the size of the primary crack in Figure 4.11 but is subjected to a higher load to develop the same stress intensity. We note that the plastic zones for the two figures are approximately equal indicating that similitude with the crack stress intensity gave similitude in the size of plastic zone. As the free surface of the crack was placed closer to the defect, the size of the plastic zone decreased. An analogy to this effect is to consider the strain energy present in the crack/defect spacing as water flowing through the area between the crack and defect. As

the area becomes smaller, the amount of water flowing or in this case the magnitude strain energy present in the crack/defect region is restricted.

Equation 2.26 is compared on the first plots of Figures 4.10 - 4.11. This calculation confirms the crack and defect must be in the given ranges in order for the plastic zones of the crack and defect to overlap.

Figures 4.12 and 4.13 show the corresponding crack opening profiles. It is seen that the elastic-plastic analysis generates a blunting of the crack tip which was essentially constant for all cases. Based on the pattern that developed with the given profiles, it appears that one can estimate what size crack will not have blunting characteristics by extrapolating a line to the crack plane as shown in Figure 4.12.

Figure 4.14 shows a direct comparison between an elastic and an elastic-plastic crack opening profile. This comparison highlights the blunting characteristic in the elastic-plastic crack opening. Furthermore, plasticity effects decreased the strain energy present at the crack tip as measured by the J-integral technique. As shown in Figure 4.14 this decrease yielded a 55 percent drop in the crack stress intensity factor for the given geometry and load condition.

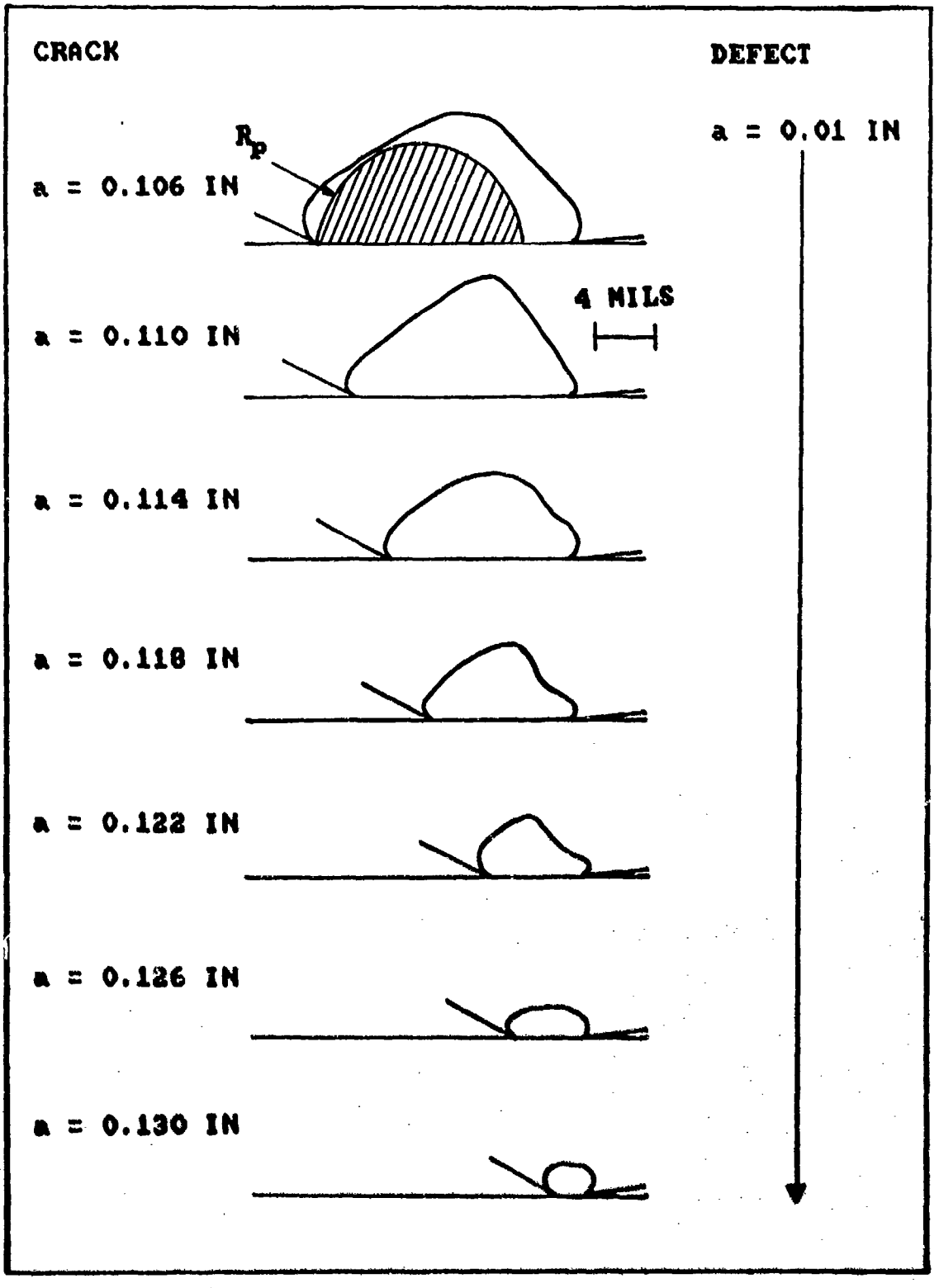

FIGURE 4.10 ELASTIC/PLASTIC ZONE SHAPES

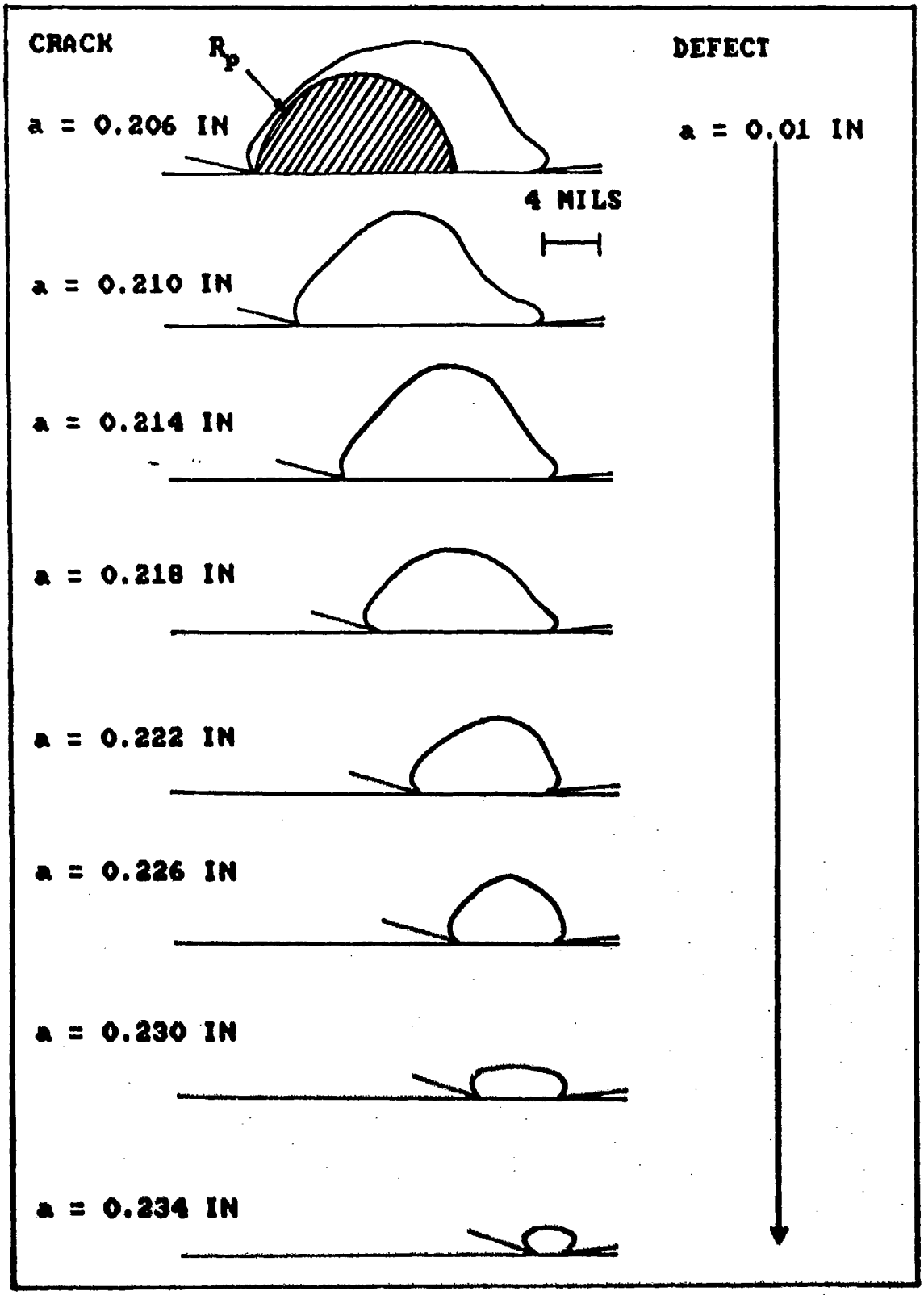

FIGURE 4.11 ELASTIC/PLASTIC ZONE SHAPES

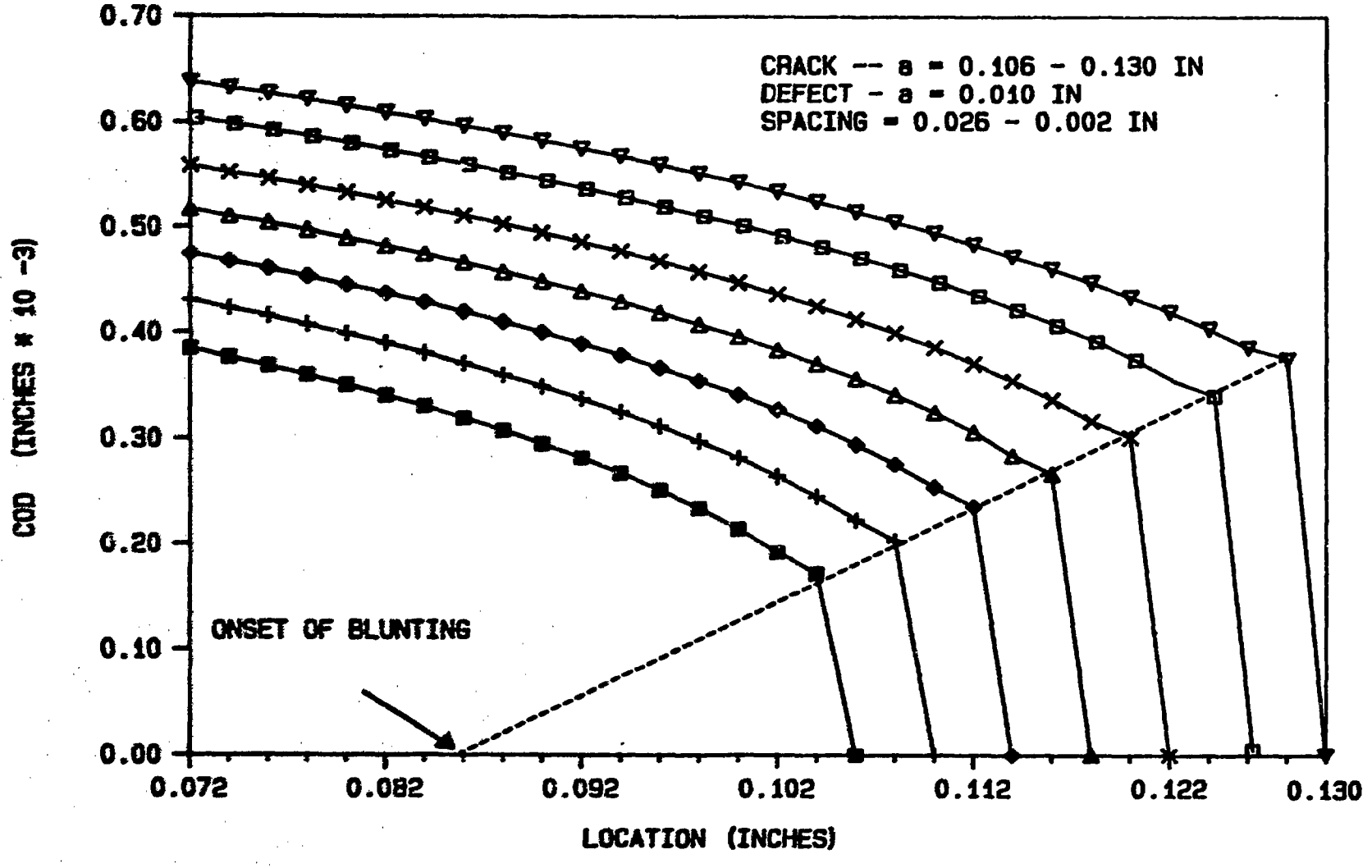

FIGURE 4.12 ELASTIC/PLASTIC CRACK OPENING PROFILES, P = 25 KIPS

FIGURE 4.13 ELASTIC/PLASTIC CRACK OPENING PROFILES, P = 18 KIPS, 100% LOAD

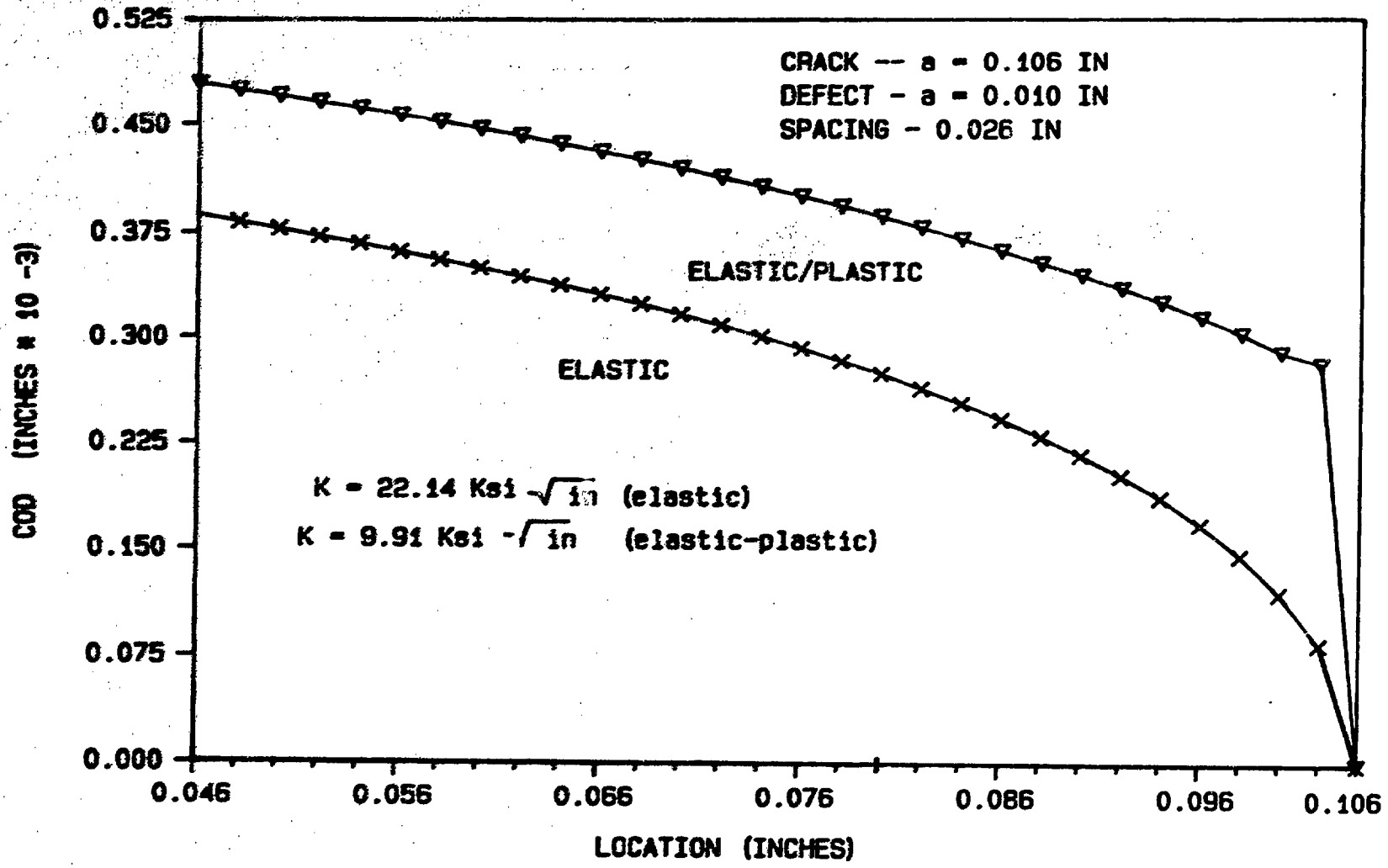

FIGURE 4.14 CRACK OPENING COMPARISON, P = 25 KIPS, 100% LOAD

Figure 4.15 illustrates the influence of the defect on the crack opening profile. A 16 percent increase in opening was evident along the entire crack profile for a crack/defect spacing of 0.026 inch.

The strain profiles between the crack and defect are shown in Figures 4.16 and 4.17. For both primary cracks, there is an increasing strain profile as the crack/defect spacing is decreased. In each figure, we note the strain curves are concave up which is a direct result of increasing strains at the crack and defect tips.

In looking at the magnitude of the strains present for the various crack/defect spacings, it becomes questionable as to how much strain can exist in the plastic zone of the material before instantaneous failure at load would occur. Since no experimental data is available for this work, one must attempt a comparison to existing finite element work by others. One assumption is to consider failure would occur when strains along the crack plane approach six to eight percent. This was the strain level Mercer (8) required to match experimental crack growth to his model of a compact tension specimen. This is a rather global assumption since we are making a comparison between an axial tension specimen and a compact tension specimen. The only similitude between this work and Mercer's is the size of the elements along the crack plane, the material thickness, and the material itself (IN-718). We note the size of the elements used in a finite

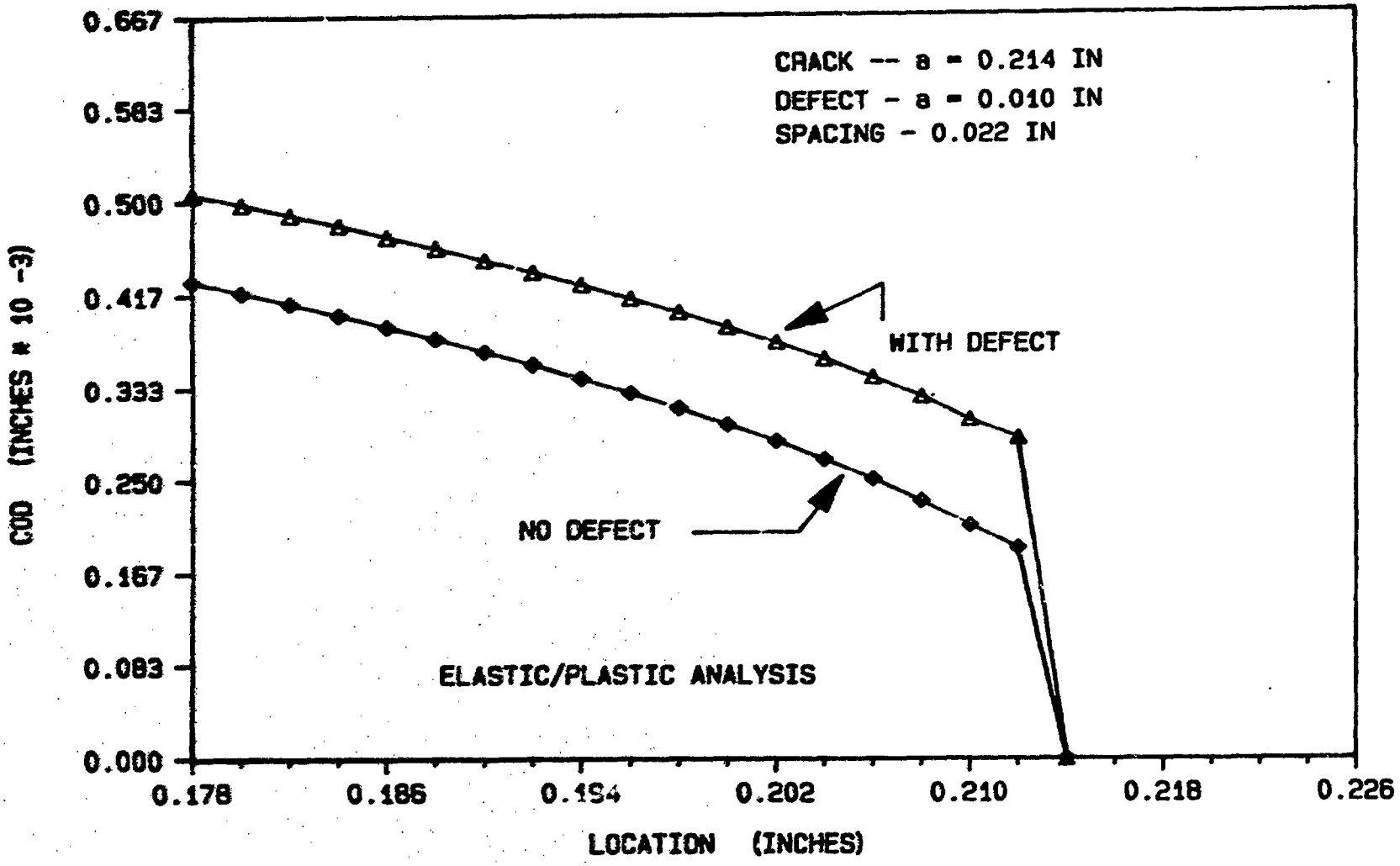

FIGURE 4.15 CRACK OPENING COMPARISON, P = 18 KIPS, 100% LOAD

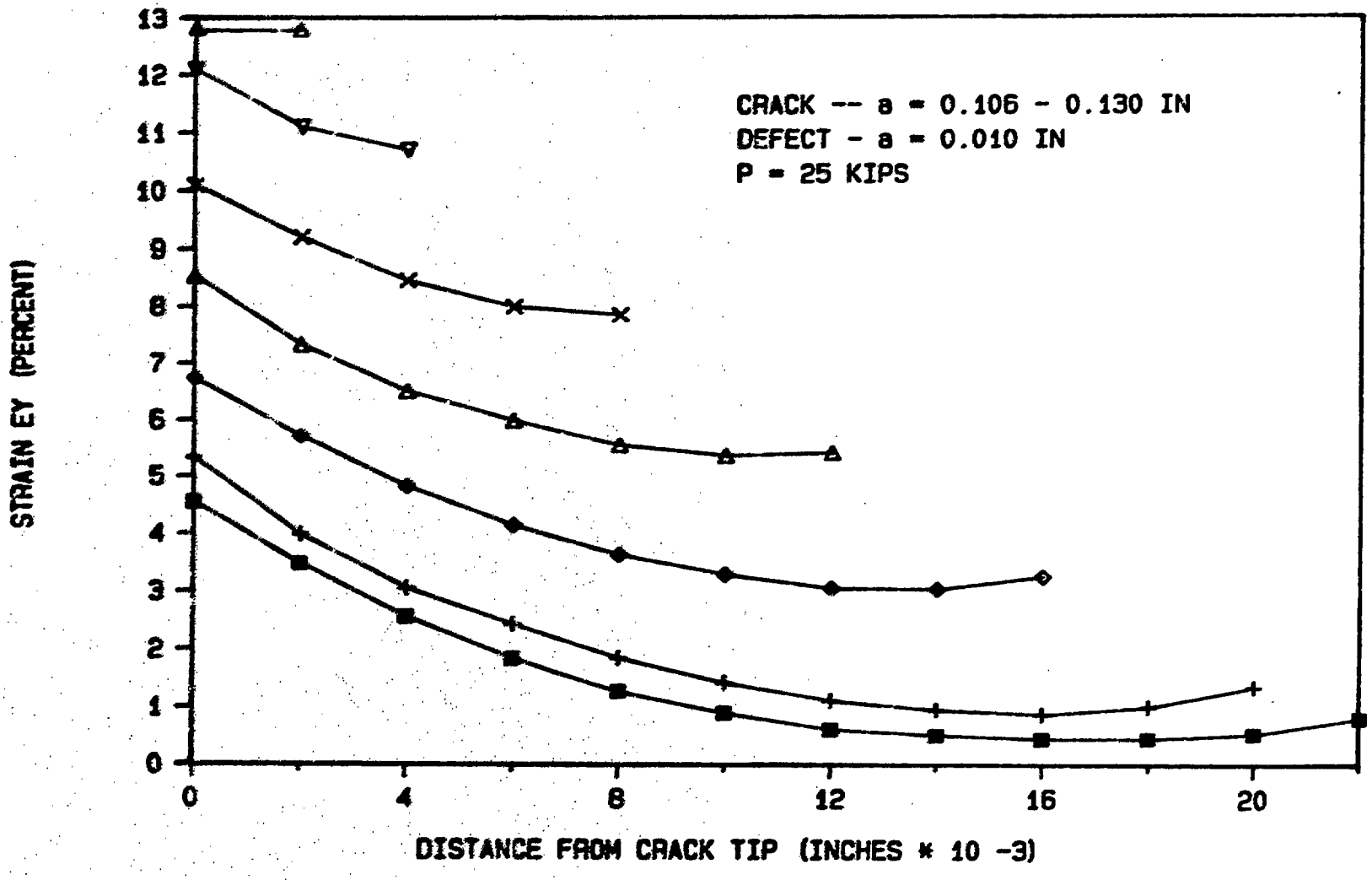

FIGURE 4.16 ELASTIC/PLASTIC STRAIN PROFILE BETWEEN CRACK AND DEFECT

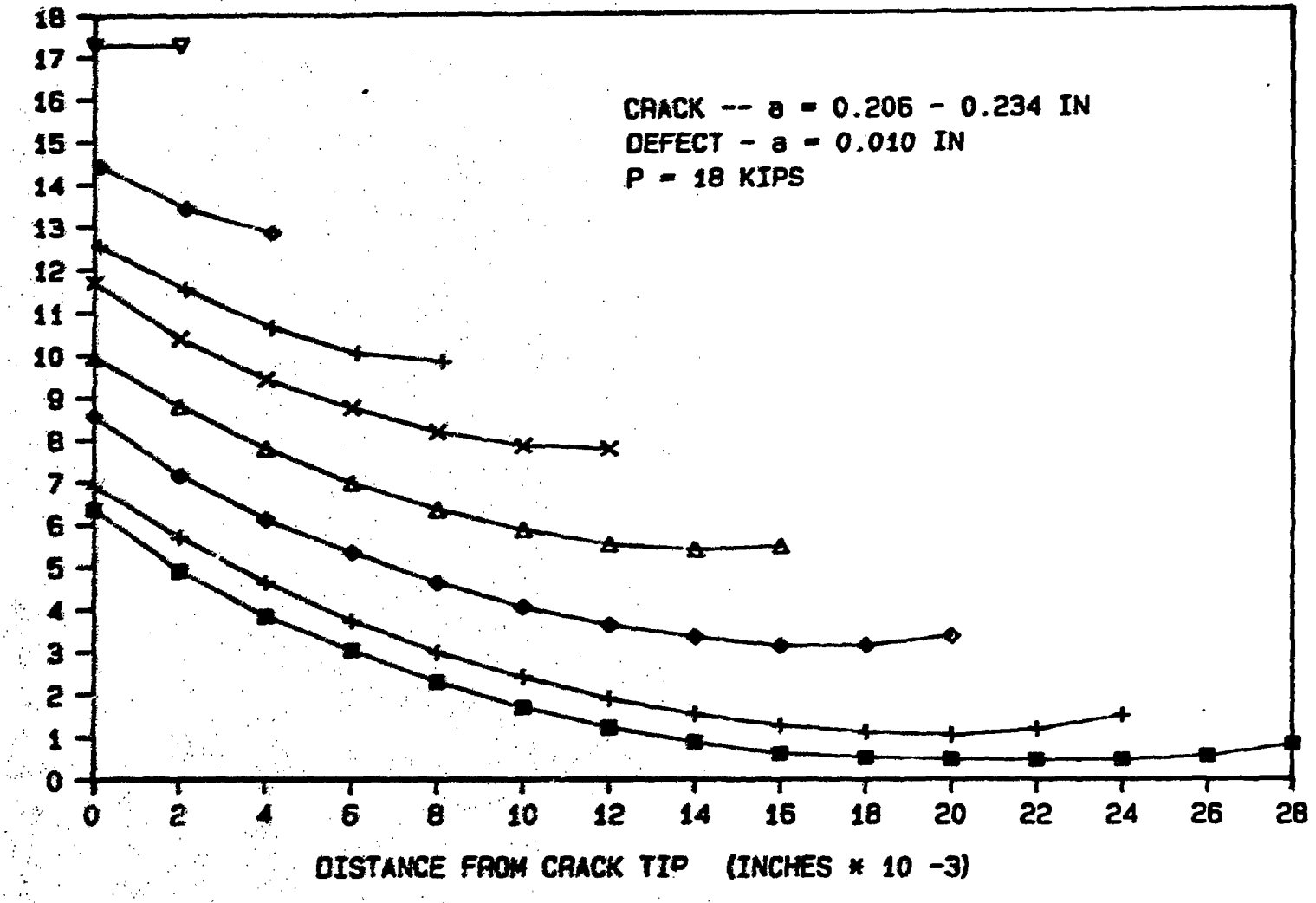

FIGURE 4.17 ELASTIC/PLASTIC STRAIN PROFILE BETWEEN CRACK AND DEFECT

element model will have a direct effect on the magnitude of the strains and therefore, plays an important role when comparing strains between models. As stated earlier, Mercer also used elements sized to 0.002 inches along the crack region and since no other work was available with this size element; his work was selected for a comparison. If one uses this criterion based on the above clarifications, we can see from the figures that failure at approximately 10 mils in Figure 4.16 and 12 mils in Figure 4.17. By selecting a maximum strain criteria for failure, one can postulate that plasticity will increase the critical spacing given by the stress intensity factor in the linear analysis.

Viscoplastic Analysis

Viscoplastic modeling at 1200 °F was accomplished with the Bodner-Partom algorithm in the SNAP program. The time, temperature, and rate dependent material behavior was accounted for with experimentally determined coefficients listed in Table 2.1.

To allow comparison with the elastic-plastic analysis, the initial crack half length and defect half length were set to (a) = 0.200 inch and (a) = 0.01 inch respectively. The same external load of 18 kips (30 ksi) was also used for the viscoplastic analysis.

Crack growth under both monotonic and cyclic load was considered. Crack growth is accomplished in the SNAP

program by the addition of "springs" to the boundary nodes along the crack plane. The boundary condition of each node is set by the spring stiffness. Free nodes have zero stiffness and constrained nodes have a stiffness equal to 1000 times the maximum diagonal entry in the structure stiffness matrix. User defined criterion set the node release tolerance and growth rate of the crack as a function of the load cycle. A detailed description of this method is given by Mercer (8).

The monotonic and cyclic load cases are depicted in Figure 4.18. For the monotonic load case, a fixed crack growth rate (da/dt) of 0.004 inch/second was selected. For the cyclic load case, a fixed crack growth rate per cycle (da/dn) of 0.004 inch/cycle was selected. However, no restriction was placed on the growth rate (da/dt) during the load phases of the cyclic case. The above rates were selected to limit the amount of computer processing time.

In actuality, thousands of cycles are required for cyclic crack growth. To attempt such an analysis with finite elements would be economically impossible. However, Wilson and Palazotto (6) state that most of the plastic strain properties of fatigue loading are characterized in one to three cycles. Thus, the limited number of cycles used in finite element analysis can still yield a good approximation to the plasticity induced features present in the problem.

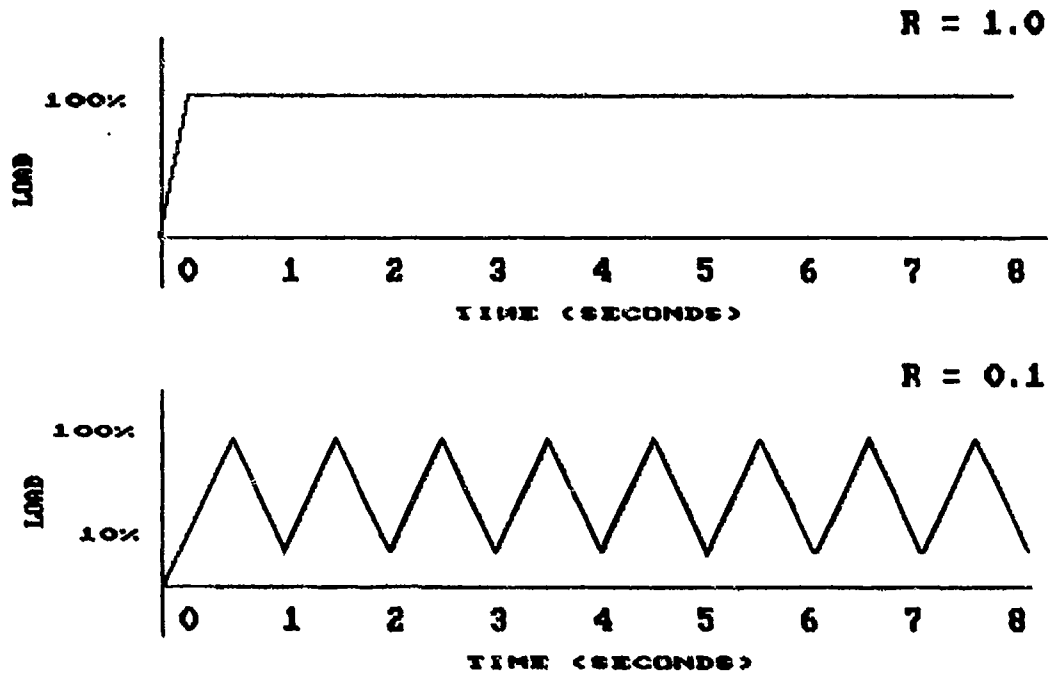

Figure 4.18 Viscoplastic Load Ratio Cases

Figures 4.19 - 4.22 depict the viscoplastic zone shapes as the crack is grown toward the defect for the monotonic and cyclic load cases. For the initial crack/defect configuration, the height of plastic zone is approximately 20 mils for monotonic loading and 16 mils for cyclic loading as compared to 8 mils for the elastic-plastic analysis. Here we see that application of the Bodner-Partom viscoplastic flow law at high temperature in combination with crack growth has increased the size of the plastic zone height by a factor of 2-3 depending on the type of load used.

For both load cases, we also see that the free surface of the defect constrains the initial plastic zone from

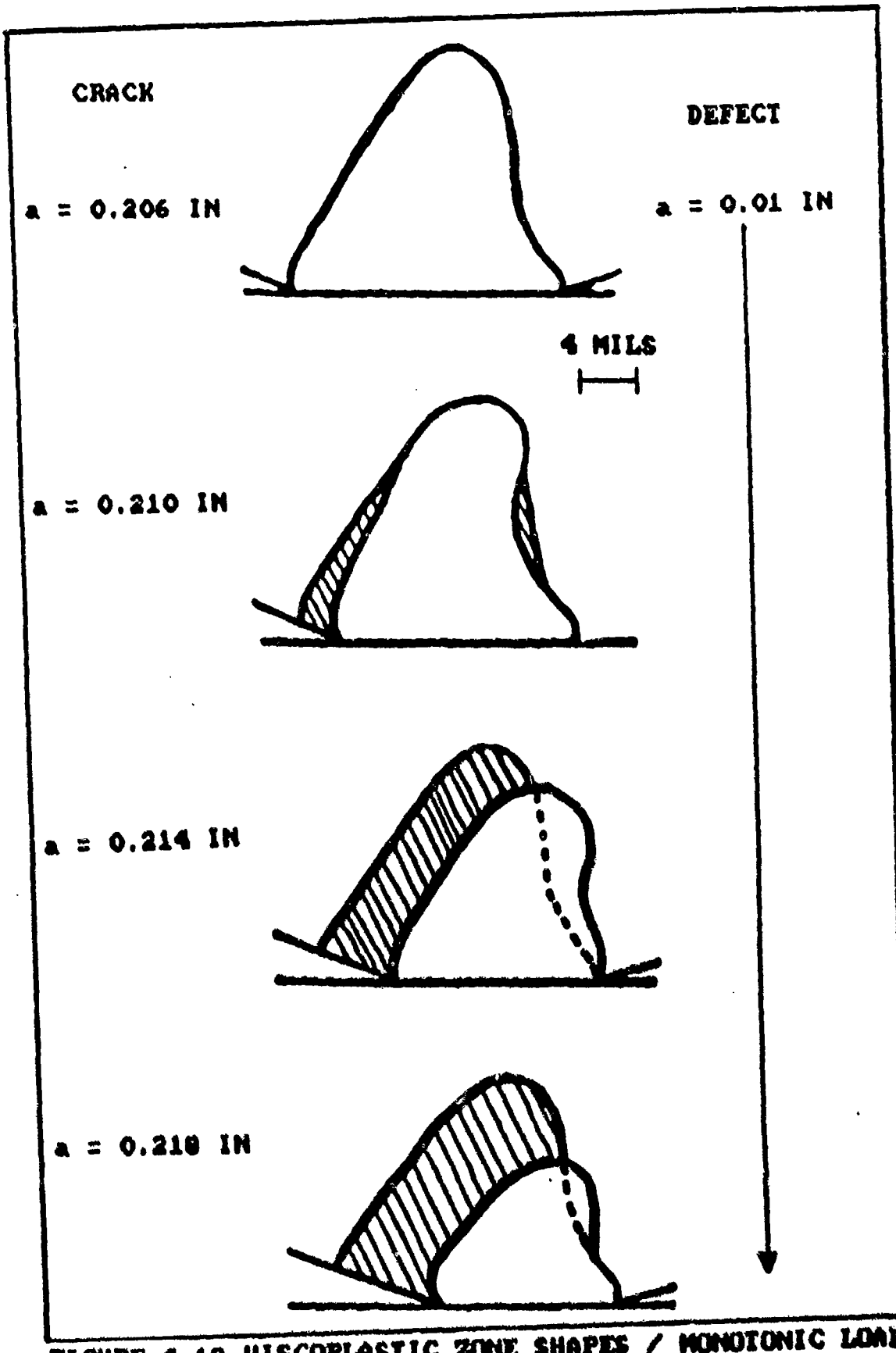

FIGURE 4.19 VISCOPLASTIC ZONE SHAPES / MONOTONIC LOAD

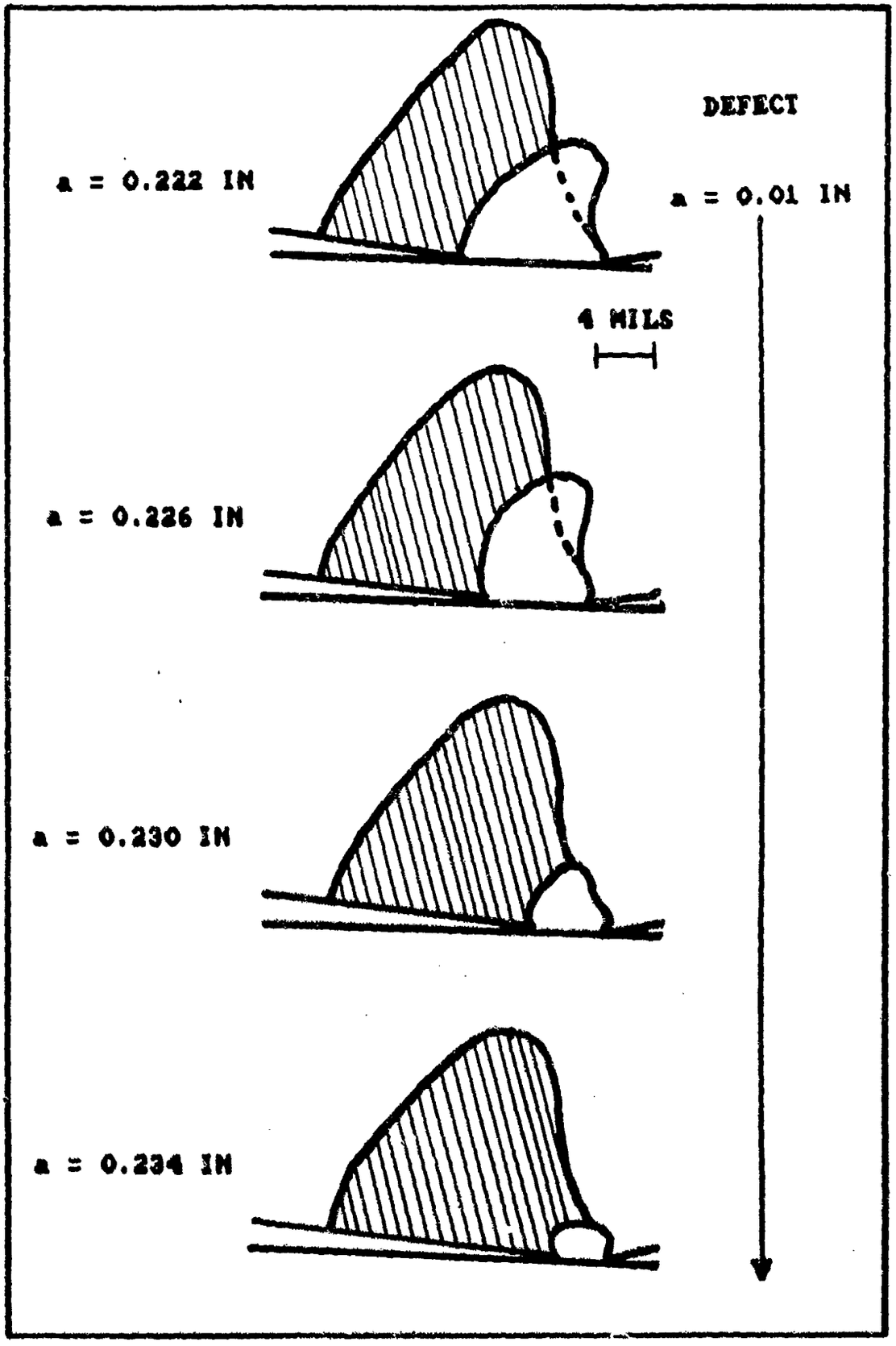

FIGURE 4.20 VISCOPLASTIC ZONE SHAPES / MONOTONIC LOAD

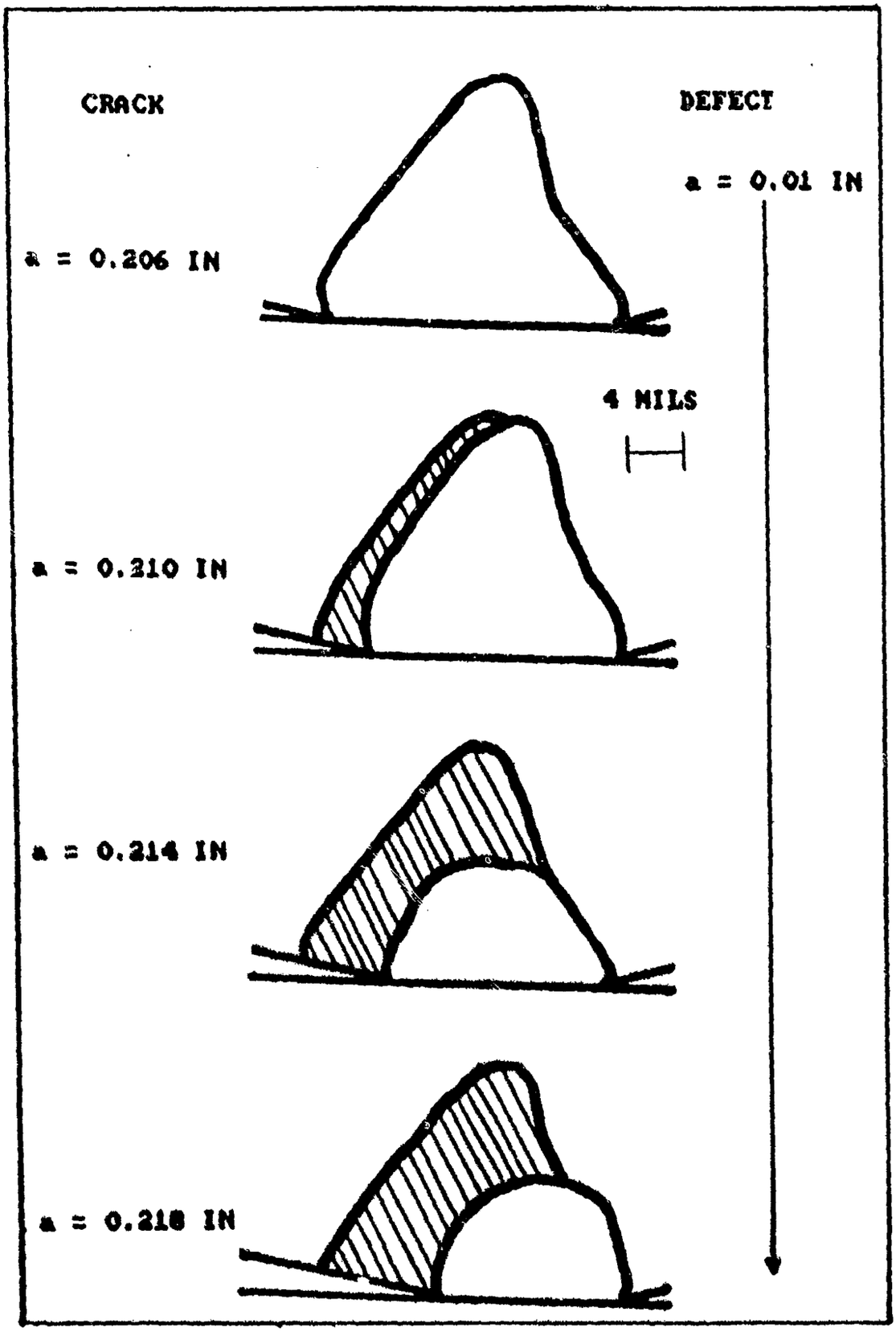

FIGURE 4.21 VISCOPLASTIC ZONE SHAPES / CYCLIC LOAD

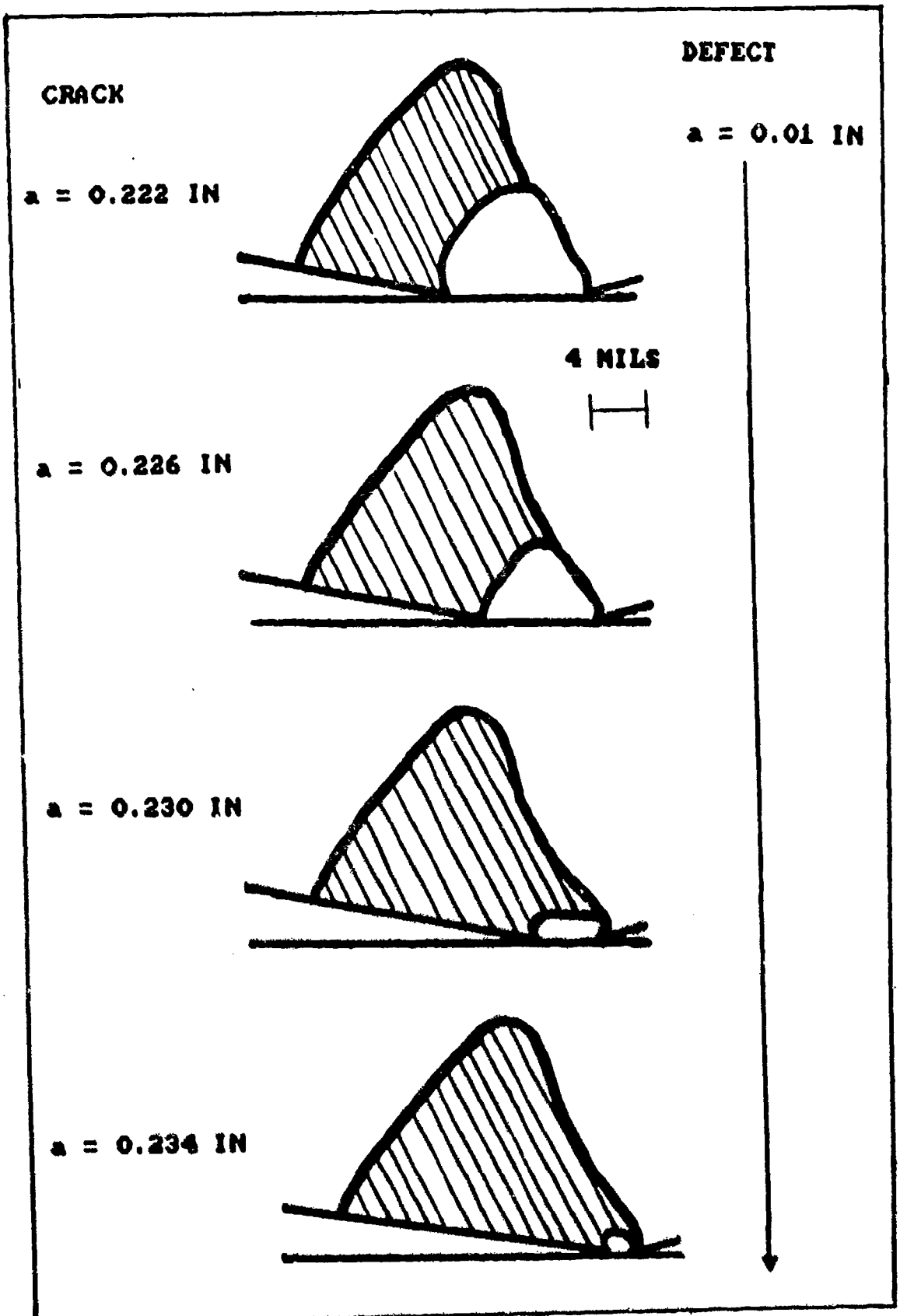

FIGURE 4.22 VISCOPLASTIC ZONE SHAPES / CYCLIC LOAD

propagating forward with the crack tip. This constraint caused a smaller "super strained" region to be formed inside the initial strain hardened region as the crack moved toward the defect. The "super strained" region is the smaller area inside the original (shaded) strain hardened region as depicted in the figures. Here, "super strained" means the remaining region that still has stresses exceeding the yield stress and a corresponding increase in the strains over the previous crack/defect configuration. As noted with the elastic-plastic analysis, the size of the "super-strained" region continues to decrease as the crack approaches the defect.

Figure 4.23 shows the plastic zones generated between the crack and defect with crack growth and compares these zones to a fixed crack of the same dimension. The increased profiles reflect the time and load dependent nature of plasticity. A 15 to 50 percent increase in the plastic zone area was due directly to crack growth in the viscoplastic analysis.

The crack opening profiles for crack growth under monotonic and maximum cyclic load are shown in Figures 4.24 and 4.25. Crack growth under monotonic load (Fig. 4.24) resulted in a sharper crack tips as compared to the maximum cyclic load (Fig. 4.25) which shows blunted crack tips. Again, the amount of blunting was essentially constant for all the crack/defect spacings considered.

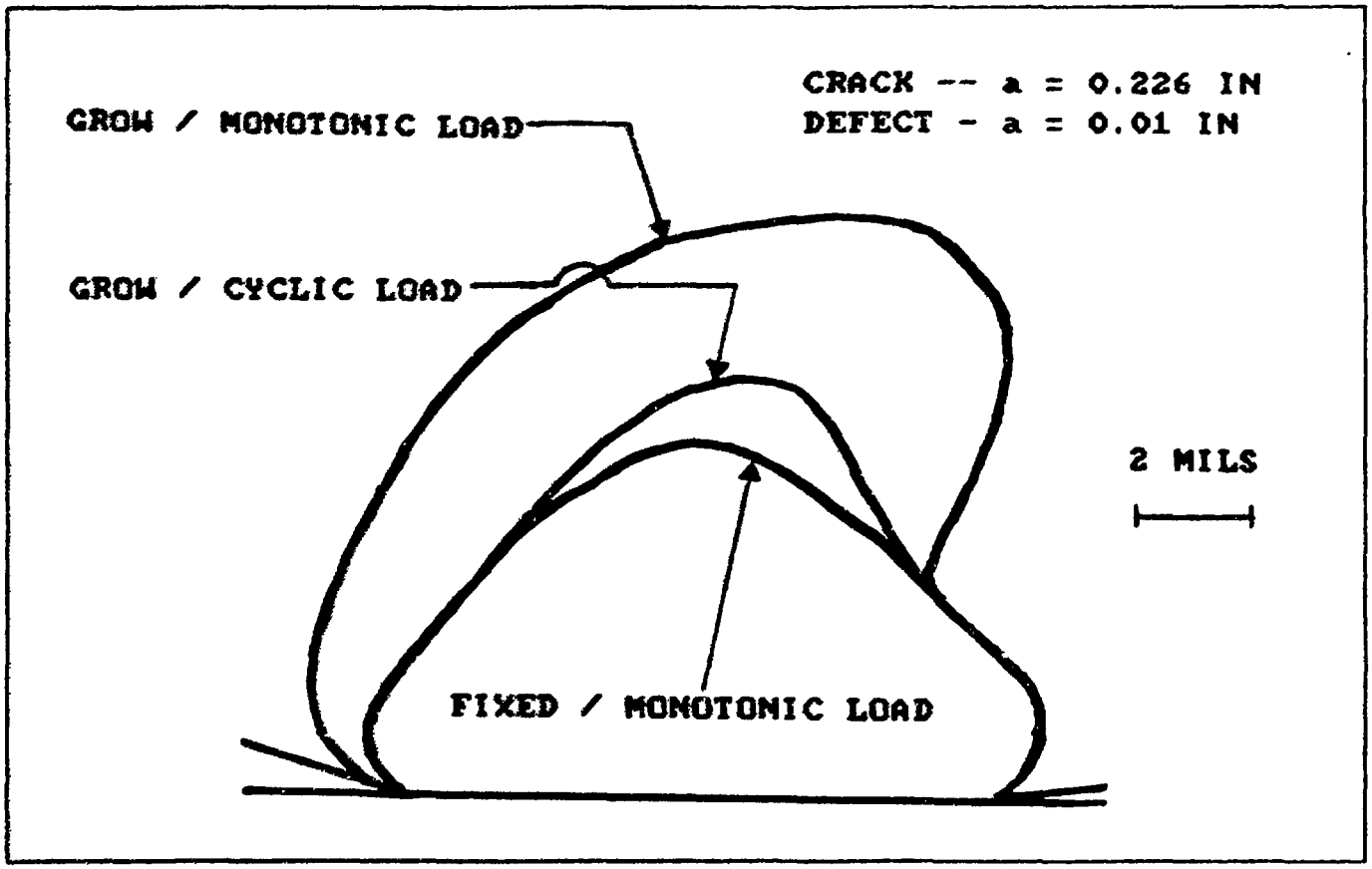

FIGURE 4.23 VISCOPLASTIC ZONE SHAPE COMPARISON

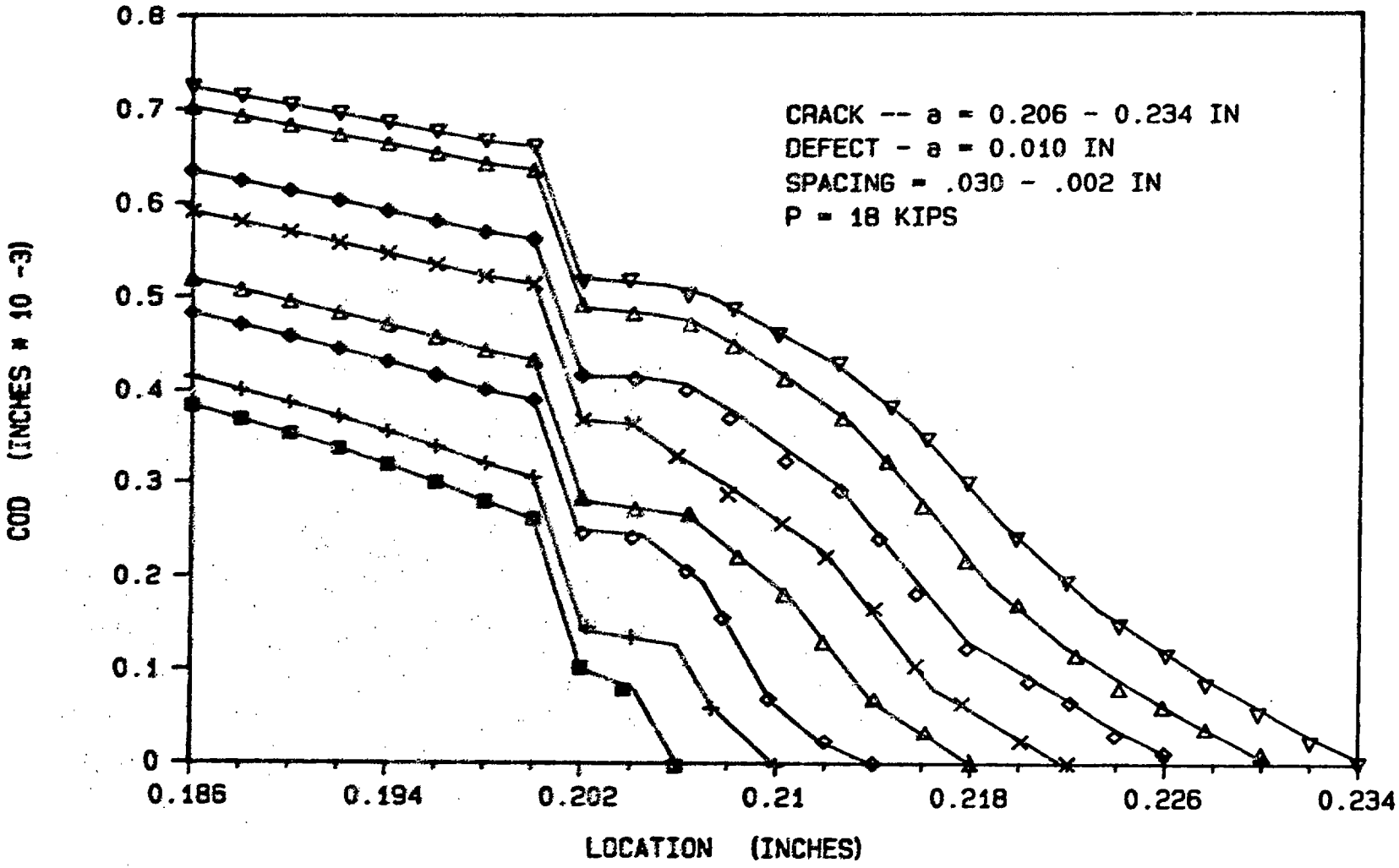

FIGURE 4.24 VISCOPLASTIC CRACK OPENING PROFILES, R = 1.0

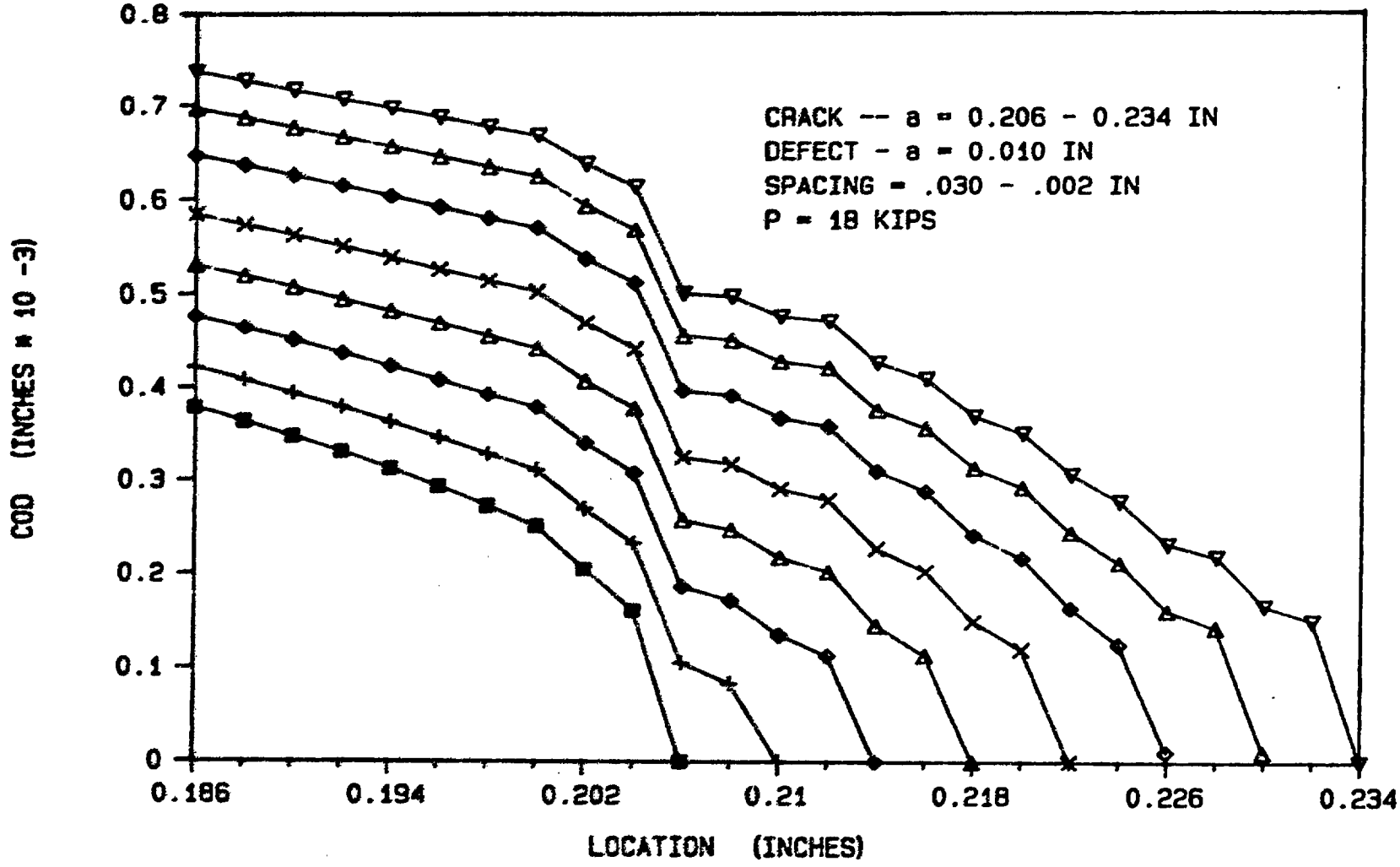

FIGURE 4.25 VISCOPLASTIC CRACK OPENING PROFILES, R = 0.1, 100% LOAD

Both load cases reflect the presence of a plastic wake forming over the crack as it moves through the strain hardened region. This presence is evidenced by the abrupt drop in the crack opening profile near the crack origin and by the jagged contour of the diminished profiles. The plastic wake formed immediately under monotonic crack growth but formed one cycle (0.004 inch) later for the cyclic load case. The decrease in the crack opening profile due to residual plastic deformation is highlighted in Figure 4.26 by the fixed crack of equal length.

Figure 4.27 shows the crack profiles at minimum cyclic load. Crack closure is established within one cycle and the amount of closure doubles as the crack moves toward the defect. Careful attention must be given to the markers used to identify the individual crack profiles to see the closure (zero displacement) for a particular crack length. Figure 4.28 highlights the closure phenomenon of one crack profile by comparing it to an elastic solution.

A comparison of a viscoplastic crack opening profile to an elastic profile at full cyclic load is presented in Figure 4.29. Again, the presence of the plasticity reduces the strain energy at the crack tip with an associated 44 percent decrease in the stress intensity factor. The stress intensity was calculated with the J-integral and application of equation 2.23.

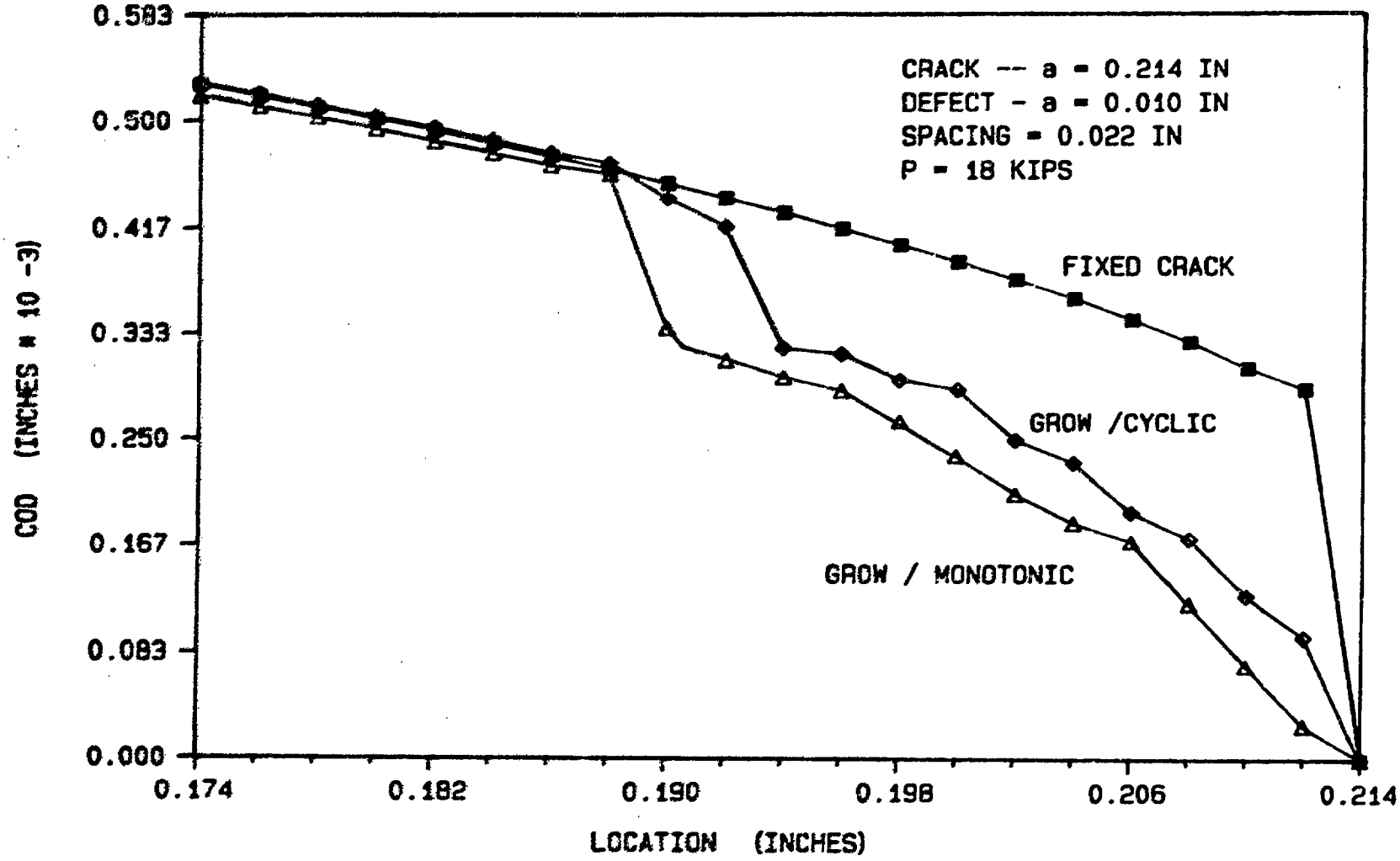

FIGURE 4.26 VISCOPLASTIC CRACK OPENING PROFILE COMPARISON

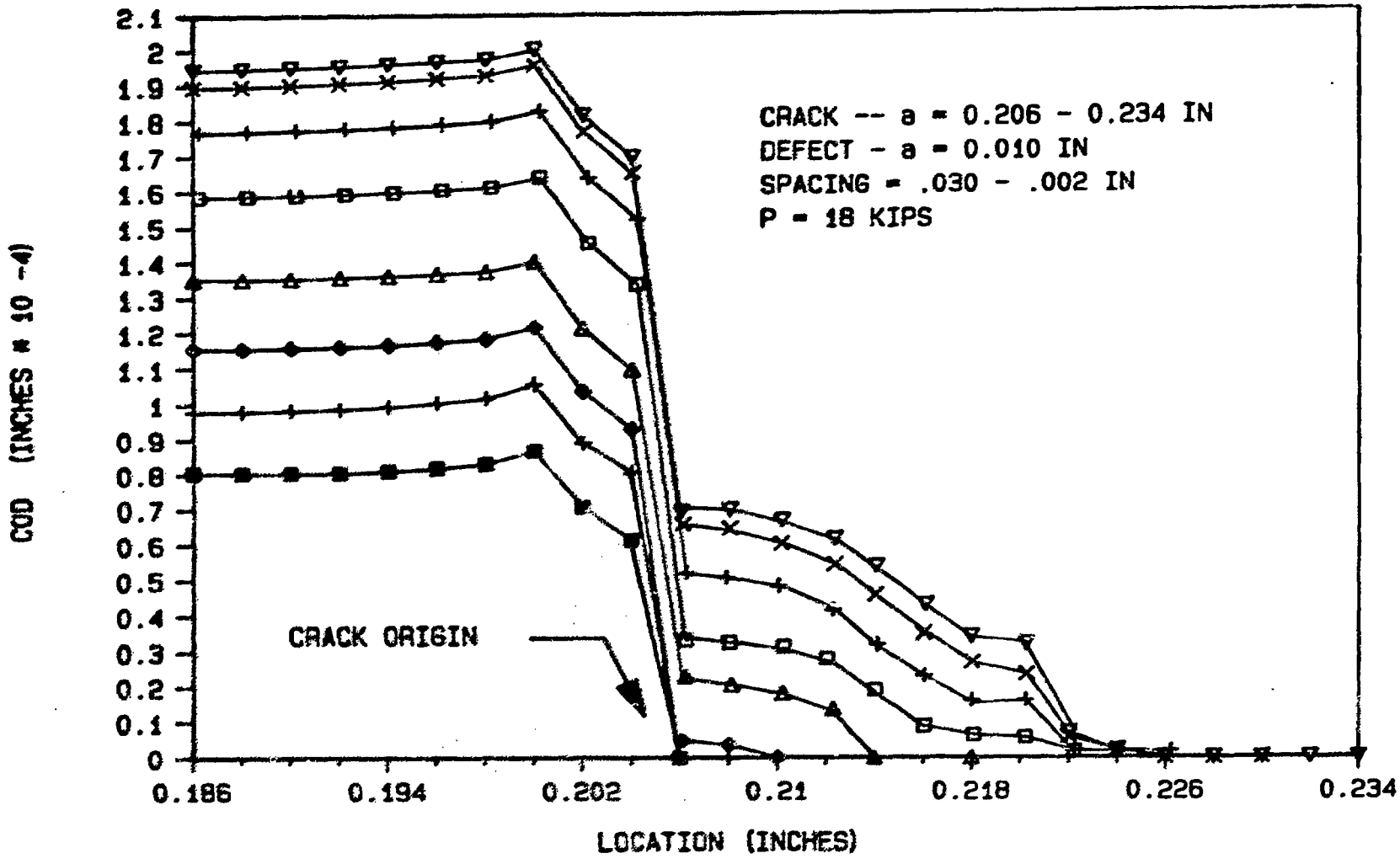

FIGURE 4.27 VISCOPLASTIC CRACK OPENING PROFILES, R = 0.1, 10% LOAD

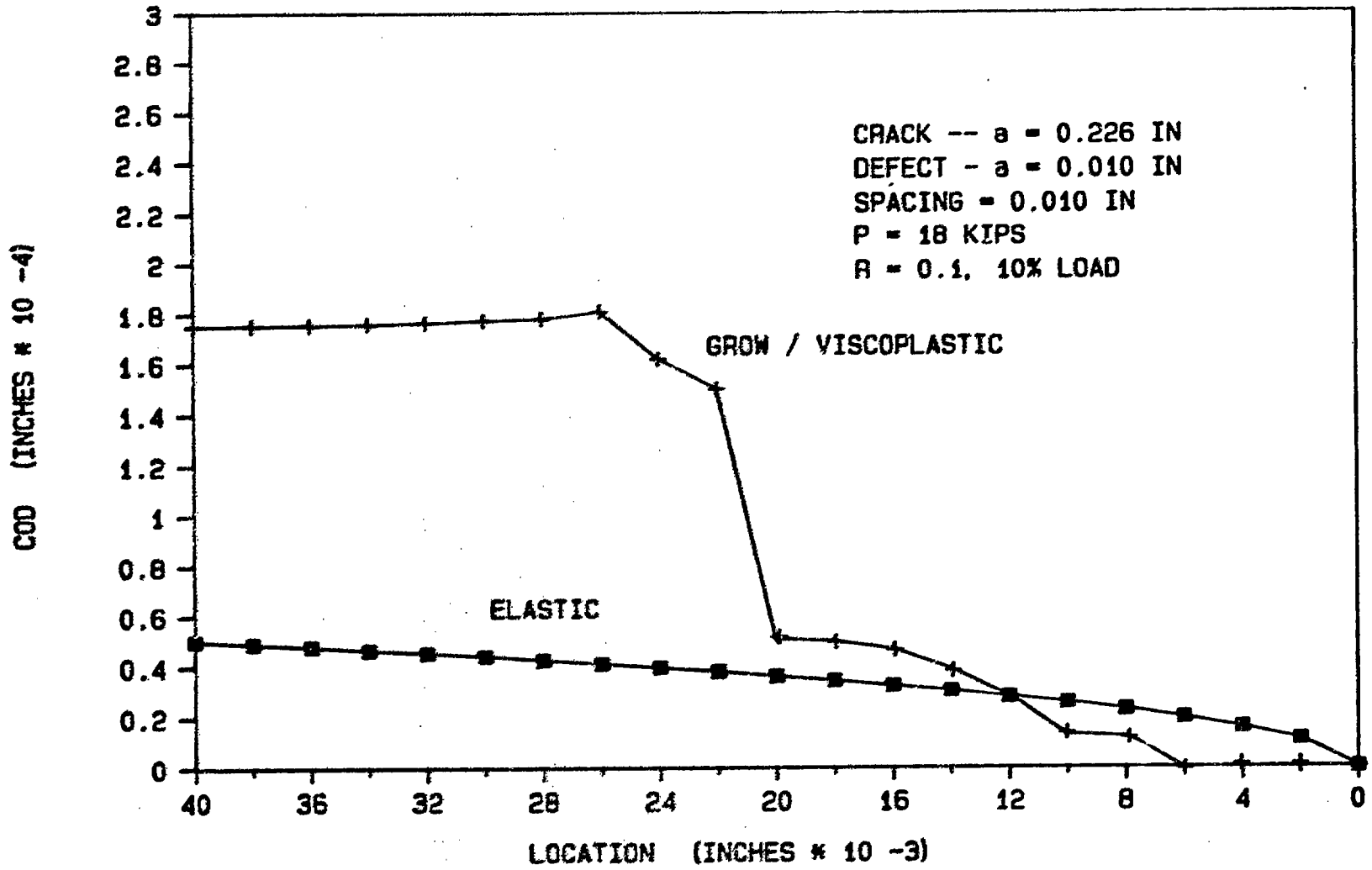

FIGURE 4.28 CRACK OPENING PROFILE COMPARISON

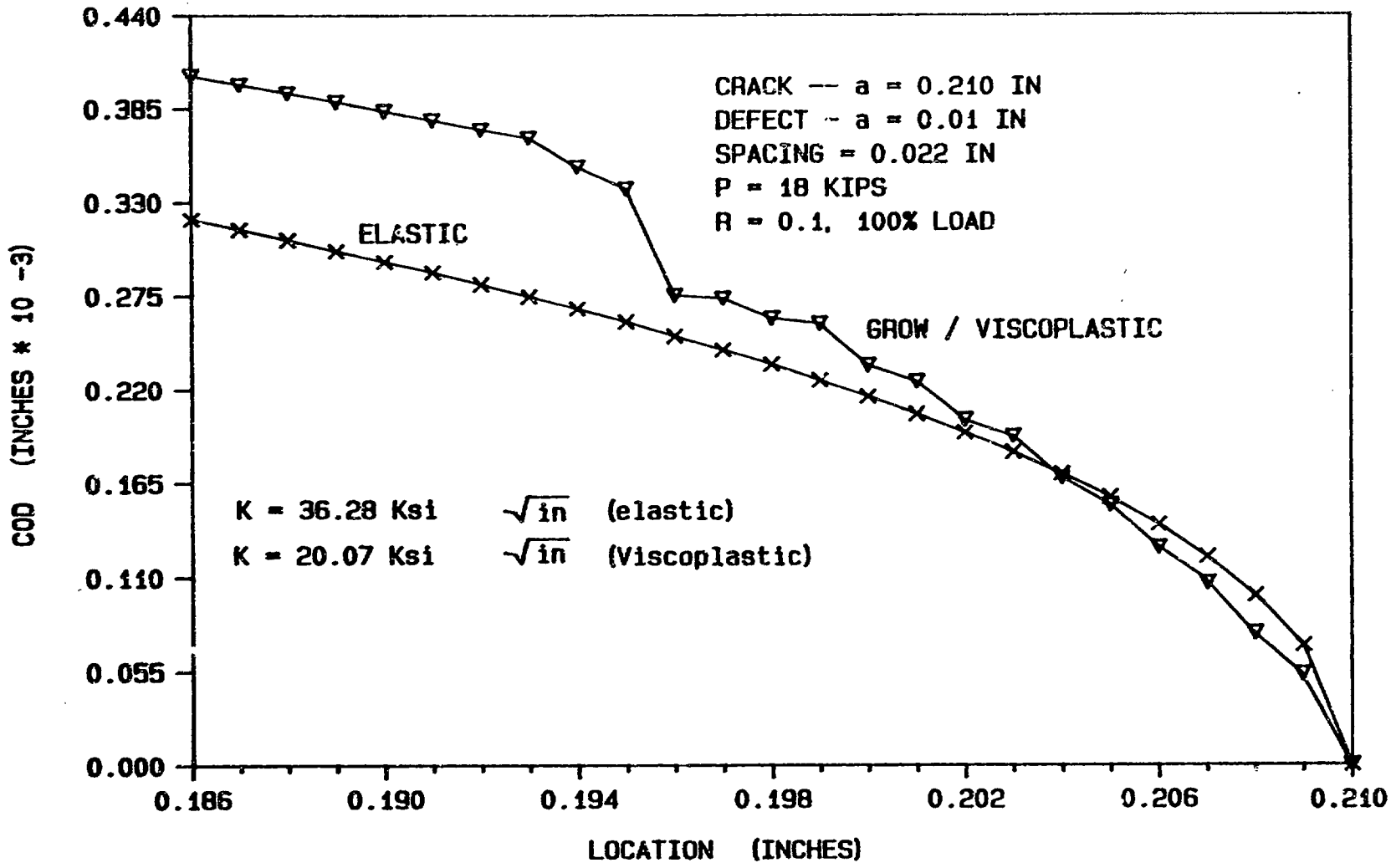

FIGURE 4.23 CRACK OPENING PROFILE COMPARISON

For both monotonic (Fig. 4.30) and maximum cyclic load (Fig. 4.31), a constant stress profile was reached along the crack plane when the crack had grown within one defect length (i.e. 0.02 inch). The cyclic analysis stabilized to a slightly higher stress of 180 ksi versus 175 ksi for the monotonic case. For 10 percent cyclic load (Fig 4.32), a fully compressive field is generated for crack/defect spacings ranging from 2 to 12 mils. Between 12 and 28 mils, we see a stress field that starts compressive, goes positive and then decreases as it approaches the defect. When the defect is 20 mils or one defect length from the crack tip we see that the stress at the defect is zero.

The strain profiles for monotonic and cyclic loading are shown in Figures 4.33 - 4.35. In Figures 4.33 and 4.34, we see the same concave up strain profiles as noted in the elastic-plastic analysis. However, for the case of 10 percent cyclic load in Figure 4.35, we see a combined concave up and concave down shape in the strain profiles. The inflection points along these curves correspond to the location where the compressive stress field converts to a positive tensile field.

As with the elastic-plastic analysis, the question of a critical strain level must be addressed. If one uses the failure criteria of eight percent strain for the crack/defect spacing, the possibility of instantaneous failure occurs at approximately 10-12 mils which is the same

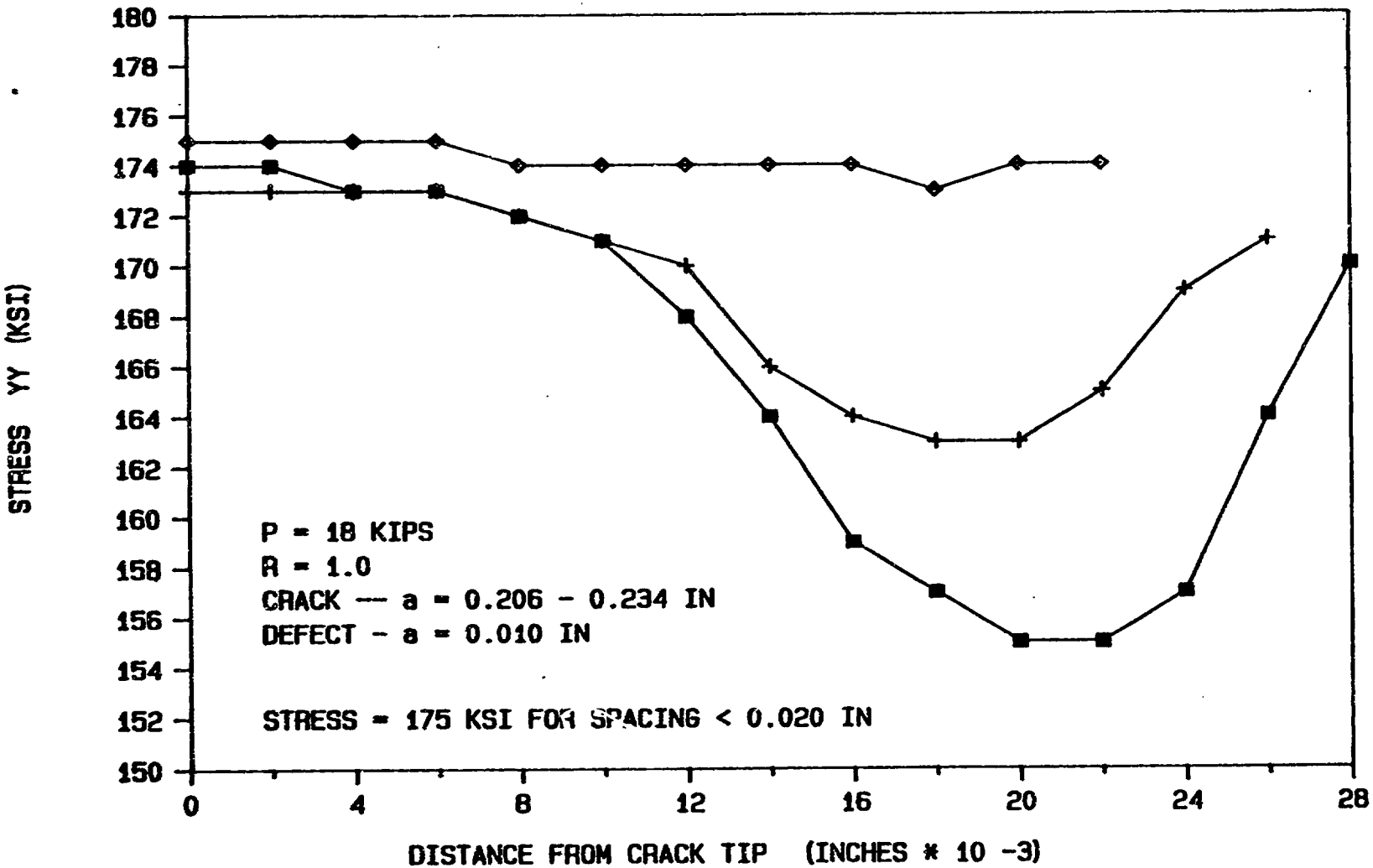

FIGURE 4.30 VISCOPLASTIC STRESS PROFILE BETWEEN CRACK AND DEFECT

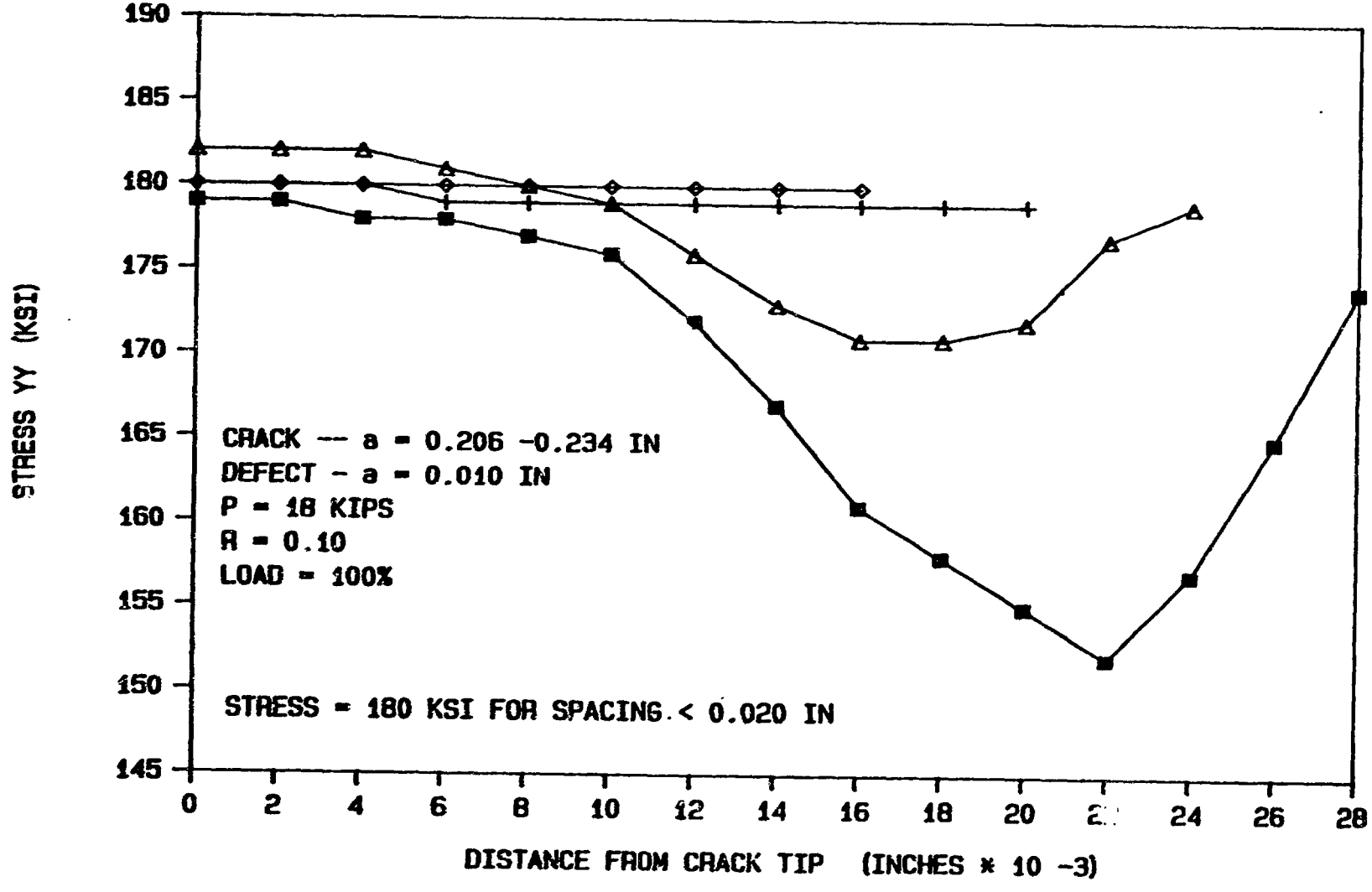

FIGURE 4.31 VISCOPLASTIC STRESS PROFILE BETWEEN CRACK AND DEFECT

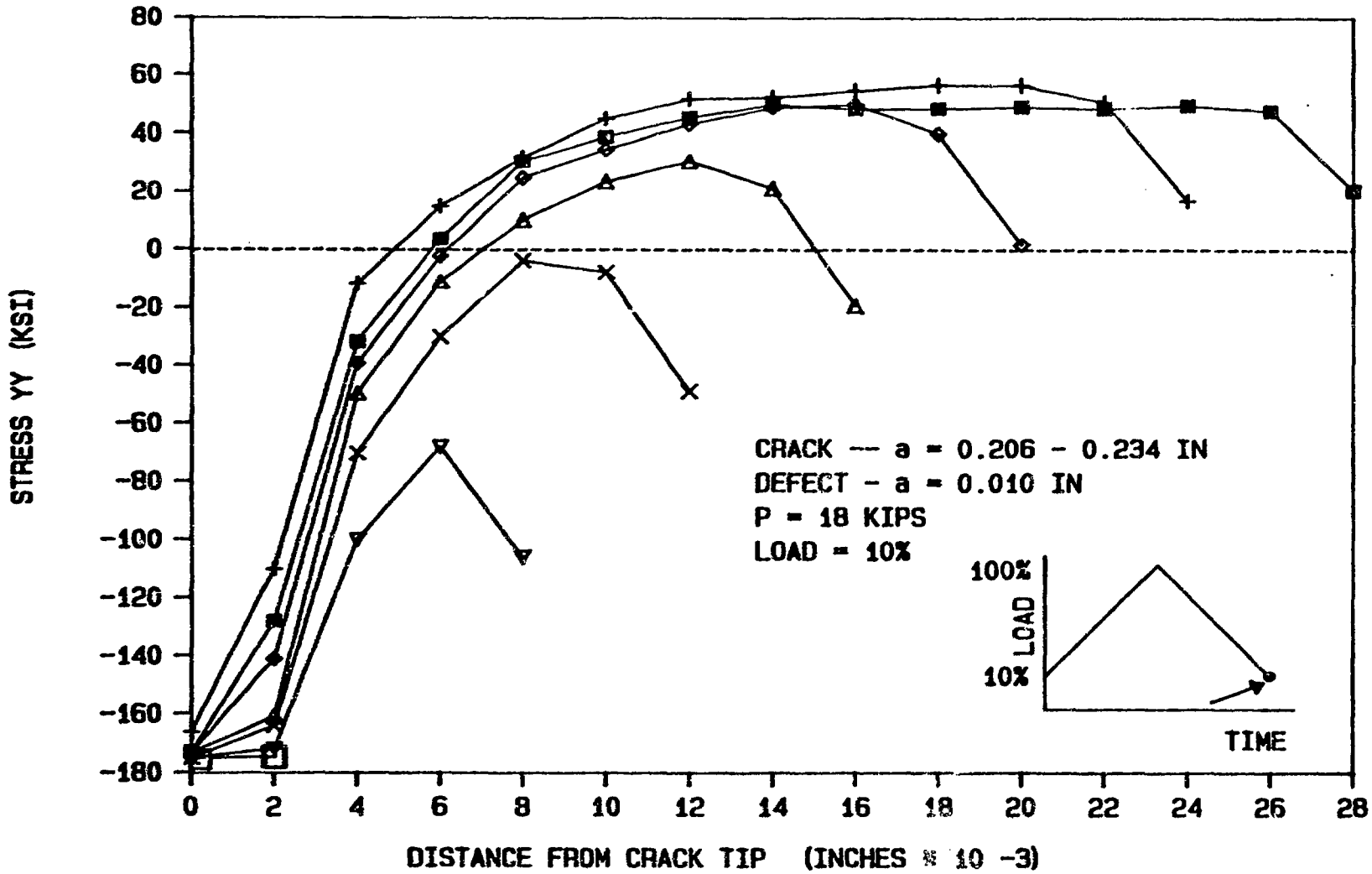

FIGURE 4.32 VISCOPLASTIC STRESS PROFILE BETWEEN CRACK AND DEFECT

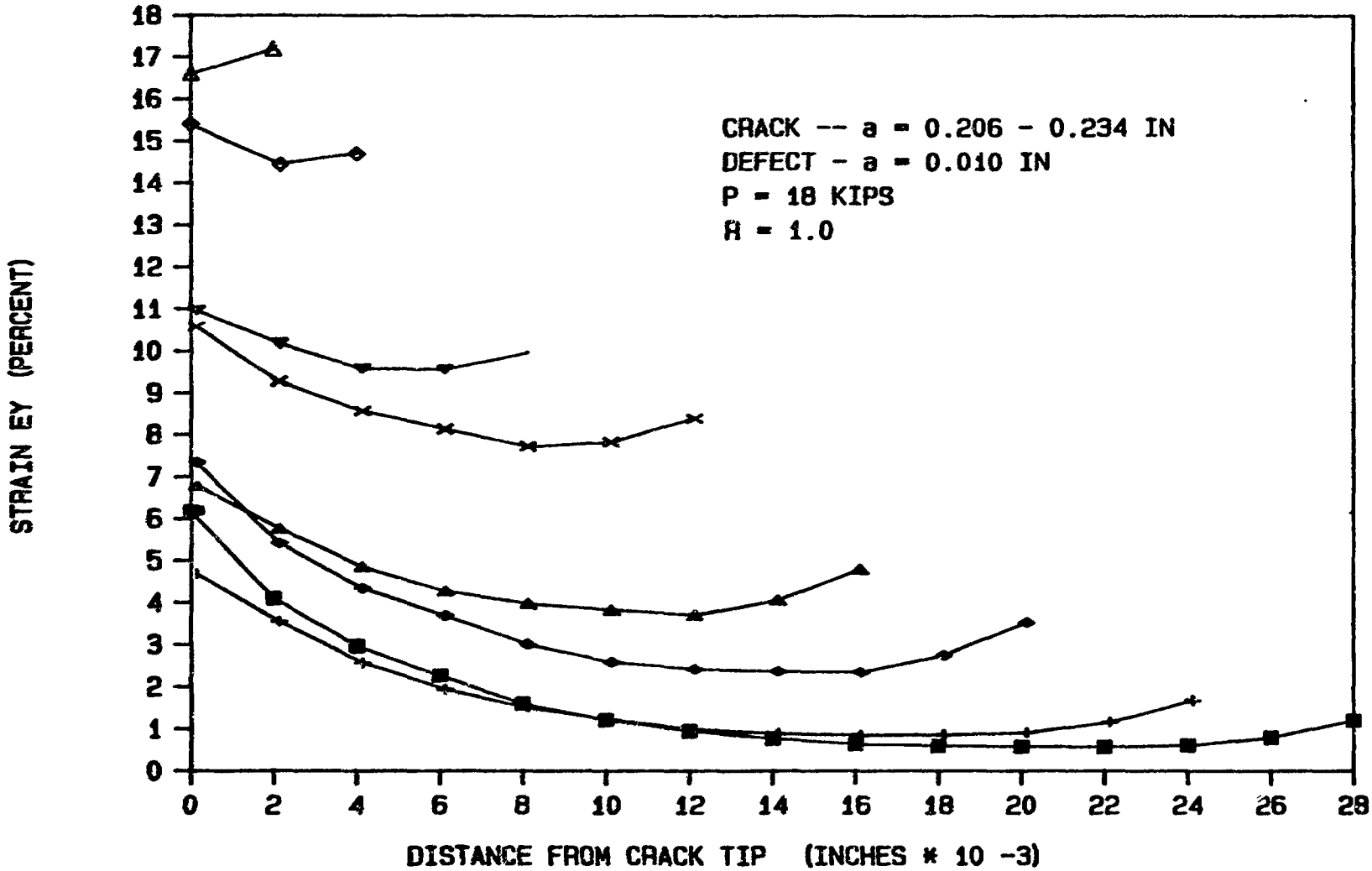

FIGURE 4.33 VISCOPLASTIC STRAIN PROFILE BETWEEN CRACK AND DEFECT

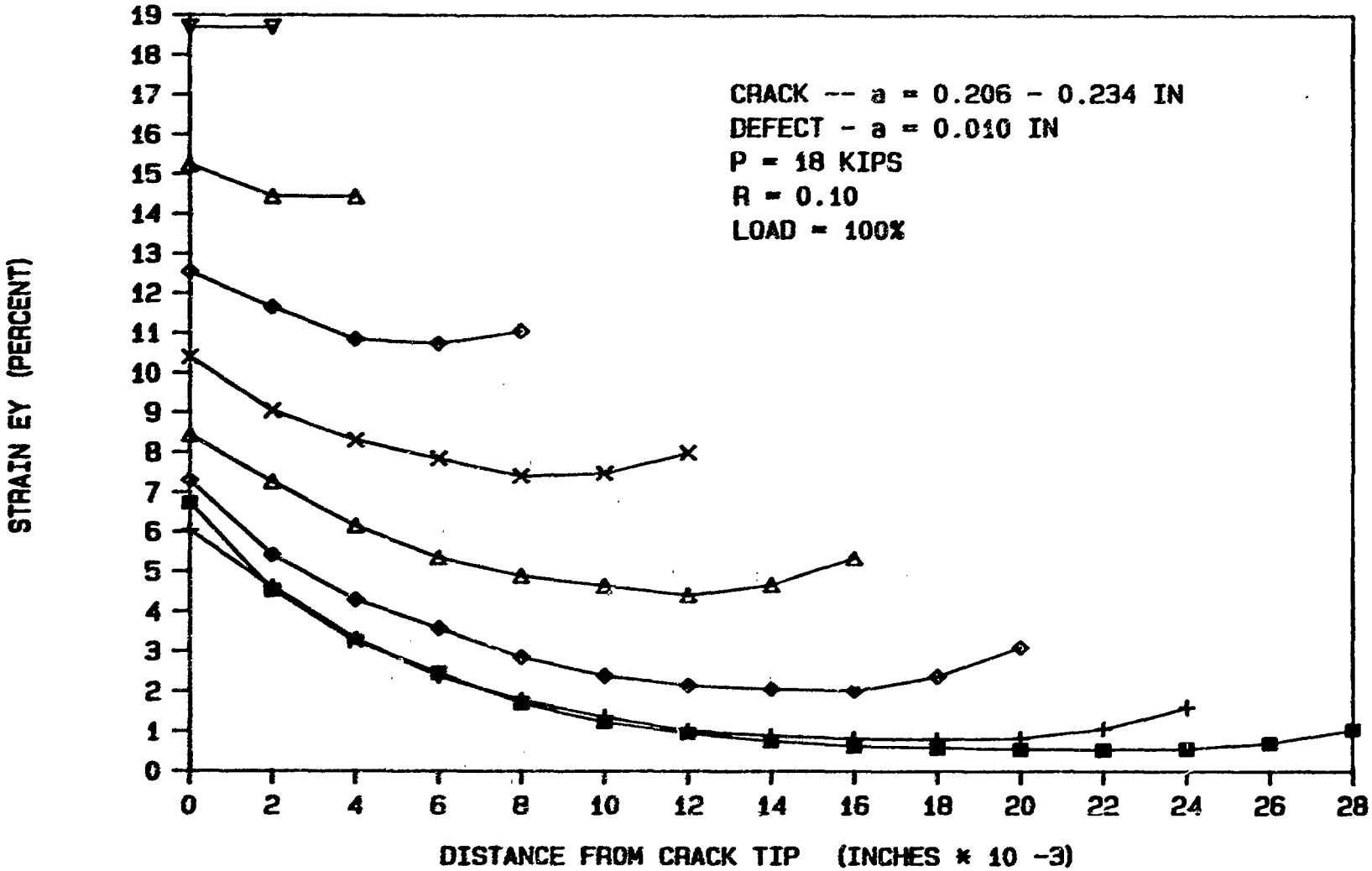

FIGURE 4.34 VISCOPLASTIC STRAIN PROFILE BETWEEN CRACK AND DEFECT

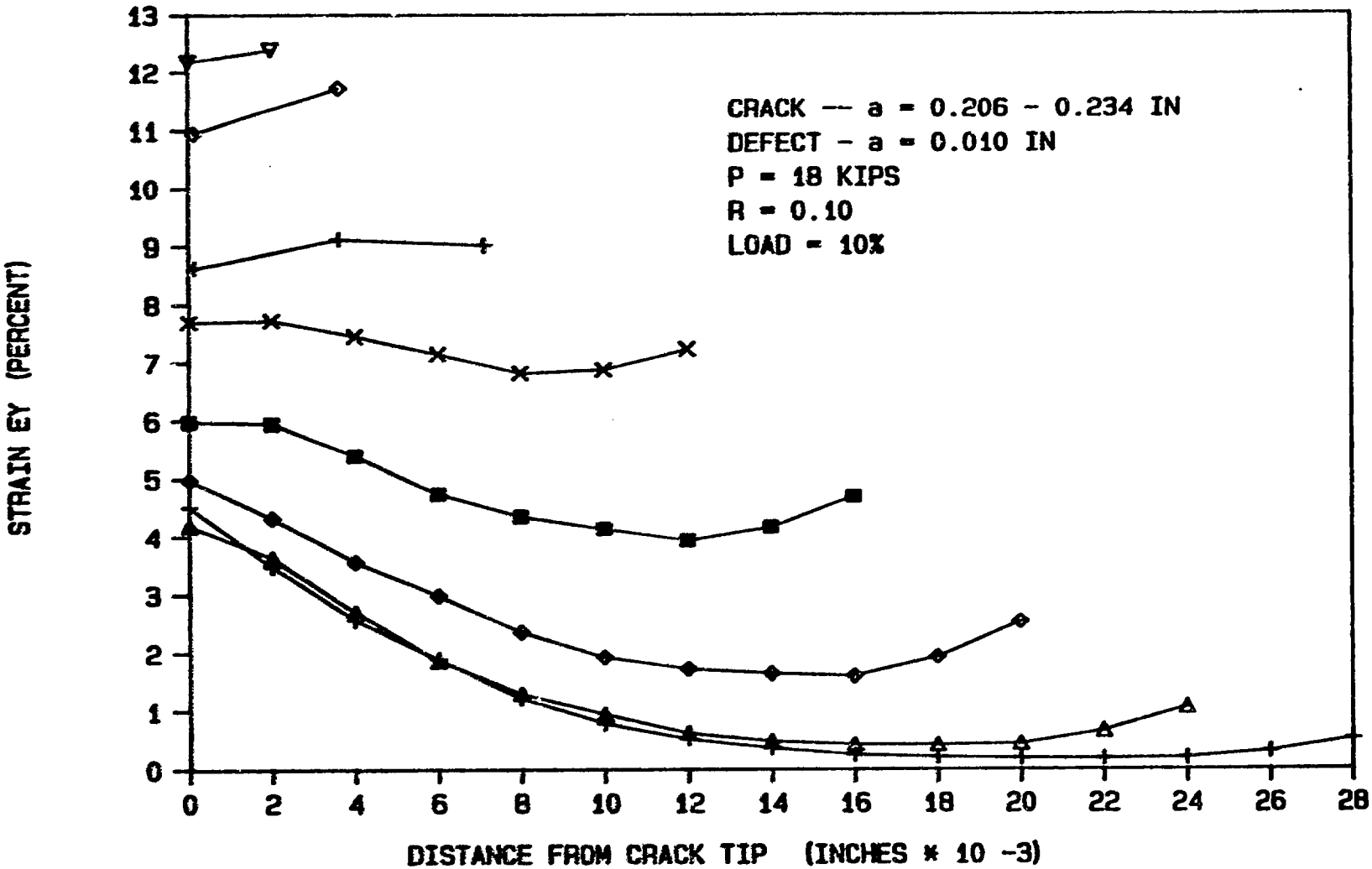

FIGURE 4.35 VISCOPLASTIC STRAIN PROFILE BETWEEN CRACK AND DEFECT

spacing given in the elastic-plastic analysis.

A second and far more realistic failure criterion in the cyclic analysis is the growth rate (da/dt) during a load increment of a cycle. As stated earlier, the growth rate per cycle (da/dn) was set to 0.004 inch/cycle. To meet this criterion, two nodes were released at a user specified stress of 160 ksi in each cycle of loading. Specifying the stress for node release allowed the node release time to be an independent variable in the solution. The corresponding release times were then recorded by the SNAP program. By subtracting the release time of the first node from the release time of the second node, the exact time increment for a 0.004 inch growth is known and the growth rate in a load cycle (da/dt) can be calculated. Table 4.2 shows the growth rate results. We see the growth rate is initially 0.018 inch/sec and then decreases to a constant rate of 0.0125 inch/sec for the next four cycles. For the seventh and eighth cycles, the growth rate is infinite. By selecting the sixth cycle as the last cycle for stable growth, we have a crack/defect spacing of 0.008 inch for instantaneous fracture. This is a 33 percent increase over the 0.006 inch prediction given by the linear stress intensity predictions. Using this method for predicting failure yields a slightly larger strain profile of approximately ten percent in the crack/defect spacing as shown in Figure 4.34.

Table 4.2 Cyclic Crack Growth Rate (da/dt)

Cycle #	da/dt (in/sec)	Cycle #	da/dt (in/sec)
1	**	5	0.0125
2	0.018	6	0.0125
3	0.0125	7	Infinite
4	0.0125	8	Infinite

** Initial Load/ No Growth

An additional check was conducted to see if the primary crack length would affect the influence range of the defect when working with viscoplastic flow law. Figures 4.36 - 4.38 show the stress-strain profiles of a crack that is approximately half the length of the original viscoplastic analysis with the same defect, spacing, and stress intensity. We see in Figure 4.38 that the stresses are in the range of 180 ksi; and the strains are about six percent at the crack and less than one percent at the defect. Figures 4.37-4.38 show the increasing strain profile between the crack and defect as the spacing is decreased. We note here that the stress/strain data is comparable to the larger primary crack indicating that the crack length still has little effect on the influence range of the defect. It is important to note that the crack stress intensity was held constant for both cases which required an increase in

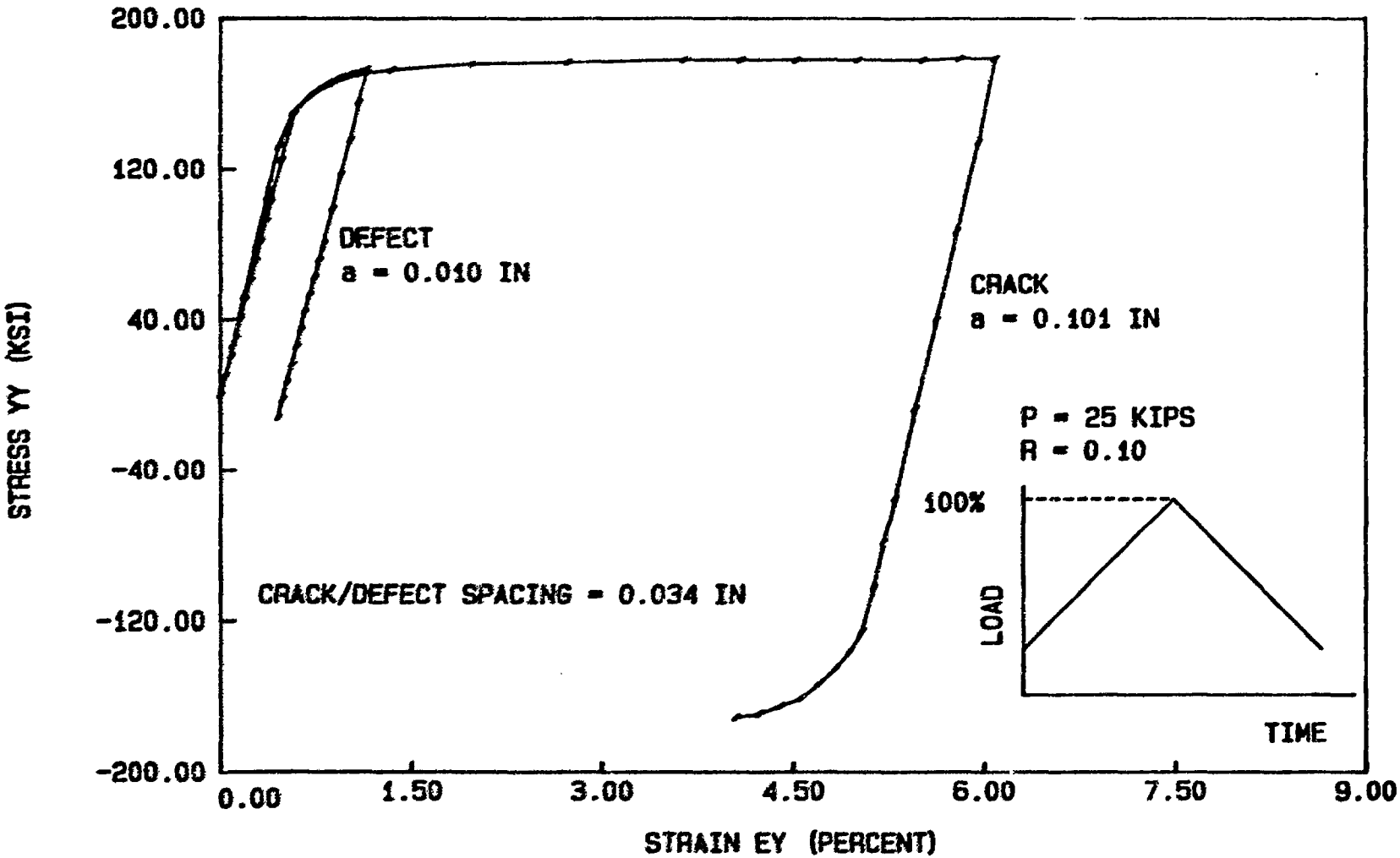

FIGURE 4.36 VISCOPLASTIC STRESS-STRAIN RESPONSE DURING CYCLIC LOADING

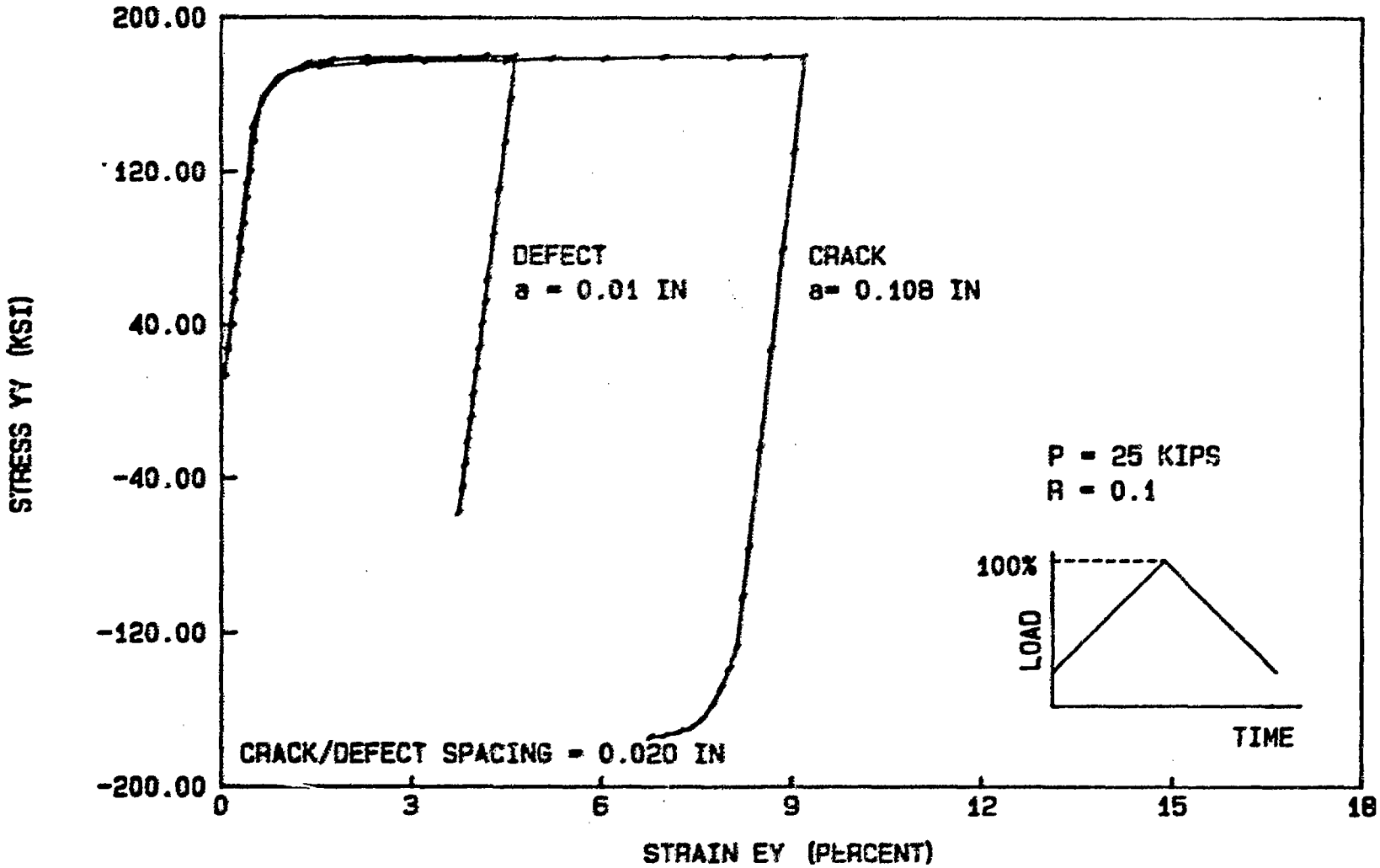

FIGURE 4.37 VISCOPLASTIC STRESS-STRAIN RESPONSE DURING CYCLIC LOADING

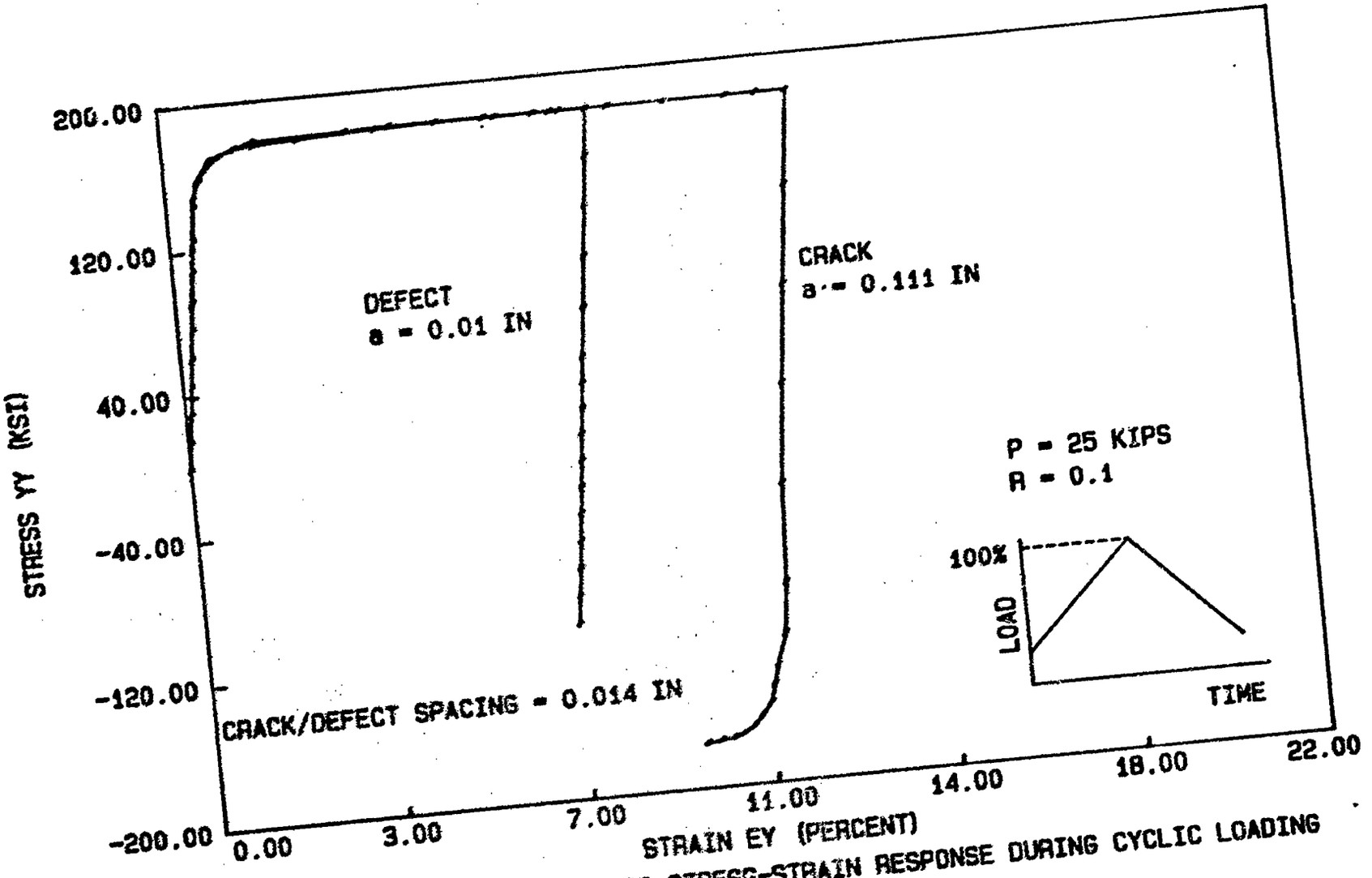

FIGURE 4.38 VISCOPLASTIC STRESS-STRAIN RESPONSE DURING CYCLIC LOADING

load for the second analysis from 18 kips to 25 kips. As long as similitude is maintained with the stress intensity, it appears the the defect size and its location are the primary factors affecting the material behavior between the crack and defect.

The analysis confirms that a defect has a prominent influence range equal to about one defect length for all three constitutive models. In addition, a critical spacing exists in the plastically deformed region where the probability of instantaneous fracture to the defect is imminent. Although no definite parameter exists to confirm the critical spacing, the critical strain and growth rate (a stress criterion) appear to be two primary indicators for estimating when instantaneous failure will likely occur.

V. Summary and Conclusions

A two-dimensional nonlinear finite element code called SNAP was used to model a center cracked axial tension specimen with two defects placed symmetrically about the crack plane. The crack/defect configuration was modeled via linear elastic, elastic-plastic, and viscoplastic constitutive equations. The material modeled was IN-718, a nickel based superalloy used in jet engines.

The following statements and conclusions are based on the analysis presented in this work:

1. Linear elastic modeling through finite element techniques provided comparative results to known infinite plate theory for a collinear crack/defect configuration. Plots of the crack stress intensity versus crack/defect spacing predict a critical spacing at which the crack stress intensity will exceed the combined crack and defect stress intensity. This phenomenon has been referred to as "pop-in" behavior and reveals that a defect can actually impede crack growth when it combines with the primary crack. In addition, the defect can shield the crack tip from finite width effects.

2. A defect has a prominent influence range equal to approximately one defect length for the three constitutive models used in this analysis. Inside this range, the defect influence on the crack opening displacement and

stress/strain fields cannot be ignored.

3. The crack sizes considered in this analysis had little affect on the crack/defect interaction. The primary driver appears to be the size of defect and the spacing from the crack tip.

4. Consideration of the strain profiles in the elastic-plastic analysis confirms the critical spacing concept revealed with the linear analysis. Selection of an eight percent strain criterion for failure increases the critical spacing over linear analysis by as much as 50 percent. As discussed earlier, the selection of the critical strain is based on the work of Mercer (8). In his analysis, eight percent strain was needed in the crack tip element to match experimental crack openings for a compact tension specimen of IN-718 subjected to a 35 Ksi$\sqrt{in}$ stress intensity.

5. Crack tip blunting and reduced strain energy at the crack tip were two additional effects present with the nonlinear analysis. The stress intensity calculated within the plastically deformed crack/defect region decreased by approximately 50 percent and the degree of crack tip blunting appeared to be independent of the crack/defect spacing.

6. Crack growth with the viscoplastic model showed that the defect will restrict the plastic zone from propagating with the crack tip. This created a smaller "super-strained" region inside the original strain hardened region as the

crack continued to grow towards the defect.

7. Cyclic crack growth with the viscoplastic model allowed the growth rate (da/dt) to be used as a failure criterion. This method also predicted a 30 percent larger critical spacing over the linear stress intensity prediction.

8. The critical strain and growth rate criterion are not exact methods for determining failure between a crack and defect. However, they do provide a plausible range for the problem.

The results presented in this work confirm the ability of finite element analysis as a tool to understand crack/defect interaction. Furthermore, some insight into how defects can alter crack growth parameters under nonlinear considerations has been provided.

Bibliography

1. Military Standard: Engine Structural Integrity Program (ENSIP), MIL-STD-1783 (USAF), 30 November, 1984.

2. Haritos G., Program Manager Aerospace Sciences, AFOSR/NA, "Structural Durability" Address to Air Force Institute of Technology, Wright-Patterson AFB OH, 5 Nov 1986.

3. Zahoor A., and Abou-Sayed I.S., "Prediction of Stable Crack Growth in Type 304 Stainless Steel", Computers and Structures, Vol.13, 137-144, 1981.

4. Hinnerichs, T.D., "Viscoplastic and Creep Crack Growth Analysis by the Finite Element Method", PhD Dissertation, AFIT/DS/AA/80-2, Air Force Institute of Technology, Department of Aeronautics and Astronautics, September, 1980.

5. Nicholas T., Palazotto A., and Bednarz E., "An Analytical Investigation of Plasticity Induced Closure Involving Short Cracks", Mechanics of Fatigue Crack Closure, ASTM STP 982,pp 361-379, 1988.

6. Wilson R. and Palazotto A., "Viscoplastic Fatigure in a Superalloy at elevated Temperatures", Fracture Mechanics, Vol. 17, ASTM STP 905, pp 265-275, 1986.

7. Palzotto A., and Henkel C.,"The Effects of Low Cycle Fatigue Comparing Compact Tension and Center-Cracked Specimens at Elevated Temperatures", Engineering Fracture Mechanics, Vol.24, 483-494, 1986.

8. Mercer J.G., "Viscoplastic Analysis of Fatigure Cracks at Notches by the Finite Element Method", PhD Dissertation, AFIT/DS/AA/86-2, Air Force Institute of Technology, Department of Aeronautics and Astronautics, September, 1986.

9. Chestnut G.L., "Cyclic Crack Growth Emanating at a Round Notch Considering Viscoplasticity", Master's Thesis, AFIT/GAE/AA/87D-3, Air Force Institue of Technology, Department of Aeronautics and Astronautics, December, 1987.

10. Rice J.R., "A Path Independent Integral and the Approximate Analysis of Strain Concentration by Notches and Cracks," Journal of Applied Mechanics, Vol. 35, 379-386, 1968.

11. Owen D.R., and Hinton E., "Finite Elements in Plasticity", Pineridge Press, Swansea, U.K., 1980.

Bibliography (Cont'd)

12. Bodner S.R., and Partom Y., "Constitutive Equations for Elastic-Viscoplastic Strain-Hardening Materials," Journal of Applied Mechanics, Vol. 42: 385-389, 1975.

13. Brockman, Robert A., SNAP: A Simple Nonlinear Analysis Program for Education and Research, University of Dayton Research Institute Report: UDR-TM-82-06, February, 1982.

14. Newman J.C., "Finite Element Analysis of Fatigure Crack Propagation Including the Effects of Crack Closure", PhD Dissertation, Dept. of Engineering Mechanics, Virginia Polytechnic Inst., 1974.

15. Matake T., and Imai Y., "Pop-In Behavior Induced by Interaction of Cracks", Engineering Fracture Mechanics, Vol. 9, 17-24, 1979.

16. Rose L.R.F., "Microcrack Interaction With a Main Crack", International Journal of Fracture, Vol. 31, 233-242, 1986.

17. Chang R., "On Crack-Crack Interaction and Coalescence in Fatigue",Engineering Fracture Mechanics, Vol. 16, 683-693, 1982.

18. Yoda M., "Subcritical Crack Growth and Crack Coalescence in Glass", Engineering Fracture Mechanics, Vol.29, 189-196, 1988.

19. Ang W.T., "A Boundary Integral Solution for the Problem of Multiple Interacting Cracks in an Elastic Material", International Journal of Fracture, Vol. 31, 259-270, 1986.

20. Rubinstein A.A., "Macrocrack - Microdefect Interaction", Journal of Applied Mechanics, Vol. 53, 505-510, 1986.

21. Yamada Y., et al., "Plastic Stress-Strain Matrix and Its Application for the Solution of Elastic-Plastic Problems by the Finite Element Method",International Journal for Mechanical Structures, Vol. 10, 343-354, 1968.

22. Hughes T.J., and Taylor, "Unconditionally Stable Algorithms for Quasi-Static Elasto/Viscoplatic Finite Element Analysis",Computers and Structures,Vol. 8, No.2, 169-173, 1978.

23. Beaman R., "The Determination of the Bodner Material Coefficients for IN-718 and Their Effects on Cyclic Loading", M.S. Thesis, AFIT/GAE/AA/84M-1, School of Engineering, Air Force Institute of Technology, Wright-Patterson AFB, Ohio, 1983.

Bibliography (Cont'd)

24. Broek, D., Elementary Fracture Mechanics, (Fourth Edition), The Hague: Martinus Nijhoff Publishers, 1986.

25. Isida M., "Effect of Width and Length on Stress Intensity Factors Of Internally Cracked Plates Under Various Boundary Conditions", International Journal of Fracture Mechanics, Vol.7, 301-316, 1971.

26. Cook R.D., Concepts and Applications of Finite Element Analysis, (Second Edition), John Wiley & Sons, 1981.

Appendix A

Simple Nonlinear Analysis Program

SNAP

The following background and user information is provided to reflect the changes made by Mercer (8) and Smith to the AFIT version of the SNAP Finite Element Code (13). The source code title is SNAP16D.F and is compatible with all VAX 11-75 compilers.

GENERAL DESCRIPTION

SNAP is a finite element solution program for two-dimensional problems in nonlinear structural mechanics. The program can be used for problems with the following characteristics:

- plane stress or plane strain assumptions
- small or moderately large displacements
- arbitrary, two-dimensional geometry
- cyclic load / monotonic loading
- crack propagation, including opening and closure
- model size less than 5000 D.O.F.
- elastic or time-independent elastic-plastic materials
- viscoplastic or time-dependent analysis

DATA PROCESSING & FILE STRUCTURE

Data processing is kept in core under control of a

simple dynamic storage allocation scheme; the only use of secondary storage is in the maintenance of element state variables and the creation output files requested by the user.

Operation of the snap program requires the following files:

File	Description
snapin.dat	primary data input deck
snapout.dat	primary data output deck
displ.dat	node displacement output file
sigstra.dat	element stress/strain output file
rstnew	restart file created at end of run
rstold	existing restart file from prior run
time	dump file for processing status

INPUT DATA CONVENTIONS

Problem input for SNAP is divided into several "data blocks", which are used as needed to define the problem to be solved. A summary of the available data blocks, their functions, and whether or not they are required for all problems is given below.

Block	Description	Required
BOUN	Define nodal constraints	YES
COOR	Define nodal coordinates	YES
CRAC	Specify nodes and directions for crack opening simulation	NO

BLOCK	DESCRIPTION	REQUIRED
CLOS	Specify nodes and directions for crack closure simulation	NO
ELEM	Define finite elements	YES
FORC	Specify concentrated forces at nodes	NO
HIST	Define loading as a function of time	YES
JINT	Define J-integral paths	NO
MESH	Generate a scaled plot of elements	NO
PARA	Select type of analysis and solution parameters	YES
PRES	Specify distributed element loads	NO
PRIN	Print specific increments of load history	NO
PROP	Define elastic material properties	YES
REST	Create a restart file for a problem	NO
STAT	Initialize material state variables	YES
SOLN	Solution start/stop after input complete	NO
SFIL	Define elements for stress and displacement files (sigstra.dat & displ.dat)	NO
TITL	Define descriptive title for a problem	YES

INPUT FORMAT

Each input data block begins with a single line containing the header of the block (e.g. "COOR"). Data blocks may be entered in any order, but each block may appear only once in the input file.

BOUNDARY CONDITIONS Input Block

Header: BOUN

BOUNDARY CONDITIONS Input Cont'd
End: Blank line

Record Format (repeat as needed)

```
.....5.....10.....15.....20.....25
  IBEG   IEND   INCR   IXFIX   IYFIX
```

Variables:

IBEG = Beginning node to be constrained

BOUNDARY CONDITIONS Input Cont'd

IEND = Ending node to be constrained

INCR = Node number increment

IXFIX = X-direction constraint code (0 = free, 1 = fixed)

IYFIX = Y-direction constraint code (0 = free, 1 = fixed)

COORDINATES Input Block

Header: COOR

END: blank line

Record Format (1):

```
....5
NUMNOD
```

Variables:

NUMNOD = Total number of nodes defined for the model.

Record Format (2):

```
..5.......10........20........30
NODE     IGEN     XCORD     YCORD
```

Variables:

NODE = Node number

IGEN = Generation increment

XCORD = X-coordinate

YCORD = Y-coordinate

CRACK Input Block

Header: CRAC

End: (none)

Record Format (1):

```
.....5
```

NUMCON

Variable:

NUMCON = Number of conditional nodes in crack front

Record Format (2):

```
....5.....10
  NODE   IDIR
```

Variables:

NODE = Node number for crack-opening constraint

IDIR = # Direction (1=X, 2=Y) of constraint
(# positive value = closed, negative = open)

Record Format (3):

```
.......5......10......15
  KRKTYPE   NSTEP    IPOP
```

Variables:

KRKTYPE = Type of element used in crack front
2 - Four noded quadr lateral
3 - Eight noded quadrilateral

NSTEP = Number of increments to reach full load

IPOP = Number of nodes released per cycle

Record Format (4):

```
........5
  ISTRESS
```

CRACK Input Cont'd

Variable:

ISTRESS = Stress required to release a node

CRACK CLOSURE Input Block

Header: CLOS

End: (none)

Record Format (1):

```
.....5
NUMCON
```

Variable:

NUMCON = Number of conditional nodes in crack front

Record Format (2):

```
.........5
    SOPEN
```

Variable:

SOPEN = Stress to open closed nodes

Record Format (3):

```
....5.....10
  NODE   IDIR
```

Variables:

NODE = Node number for crack-opening constraint

IDIR = # Direction (1=X, 2=Y) of constraint
(# initially all nodes have a negative value)

ELEMENTS Input Block

Header: ELEM

End: blank line

ELEMENTS Input Cont'd

Record Format (1):

```
....5
```

NELEM

Variable:

NELEM = Number of elements in model

Record Format (2):

```
.....5.....10.....15.....20.....25.....30.....35
 IELEM  IEGEN   INGEN  NODE(1)  NODE(2) NODE(3) NODE(4)
.....40.....45.....50.....55.....60
 NODE(5)  NODE(6)    NODE(7)   NODE(8)    INTORD
```

Variables:

IELEM = Element number

IGEN = Element generation increment (* not used)

INGEN = Node number increment generation (* not used)

NODE (i) = i-th connected node for this element

INTORD = Numerical integration order
(1 or 3 = 1-point or 3-point rule, for triangles)
(4 or 9 = 2x2 or 3x3 Gauss rule, for quadrilaterals)

* IEGEN AND INGEN are not used if mesh is generated with external program such as PDA-PATRAN.

Forces Input Block

Header: FORC

End: blank line

Record Format: (repeat as needed)

```
......5.......10.................20
   NODE     IDIR                FORCE
```

Variables:

FORCES Input Cont'd

NODE = Node number at which the force is applied.

IDIR = DIrection (1 = X, 2 = Y) of the force

FORCE = Force magnitude

HISTORY Input Block

Header: HIST

End: (none)

Record Format (1):

```
.....5
NUMPTS
```

Variable:

NUMPTS = Number of points (t, f(t)) to be defined on force time history curve

---

Record Format (2): (repeat as needed)

```
.........10..............20
        TIME             FUNC
```

Variables:

TIME = Reference value of time (loading parameter)

FUNC = Corresponding scale factor for applied loads

J-INTEGRAL Input Block

Header: JINT

End: (none)

Record Format (1):

```
................20
               TITLE
```

Variable:

TITLE = 20 character title block

J-INTEGRAL Input Cont'd

Record Format (2):

```
 .....5.........10
INUMBER       MODEL
```

Variables:

INUMBER = Number of Paths

MODEL = Type of Constitutive Model
- 1 -- Elastic
- 2 -- Elastic Plastic

Record Format (3):

```
 ....5
ETOTAL
```

Variable:

ETOTAL = Total Number of Elements in path

Record Format (4): (repeat as needed)

```
 .....5.......10.......15........20........25.........80
 ELEM(1)  ELEM(2)  ELEM(3)   ELEM(4)   ELEM(5)...ELEM(16)
```

Variable:

ELEM(i) = i-th element number containing J-integral path

Record Format (5): (repeat as needed)

```
 .....5.......10.......15........20........25.........80
IDIR(1)   IDIR(2)  IDIR(3)   IDIR(4)   IDIR(5)...IDIR(16)
```

Variable:

IDIR(i) = i-th path direction (See Diagram Below)
* NOTE EACH ELEMENT HAS TWO DIRECTIONS *

ELEMENT PATH DIAGRAM

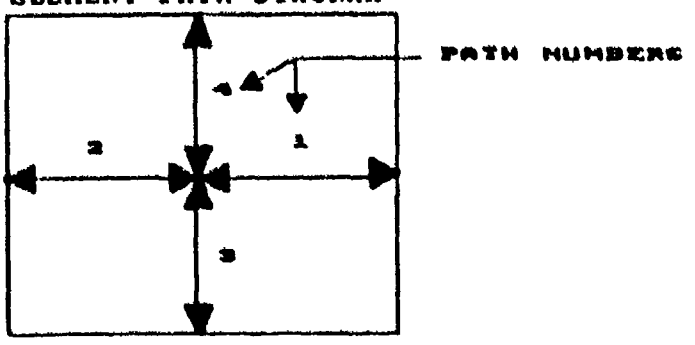

+ DIRECTION = UP AND TO THE RIGHT

- DIRECTION = DOWN AND TO THE LEFT

MESH PLOTTING Input Block

Header: MESH

End: (none)

Record Format (1):

```
 ......5.....10......20.....30.....40.....50......60
    IOPT   INUM   SCALE   XMIN   XMAX   YMIN    YMAX
```

Variables:

IOPT = Option for mesh plotting
       0 -- No plot
       1 -- Plot mesh

INUM = Option for plotting element numbers
       0 -- No numbers
       1 -- Plot numbers

SCALE = Plotting magnification scale
        1-99 -- allowable values

XMIN = Minimum X-value of plot region

XMAX = Maximum X-value of plot region

YMIN = Minimum Y-value of plot region

YMAX = Maximum Y-value of plot region

** This routine is disabled in snap16d.f since no 1038 device driver is available on the AFIT/ICC. ASD/CYBER version of SNAP (snap16c.f) supports this routine.

PARAMETERS Input Block

Header: PARA

End: (none)

Record Format (1):

```
 ......5.......10........15.........20........25......30
  IPLANE   ISMALL    IMODEL     NCSTEP     ISPRT    IGPT
```

Variables:

IPLANE = Problem type
         0 -- Plane strain
         1 -- Plane stress

PARAMETERS Input Cont'd

ISMALL = Kinematics option
- 0 -- Large displacements
- 1 -- Small displacements

IMODEL = Constitutive model type
- 1 -- Elastic
- 2 -- Elastic, perfectly plastic
- 5 -- Bodner-Partom viscoplastic
- 10 -- Bilinear Elastic plastic

NCSTEP = Total number of time step changes

ISPRT = integration point stress/strain data flag
- 0 -- none
- 1 -- Print data

IGPT = Gauss point coordinate flag
- 0 -- no data print
- 1 -- print coordinate data

Record Format (2):

```
....5.....10.....15.....20.....30.....40.....50
NSTEP  IPFREQ   ITOPT   MAXIT   EQTOL   DISTOL   DELTAT
```

Variables:

NSTEP = Number of solution increments

IPFREQ = Printing/file output frequency (in increments)

ITOPT = Nonlinear solution option
- 0 -- Corrected step-by-step
- 1 -- Constant stiffness (pseudoforce)
- 2 -- Modified Newton iteration
- 3 -- Full Newton iteration
- 4 -- Combined Newton iterations

MAXIT = Maximum number of iterations per step

EQTOL = Convergence tolerance on force residuals

DISTOL = Convergence tolerance on displacement corrections

DELTAT = Time (load parameter) step size

PARAMETERS Input Cont'd

Record Format (3) (repeat as needed)

```
 ......5.......15........20......30.........35......45....80
ICSTEP(1)   CDT(1) ICSTEP(2)  CDT(2)  ICSTEP(3)  CDT(3).....
```

(MAXIMUM STEP CHANGES = 200)

Variables:

ICSTEP (i) = i-th increment or step

CDT(i) = i-th time step size

This record enables the user to apply different time step increments during a load cycle.

PRESSURES Input Block

Header: PRES

End: (blank line)

Record Format: (repeat as needed)

```
 ..5........10...........20........30.........40
 IEL     IEDGE        PRESSA     PRESSB      PRESSC
```

Variables:

IEL = Element to which pressure is applied

IEDGE = Edge Number
1 = top, 2 = left side, 3 = bottom 4 = right side

PRESSA = Pressure value at first node point on the edge

PRESSB = Pressure value at second node point on the edge

PRESSC = Pressure value at third node point on the edge

PRINT Input Block

Header: PRIN

End: (none)

PRINT Input Cont'd
Record Format (1):

```
........5
   IPRINT
```

Variable:

IPRINT = Number of increments to print (MAXIMUM 200)
Allows user to print increment that are skipped by IPFREQ in PARAMETERS block.

Record Format (2):

```
......5........10.....15.....20.....25.....80
ICSTEP(1) ICSTEP(2).........
```

Variable:

ICSTEP(i) = i-th increment

PROPERTIES Input Block

Header: PROP

End: (none)

Record Format:

```
......10.............20
    ELAS             POIS
```

Variables:

ELAS = Elastic modulus

POIS = Poison's ratio 0 < POIS < 0.50

STATE VARIABLES Input Block

Header: STAT

End: (none)

Record Format (1):

```
.....5.......10
NSTATE   NCONST
```

Variables:

STATE VARIABLES Input Cont'd

NSTATE = Number of internal state variables to be defined

NCONST = Number of constant parameters to be defined

Record Format (2): (repeat as needed)

```
.....10........20..........30..........40..........80
STATE(1)  STATE(2)   STATE (3)    STATE(4)... STATE (8)
```

Variables:

STATE(i) = Initial value of the i-th internal state variable.

Record Format (3): (repeat as needed)

```
.....10........20..........30..........40..........80
CONST(1)  CONST(2)   CONST (3)    CONST(4)... CONST (8)
```

Variable:

CONST(i) = Value of i-th constant parameter value. (MAXIMUM 20)

STRESS/STRAIN & DISPLACEMENT FILES Input Block

Header: SFIL

End: (none)

Record Format (1): (repeat as needed)

```
......5.......10
IELEM(1)  ISTR(1)
```

Variables:

IELEM = Number of elements to be output (200 maximum)

ISTR = Stress/strain Designator
1 = XX
2 = YY (DEFAULT)

Record Format (2): (repeat as needed)

```
.....10........20..........30..........40..........80
JELM(1)    JELM(2)    JELM (3)     JELM(4)......JELM(8)
```

Variables:

STRESS/STRAIN & DISPLACEMENT FILES Input Cont'd

JELM(i) = Element numbers whose stress/strain will be written
sigstra.dat

Record Format (3):

```
......5
 MNODES
```

Variables:

MNODES = Number of Nodes whose displacement will be written
to displ.dat

Record Format (4):

```
......5........10.....15.....20.....25.....80
MNODE(1)   IDIR(1).........
```

Variables:

MNODE(i) = i-th node number

IDIR(i) = i-th displacement direction
1 = X
2 = Y

TITLE Input Block

Header: TITL

End: (none)

Record Format:

```
.........................80
```

Variables:

TITLE = Alphanumeric problem title (up to 80 characters)

MATERIAL MODEL VARIABLE DESCRIPTIONS

IMODEL = 1: LINEAR ELASTIC MATERIAL

Constants: (none)

State Variables: (none)

IMODEL = 2: ELASTIC - PERFECTLY PLASTIC

Constants: (none)

State Variables:

1. Yield Stress
2. Effective Stress (initially set to zero)
3. Elastic/Elastic Plastic Work

IMODEL = 5: BODNER-PARTOM VISCOPLASTIC MATERIAL

Constants:

1. DO
2. ZO
3. Z1
4. Z2
5. n (floating point)
6. m (floating point)
7. A (floating point)

State Variables:

1. Plastic Strain Exx
2. Plastic strain Eyy
3. Plastic strain Ezz
4. Plastic strain 2*Exy
5. Z
6. Plastic work
7. Total Work (Elastic + Plastic)

IMODEL = 10: BILINEAR ELASTIC-PLASTIC MATERIAL

Constants:

1. Yield stress
2. Strain-hardening slope

State Variables:

1. Plastic Strain in X-direction
2. Plastic Strain in Y-direction
3. Plastic Strain in Z-direction
4. Plastic Strain in XY-direction
5. Effective Plastic Strain
6. Effective Stress
7. Current Yield Stress
8. Elastic + Plastic Work

EXAMPLE OF INPUT DECK

```
COOR
 1057
    1        0.00000    0.00000
    2        0.00200    0.00000
    3        0.00000    0.00200
    4        0.00400    0.00000
    .            .          .
    .            .          .
    .            .          .
 1054        0.49238    0.00200
 1055        0.49238    0.00000
 1056        0.50000    0.00200
 1057        0.50000    0.00000

ELEM
  960
    1          1    2    6    3    0    0    0    0    4
    2          2    4    7    6    0    0    0    0    4
    3          4    5   10    7    0    0    0    0    4
    4          5   11   12   10    0    0    0    0    4
    .          .    .    .    .    .    .    .    .    .
    .          .    .    .    .    .    .    .    .    .
    .          .    .    .    .    .    .    .    .    .
  957        929  951  950  925    0    0    0    0    4
  958        974  973  950  951    0    0    0    0    4
  959        898  925  924  897    0    0    0    0    4
  960        925  950  949  924    0    0    0    0    4

BOUN
  752                1
  753                1
  754                1
  794                1
  801                1
  803                1
  804                1
  805                1
  807                1
  808                1
  809                1
  848                1
  855                1
  889                1
  895                1
  920                1
  923                1
  945                1
  948                1
  969                1
  972                1
  993                1
  996                1
 1008                1
 1010                1
 1022                1
 1025                1
 1045                1
 1050                1
 1055                1
 1057                1
    1          1
    3          1
    8          1
   23          1
   71          1
  139          1
  189          1
  251          1
  325          1
  385          1
  456          1
  503          1
```

```
TITL
QUAD4 MESH: VISCOPLASTIC  CYCLIC RUN  (SUB = 0.02) a = .204 FIXED
FORC
 503      2       .576
 519      2     1.152
 584      2     1.152
 642      2     1.152
 700      2     1.152
 755      2     1.152
 810      2     1.152
 857      2     1.152
 897      2     2.776
 924      2     4.399
 949      2     2.199

CRAC
  129
    1   -2     2   -2     4   -2     5   -2    11   -2    14   -2    15   -2    16   -2
   17   -2    19   -2    20   -2    21   -2    36   -2    42   -2    44   -2    45   -2
   46   -2    48   -2    49   -2    50   -2    51   -2    53   -2    54   -2    55   -2
   56   -2    58   -2    59   -2    60   -2    61   -2    63   -2    64   -2    65   -2
   66   -2    68   -2    69   -2    70   -2   118   -2   126   -2   130   -2   133   -2
  134   -2   136   -2   137   -2   138   -2   187   -2   194   -2   196   -2   197   -2
  198   -2   200   -2   201   -2   202   -2   203   -2   205   -2   206   -2   207   -2
  208   -2   210   -2   211   -2   212   -2   213   -2   215   -2   216   -2   217   -2
  218   -2   220   -2   221   -2   222   -2   291   -2   299   -2   303   -2   306   -2
  307   -2   309   -2   310   -2   311   -2   369   -2   376   -2   378   -2   379   -2
  380   -2   382   -2   383   -2   384   -2   441   -2   447   -2   449   -2   450   -2
  451   -2   453   -2   454   -2   455   -2   501   -2   510   -2   512   -2   513   -2
  514   -2   516   -2   517   -2   518   -2   569   -2   575   -2   577   -2   578    2
  579    2   581    2   582    2   583    2   626    2   633    2   635    2   636    2
  637    2   639    2   640    2   641    2   685    2   691    2   693    2   694   -2
  695   -2   697   -2   698   -2   699   -2   740   -2   746   -2   748   -2   749   -2
  750    2
    2   34     1
960.0

CLOS
  128
0.004
    1   -2     2   -2     4   -2     5   -2    11   -2    14   -2    15   -2    16   -2
   17   -2    19   -2    20   -2    21   -2    36   -2    42   -2    44   -2    45   -2
   46   -2    48   -2    49   -2    50   -2    51   -2    53   -2    54   -2    55   -2
   56   -2    58   -2    59   -2    60   -2    61   -2    63   -2    64   -2    65   -2
   66   -2    68   -2    69   -2    70   -2   118   -2   126   -2   130   -2   133   -2
  134   -2   136   -2   137   -2   138   -2   187   -2   194   -2   196   -2   197   -2
  198   -2   200   -2   201   -2   202   -2   203   -2   205   -2   206   -2   207   -2
  208   -2   210   -2   211   -2   212   -2   213   -2   215   -2   216   -2   217   -2
  218   -2   220   -2   221   -2   222   -2   291   -2   299   -2   303   -2   306   -2
  307   -2   309   -2   310   -2   311   -2   369   -2   376   -2   378   -2   379   -2
  380   -2   382   -2   383   -2   384   -2   441   -2   447   -2   449   -2   450   -2
  451   -2   453   -2   454   -2   455   -2   501   -2   510   -2   512   -2   513   -2
  514   -2   516   -2   517   -2   518   -2   569   -2   575   -2   577   -2   578   -2
  579   -2   581   -2   582   -2   583   -2   626   -2   633   -2   635   -2   636   -2
  637   -2   639   -2   640   -2   641   -2   685   -2   691   -2   693   -2   694   -2
  695   -2   697   -2   698   -2   699   -2   740   -2   746   -2   748   -2   749   -2

PROP
   23569.0       0.30

STAT
    7    8
    0.          0.          0.          0.        235.3       0.          0.
1000000.    235.5       260.3       104.1       3.0       3.675     .0015     7.0
```

```
PARA
    1     1   05   41    0
   34    34    1  100     0.10      1.0E-9   0.025
   10  .500E-01  013  .200E-01  017  .100E-01  019  .500E-01  024  .250E-01
   44  .500E-01  047  .200E-01  051  .100E-01  053  .500E-01  058  .250E-01
   78  .500E-01  081  .200E-01  085  .100E-01  087  .500E-01  092  .250E-01
  112  .500E-01  115  .200E-01  119  .100E-01  121  .500E-01  126  .250E-01
  146  .500E-01  149  .200E-01  153  .100E-01  155  .500E-01  160  .250E-01
  180  .500E-01  183  .200E-01  187  .100E-01  189  .500E-01  194  .250E-01
  214  .500E-01  217  .200E-01  221  .100E-01  223  .500E-01  228  .250E-01
  248  .500E-01  251  .200E-01  255  .100E-01  257  .500E-01  262  .250E-01
  282  .500E-01  285

PRIN
    2
   19    34  000  000  000  000  000  000
SOLN
    0
HIST
   17
0.          0.0
0.5         1.0
1.0         0.1
1.5         1.0
2.0         0.1
2.5         1.0
3.0         0.1
3.5         1.0
4.0         0.1
4.5         1.0
5.0         0.1
5.5         1.0
6.0         0.1
6.5         1.0
7.0         0.1
7.5         1.0
8.0         0.1

REST
    0    34
  JINT
  J INTEGRAL
      1     2
     94
    118   117   116   115   114   113   112   111   110   109   108   107   106   105   104   103
    102   101   100    99    98    97    96    95    94    93    92    91    90    89    88    87
     86    85    84    83    82    81    80    79    78    77    76    75    74    73    72    71
     70    69    68    67    66    65    64    63    62    61    60    59    58    57    56    55
     54    53    52    51    50    49    48    47    46    45    44    43    42    41    40    39
     38    37    36    35    34    33    32    31    30    29    28    27    26    25
      3    -2    -1    -2    -1    -2    -1    -2    -1    -2    -1    -2    -1    -2    -1    -2
     -1    -2    -1    -2    -1    -2    -1    -2    -1    -2    -1    -2    -1    -2    -1    -2
     -1    -2    -1    -2    -1    -2    -1    -2    -1    -2    -1    -2    -1    -2    -1    -2
     -1    -2    -1    -2    -1    -2    -1    -2    -1    -2    -1    -2    -1    -2    -1    -2
     -1    -2    -1    -2    -1    -2    -1    -2    -1    -2    -1    -2    -1    -2    -1    -2
     -1    -2    -1    -2    -1    -2    -1    -2    -1    -2    -1    -2    -1    -2    -1    -2
     -1    -2    -1    -2    -1    -2    -1    -2    -1    -2    -1    -2    -1    -2    -1    -2
     -1    -2    -1    -2    -1    -2    -1    -2    -1    -2    -1    -2    -1    -2    -1    -2
     -1    -2    -1    -2    -1    -2    -1    -2    -1    -2    -1    -2    -1    -2    -1    -2
     -1    -2    -1    -2    -1    -2    -1    -2    -1    -2    -1    -2    -1    -2    -1    -2
     -1    -2    -1    -2    -1    -2    -1    -2    -1    -2    -1    -2    -1    -2    -1    -2
     -1    -2    -1    -2    -1    -2    -1    -2    -1    -2    -1    -3

  SPIL
    173     2
     80    81    82    83    84    85    86    87    88    88    89    90    91    92    93    94
     95    96    97    98    99   100   101   102   103   104   105   106   107   108   109   110
    111   112   113   114   115   116   117   118   119   120   121   122   123   124   125   126
    127   128   326   329   331   337   336   339   341   347   346   349   351   357   356   359
    361   367   366   369   371   377   376   379   381   387   386   389   391   397   396   399
    401   407   406   409   411   417   416   419   421   427   426   429   431   437   436   439
    441   447   446   328   330   338   340   348   350   358   360   368   370   378   380   388
    390   398   400   408   410   418   420   428   430   438   440   448   325   332   335   334
    344   343   345   352   355   354   364   363   365   372   375   374   384   383   385   392
    395   394   404   403   405   412   415   414   424   423   425   432   435   434   444   443
    445   333   342   353   362   373   382   393   402   413   422   433   442
     26
    510     2   512     2   513     2   514     2   516     2   517     2   518     2   569     2
    575     2   577     2   578     2   579     2   581     2   582     2   583     2   626     2
    633     2   635     2   636     2   637     2   639     2   640     2   641     2   685     2
    691     2   693     2
```

APPENDIX B

SWAP PROGRAM SOURCE CODE

```
C     PROGRAM SWAP (INPUT,OUTPUT,CHOICES VIA SCREEN)
C
C     THIS PROGRAM ACTS AS AN INTERFACE BETWEEN THE PATRAN
C     NEUTRAL FILE, THE NASTRAN BANDIT ALGORITHM, AND THE
C     SNAP INPUT DATA FILE
C
C     THREE OPTIONS ARE AVAILABLE TO THE USER:
C
C
C       1. GENERATE BANDIT INPUT DATA FILE  FROM
C          THE PATRAN NEUTRAL FILE
C
C       2. GENERATE A SNAP INPUT DECK USING THE
C          USING THE PATRAN NEUTRAL FILE AND
C          AND BANDIT RESULTS
C
C       3. GENERATE SNAP INPUT DATA  FROM
C          PATRAN NEUTRAL FILE ONLY
C
C
C     FILES ARE AS FOLLOWS:
C
C       PATRAN.DAT  -- PATRAN NEUTRAL FILE (INPUT)
C
C       BANDIT.DAT -- BANDIT INPUT DATA (NASTRAN OUTPUT)
C
C       BANDIT.LOG -- BANDIT RENUMBERING RESULTS (INPUT)
C
C       SNAP.INP  -- SNAP INPUT DATA (OUTPUT)
C
C     ***************************************
C
      DIMENSION NCON(3000,8),X(4000),Y(4000)
      DIMENSION IOLD(4000),INEW(4000)
      CHARACTER*8 ITYPE
C
      OPEN (UNIT=8,FILE='PATRAN.DAT',STATUS='OLD')
      OPEN (UNIT=9,FILE='BANDIT.DAT',STATUS='NEW')
      OPEN (UNIT=10,FILE='BANDIT.LOG',STATUS='OLD')
      OPEN (UNIT=11,FILE='SNAP.INP',STATUS='NEW')
C
      REWIND 8
      REWIND 9
      REWIND 10
      REWIND 11
      Z = 0.0
```

```
* PROGRAM SWAP CONT'D *
      WRITE(6,2000)
      WRITE(6,2100)
      READ (5,*) IOPT
      IF (IOPT .EQ. 1 )  WRITE (9,5000)
      IF ((IOPT .NE. 2) .AND. (IOPT.NE. 3)) GO TO 50
      WRITE(6,1050)
      READ(5,*) INTORD
50    CONTINUE
C
      READ (8,1000) NODES,NEL
CC      WRITE(6,*) NODES,NEL
      DO 100 I = 1,NODES
      READ (8,960) INODE
      READ (8,1100) X(INODE),Y(INODE)
      READ (8,960)
CC      WRITE (6,*) INODE
CC      WRITE (6,*) X(INODE),Y(INODE)
100   WRITE (9,1150) INODE,X(INODE),Y(INODE),Z
C
C     READ ELEMENT CONNECTIVITY FROM PATRAN NEUTRAL FILE
C
      DO 200 I = 1,NEL
      READ (8,970) IEL
      READ(8,1200) (NCON(IEL,J),J=1,8)
CC      WRITE (6,*) IEL
CC      WRITE (6,*) (NCON(IEL,J),J=1,8)
      ITYPE = 'CIS2D8  '
      ITYP2 = '+CIS    '
      MID = 1
      ITEST = 0
      IF (NCON(IEL,5) .GT. 0) GO TO 22
      ITYPE = 'CQUAD1  '
      ITEST = 1
22    IF (NCON(IEL,4) .GT. 0) GO TO 23
      ITYPE = 'CTRI    '
      ITEST = 2
23    IF (IOPT .GT. 1) GO TO 200
      IF (ITEST .EQ. 1) GO TO 24
      IF (ITEST .EQ. 2) GO TO 25
      WRITE (9,2200) ITYPE,IEL,MID,(NCON(IEL,J),J=1,6),
     +   ITYP2,IEL,  ITYP2,IEL,(NCON(IEL,K),K=7,8)
      GO TO 200
24    WRITE (9,2224) ITYPE,IEL,MID,(NCON(IEL,J),J=1,4)
      GO TO 200
25    WRITE (9,2225) ITYPE,IEL,MID,(NCON(IEL,J),J=1,3)
200   CONTINUE
C     END IF GENERATING NASTRAN TYPE DATA FOR BANDIT INPUT
C
      IF (IOPT .EQ. 1 ) WRITE (8,3200)
      IF (IOPT .EQ. 1 ) WRITE(9,5010)
      IF (IOPT .EQ. 1) GO TO 900
```

```
* PROGRAM SWAP CONT'D
      IF (IOPT .EQ. 3) GO TO 710

C     READ RENUMBERING DATA FROM BANDIT OUTPUT
C
      READ (10,1500) (IOLD(J),INEW(J),J=1,NODES)
C      DO 300 I=1,NODES
C      WRITE(6,*) IOLD(I),INEW(I)
C      WRITE(6,*) X(I),Y(I)
C300   CONTINUE
C
C     CONVERT NODAL COORDINATES
C
      DO 400 I = 1,NODES
      M = I
      N = INEW(I)
      X(N) = X(M)
      Y(N) = Y(M)
C      WRITE(6,*) M,INEW(I)
400   CONTINUE
C
C     CONVERT ELEMENT CONNECTIVITIES
C
      DO 500 IEL = 1,NEL
C
      DO 450 J = 1,8
      M = NCON(IEL,J)
      IF (M .LE. 0) GO TO 450
      NCON(IEL,J) = INEW(M)
450   CONTINUE
C
500   CONTINUE
C
C     WRITE OUT RESULTS IN SNAP FORMAT
C
710   WRITE (11,2700)
      WRITE (11,2750) NODES
      DO 750 INODE = 1,NODES
750   WRITE (11,2780) INODE,X(INODE),Y(INODE)
      WRITE(11,2900)
      WRITE(11,2800)
      WRITE(11,2750) NEL
      DO 800 IEL = 1,NEL
800   WRITE(11,2850) IEL,(NCON(IEL,J),J=1,8) , INTORD
      WRITE (11,2900)
      WRITE(6,3100)
900   CONTINUE
      STOP
950   FORMAT(5X,I5)
970   FORMAT(5X,I5,/)
1000  FORMAT(/,/,30X,I5,2X,I5,/)
1050  FORMAT(41H INPUT ELEMENT INTEGRATION ORDER FOR SNAP  )
```

```
* PROGRAM SWAP CONT'D *
1100  FORMAT(3E16.9)
1150  FORMAT(8HGRID    ,I8,8X,3F8.5)
1200  FORMAT(8(4X,I4))
1500  FORMAT(32X,8I8)
2000  FORMAT(//40H**************************************************,//
     +          40H      NODAL RENUMBERING PROGRAM                  ,//
     +          40H**************************************************,/)
2050  FORMAT(   40H              FILE  NUMBERING:                    ,/
     +          40H PATRAN.DAT = PATRAN NEUT FILE (INP)             ,/
     +          40H BANDIT.DAT = DATA FILE BANDIT(OUTPT)            ,/
     +          40H BANDIT.LOG = BANDIT RENUMBERING RESULTS         ,/
     +          40H                (INPUT)                          ,/
     +          40H SNAP.INP = COORDS AND CONNECTIVITIES            ,/
     +          40H              IN SNAP FORMAT (OUTPUT)            ,/)
2100  FORMAT(   40H CHOOSE OPTIONS:                                 ,/
     +          40H  1. GENERATE BANDIT INPUT DATA                  ,/
     +          40H       FROM NEUTRAL FILE                         ,/
     +          40H  2. RENUMBER USING BANDIT RESULTS               ,/
     +          40H       GENERATE SNAP DATA FILE                   ,/
     +          40H  3. REFORMAT PATRAN DIRECTLY TO SNAP            ,/ )
2200  FORMAT(A8,8I8,A4,I4,/A4,I4,2I8)
2224  FORMAT(A8,6I8)
2225  FORMAT(A8,5I8)
2700  FORMAT(4HCOOR)
2750  FORMAT(I5)
2780  FORMAT(I5,5X,2F10.5)
2800  FORMAT(4HELEM)
2850  FORMAT(I5,10X,9I5)
2900  FORMAT(1X)
3100  FORMAT (40H SNAP FILE WRITTEN.                                ,/
     +         40H  OUTPUT FILE IS:                                 ,/
     +         40H  SNAP.INP   SNAP DATA FILE                       ,/)
3200  FORMAT(40H BANDIT DATA (BANDIT.DAT) IS READY                  ,/)
C
C  * NOTE CHANGE MATERIAL CARD TO MATCH REQUIRED ELEMENT
C
5000  FORMAT(41HNASTRAN TITLEOPT=-1,BANDTPCH=1,BANDTRUN=1,/
     +      30HID SNAP,BANDIT ON NESH                                ,/
     +      30HAPP DISPLACEMENT                                      ,/
     +      30HTIME 2                                                ,/
     +      30HSOL 1,0                                               ,/
     +      30HCEND                                                  ,/
     +      30HSPC=1                                                 ,/
     +      30HSTRESSES=ALL                                          ,/
     +      30HBEGIN BULK                                            ,/
     +      50HSPC1             1   345126        1       14              )
5010  FORMAT(50HPQUAD1            1         1       .5
     +       50HMAT1              1   10.0E6                .30     .100
     +        7HENDDATA   )
      END
```

VITA

LeRoy K. Smith was born on 27 December 1960 at Pierre, South Dakota. He graduated from high school in Murdo, SD in 1979. He then attended South Dakota State University in Brookings, SD. In December 1983 he was awarded a B.S. in Mechanical Engineering with high honor and was commissioned as a second lieutenant in the United State Air Force. He was then assigned to HQ Space Division, Los Angeles, CA. During this assignment he served as a facility integration engineer for the Automated Remote Tracking Station (ARTS) System Program Office. He then entered the School of Engineering, Air Force Institute of Technology, in June 1987.

UNCLASSIFIED
ECURITY CLASSIFICATION OF THIS PAGE

REPORT DOCUMENTATION PAGE

Form Approved
OMB No. 0704-0188

1a. REPORT SECURITY CLASSIFICATION UNCLASSIFIED	1b. RESTRICTIVE MARKINGS None
2a. SECURITY CLASSIFICATION AUTHORITY	3. DISTRIBUTION/AVAILABILITY OF REPORT Approved for public release; Distribution unlimited
2b. DECLASSIFICATION/DOWNGRADING SCHEDULE	
4. PERFORMING ORGANIZATION REPORT NUMBER(S) AFIT/GAE/AA/88D-35	5. MONITORING ORGANIZATION REPORT NUMBER(S)
6a. NAME OF PERFORMING ORGANIZATION School of Engineering 6b. OFFICE SYMBOL (If applicable) AFIT/ENY	7a. NAME OF MONITORING ORGANIZATION
6c. ADDRESS (City, State, and ZIP Code) Air Force Institute of Technology Wright-Patterson AFB OH 45433-6583	7b. ADDRESS (City, State, and ZIP Code)
8a. NAME OF FUNDING/SPONSORING ORGANIZATION Air Force Wright Aero Lab 8b. OFFICE SYMBOL (If applicable) MLLN	9. PROCUREMENT INSTRUMENT IDENTIFICATION NUMBER
8c. ADDRESS (City, State, and ZIP Code) AFWAL/MLLN Wright-Patterson AFB OH 45433-6583	10. SOURCE OF FUNDING NUMBERS PROGRAM ELEMENT NO. / PROJECT NO. / TASK NO. / WORK UNIT ACCESSION NO.

11. TITLE (Include Security Classification)

See box 19

12. PERSONAL AUTHOR(S)
LeRoy K. Smith, Capt, USAF

13a. TYPE OF REPORT	13b. TIME COVERED	14. DATE OF REPORT (Year, Month, Day)	15. PAGE COUNT
Thesis	FROM _____ TO _____	1988 December	115

16. SUPPLEMENTARY NOTATION

17. COSATI CODES			18. SUBJECT TERMS (Continue on reverse if necessary and identify by block number)
FIELD	GROUP	SUB-GROUP	Crack Growth, Finite Elements, Viscoplasticity, Theses. (jhd)
12	01		

19. ABSTRACT (Continue on reverse if necessary and identify by block number)

TITLE: MACROCRACK-MULTIPLE DEFECT INTERACTION CONSIDERING ELASTIC, PLASTIC, AND VISCOPLASTIC EFFECTS

Thesis Chairman: Dr Anthony Palazotto
Professor of Aeronautics and Astronautics

Approved for release in accordance with AFR 190-1.
12 Jan 1989

20. DISTRIBUTION/AVAILABILITY OF ABSTRACT ☑ UNCLASSIFIED/UNLIMITED ☐ SAME AS RPT ☐ DTIC USERS	21. ABSTRACT SECURITY CLASSIFICATION UNCLASSIFIED
22a. NAME OF RESPONSIBLE INDIVIDUAL Dr A Palazotto, Professor	22b. TELEPHONE (Include Area Code) 513-255-2998 22c. OFFICE SYMBOL AFIT/ENY

DD Form 1473, JUN 86 *Previous editions are obsolete.* SECURITY CLASSIFICATION OF THIS PAGE

UNCLASSIFIED

BOX 19:

A finite element investigation was conducted to analyze an axial tension specimen with collinear defects placed symmetrically about a center crack. The material modeled was IN-718, a nickel-based superalloy used in jet engines. The effects of crack/defect interaction were compared using elastic, elastic plastic, and viscoplastic constitutive models. A 2-D nonlinear finite element code called SNAP was used. This program has the capability to simulate crack growth and closure by releasing or closing nodes along the crack plane.

Elastic stress intensity solutions were developed for two different finite width specimens. The stress intensity versus crack length plots compared well with infinite theory. Results reflect the defect can partially shield the crack from finite width effects. A critical spacing was also noted where the stress intensity of the crack exceeded the stress intensity for the combined length of the crack and defect.

Finite element analysis of a crack/defect configuration, considering elastic-plastic and elastic-viscoplastic effects, provided crack opening profiles, plastic zone profiles, and stress/strain fields. In general, the defect has a prominent influence range equal to approximately one defect length for all constitutive models. The presence of a defect increases the magnitude of the crack opening and stress/strain fields in front of the crack tip. Keywords: → to field 18